MINERALOGY AND STABLE ISOTOPE GEOCHEMISTRY OF THE STRATIFORM REPLACEMENT ZONE, VIBURNUM TREND, SOUTHEAST MISSOURI, USA

by

Daniel Slane

A Thesis
Submitted to the Faculty of Graduate Studies of
The University of Manitoba
In Partial Fulfillment of the Requirements
For the Degree of

MASTER OF SCIENCE

Department of Geological Sciences
University of Manitoba
Winnipeg, Manitoba

Abstract

As the mines on the Viburnum Trend continue to age, there is an increasing need to find mineralization of sufficient tonnage and grade. The objective of this study is to determine if there are any trends in oxygen or carbon isotopes that can be used as an exploration tool within the Stratiform Replacement Zone of the Viburnum Trend. Micro drilled samples were collected, and carbon and oxygen isotope values analyzed within and at increasing distances from mineralized areas. While there are trends in oxygen isotope values between mineralized and unmineralized samples, there is weak correlation between the barren oxygen isotope values and distance from mineralization. Mineralized samples show less variability among the oxygen isotope values compared with unmineralized samples. The weak correlation between oxygen isotope values and distance from mineralization is interpreted to be caused by a complex relationship between variable amounts of recrystallized dolomite and different sulfide generations.

Acknowledgements

I would like to thank Ross Conner, V.P. of Exploration & Development and Tom Schott, District Exploration Manager, for permission to complete this study. The Exploration Department within The Doe Run Resources Corporation provided technical and logistical support throughout the project. I would also like to thank engaging discussions and improvements to earlier drafts from Jim Palmer, which improved the overall quality and relevance of this work. Financial support was provided by the Doe Run Resources Corporation.

The underground sampling within the mines could not have been completed without the assistance of the Mine Geologists at each site, including Kevin Koob, Craig Gripp, Bob Ridings and Richard Anderson. Helpful information and assistance was also provided by Craig Hall and Bob Hemmann. Terry Peppers, Jim Wisdom and Vannessa White also helped out by helping locate drill core samples in the early stages of the project.

My advisor, Mostafa Fayek provided invaluable guidance on the project from data collection, to interpretation, to thesis writing. Laboratory work with the SIMS, microprobe, Stable Isotope Lab, and SEM could not have been completed without the assistance of the following lab managers: Ryan Sharpe, Brandi Shabaga, Neil Ball, and Misuk Yun.

The support of my family, and especially my wife, Heather Slane, was absolutely critical.

Dedication

I dedicate to this my late brother, Nathanial J. Slane.

Table of Contents

List of Tables

List of Figures

Chapter 1: **Introduction**

The Missouri Lead District, located in the south-central United States (Figure 1.1), is the second largest producer of lead in the world. The deposits in this region have been mined continuously since 1864, with the earliest records of mining dating from the early 1700's. The district has also been a minor producer of zinc and copper since its discovery. The Missouri Lead District is sub-divided into two major areas based on the location of mineralization and the history of mining in the area: the Old Lead Belt and the Viburnum Trend. The Old Lead Belt was first mined in the early 1700's and all operations ceased by the late 1960's. The Viburnum Trend was discovered in the late 1950's and is the location of current mining operations (Gerdemann & Myers, 1972). There are currently 6 mines, which feed 4 mills producing lead, zinc, and copper concentrates. Average ore grade is 4% Pb, 1% Zn and 0.15% Cu. The mining division produces approximately 250,000 tons of concentrate annually (The Doe Run Company, 2015).

Figure 1.1: Map of Missouri showing mineral districts (Gerdemann & Myers, 1972).

1.1 District History

The Viburnum Trend was discovered in the 1950's by the St. Joseph Minerals Corporation (St. Joe), which at the time was experiencing a reduction in available ore reserves from the Old Lead Belt (OLB). As a result, the company began an exploration program to the North and West, reaching a maximum distance of 35 miles from the OLB. St. Joe's first success in finding ore outside of the OLB was a drill hole collared near the town of Potosi, located approximately 40 miles Northeast of the Viburnum Trend. This drill hole resulted in the Indian Creek Mine, which was the first outside of the OLB (Lasmanis, 1997). The first

successful drill hole by St. Joe along the Viburnum Trend was completed in 1955 at the North end of the district (Figure 1.2).

The discovery of economic lead mineralization West of the OLB resulted in a land rush with multiple mining companies competing for land on the Viburnum Trend. Some notable companies which either explored or mined the Viburnum Trend as a result of this rush include Hecla Mining Company, Phelps-Dodge Corporation (predecessor to Freeport-McMoRan Inc.), Cyprus Amax Minerals Company, Homestake Mining Company and the American Smelting And Refining Company (Lasmanis, 1997).

(Removed Due to Copyright)

Figure 1.2: Map of southeast Missouri showing different sub districts
(Shelton et al., 2009).

The Viburnum Trend is 40 miles long and 2 miles wide. Over 21 miles of underground roads connect four mines, while two mines have separate access. The mining method is room and pillar, with drifts 32 ft. wide and 16-20 ft. tall. The mines are arranged in a North-South orientation and are almost entirely connected. While the stratigraphy is largely flat-lying, there is a gradual southerly dip of 1-2 degrees. Depths below surface for mining range from 700 ft. at the # 29 Mine to 1,200 ft. at the Sweetwater mine, which is situated at the very southern tip of the Viburnum Trend. Ore is hoisted in vertical shafts and processed

at one of the nearby mills. Concentrate is produced from these mill sites and transported to a port on the Mississippi River (~80 miles east of the Viburnum Trend) where it is loaded onto ships bound for overseas customers. Figure 1.3 shows the location of current mining operations and the site of closed operations which are relevant to this study (Gerdemann & Myers, 1972; The Doe Run Company, 2015).

Figure 1.3: Mine location map of the Viburnum Trend (Google Earth).

1.2 Previous Work

Previous work on sphalerite mineralization has focused on analyzing the trace element chemistry of different colors of sphalerite located within specific mines. Some work has also been completed on sphalerite as a way of comparing fluids between different districts (Mavrogenes *et al.*, 1992; Viets *et al.*, 1992). Carbon and oxygen isotope studies have also been completed with the focus on determining fluid sources for mineralization on the Viburnum Trend (Gregg, 1985; Shelton *et al.*, 2009).

Viets *et al.* (1992) studied the trace element profiles of sphalerites using micro drilled spahlerite samples which were analyzed with a six step semi-quantitative DC spectrographic arc analysis. Two paragenetic stages of sphalerite were studied: early sphalerite associated with main stage fluids and late stage sphalerite associated with cubic galena. They concluded that these distinct sphalerite generations were sourced from two different basins. This was based on K/Cl ratios and trace element differences in inclusions from representative sphalerite grains. The K/Cl ratios in fluids associated with early, main stage sphalerite contained elevated K levels with significantly higher concentrations of Cu, Ge, Ga, Ag and Co compared with the late stage sphalerite.

Fluids associated with early stage sphalerite were interpreted to have been sourced from the LaMotte Formation, similar to fluids associated with other main stage sulfides in the Viburnum Trend. Fluids associated with late-stage sphalerite, however, were interpreted to have been sourced from a different basin (such as the Illinois or Forest City basins) and the authors suggested that these fluids were associated with other mineral districts in the Tri-

State area, Mississippi-Valley (Wisconsin), Central Missouri and Northern Arkansas (Viets *et al.*, 1992).

Work was completed on the West Fork Mine (now Fletcher) to determine the causes of color variation of sphalerite (Mavrogenes *et al.*, 1992). At least 6 different colors of sphalerite have been identified at the West Fork Mine, as well as Wurtzite (a polymorph of sphalerite) and Schalenblende (an intergrowth of sphalerite and wurtzite). Overall, Mavrogenes *et al.* (1992) determined that deposition of the different zones of sphalerite at the West Fork Mine were caused by fluids with a pH of approximately 5 and must have been the result of fluids which were channeled from remote and separate basins. In addition, compositions of different sphalerites were analyzed to determine the causes of the color variations. The authors determined that different colors of sphalerite were due to the varying concentrations of germanium, copper and other trace elements (Mavrogenes *et al.*, 1992).

Oxygen and carbon isotopic analyses of late calcite and select hydrothermal dolomite crystals from the Magmont West Mine as well as in unmineralized drill holes several miles away were completed to identify isotopic trends at increasing distances from mineralization. An oxygen isotope trend (higher $\delta^{18}O$ values with increasing distance) was identified. This $\delta^{18}O$ enrichment trend was interpreted to be with the result of fluids associated with late chalcopyrite mineralization. The mineralizing fluids associated with the Magmont West Mine were interpreted to be sourced from local recycling of fluids in a closed system. In addition, baseline oxygen and carbon isotope values for unmineralized

Bonneterre Formation limestone were found to range between18.6 to 21.7 ‰ $\delta^{18}O$ (SMOW) and -1.5 to + 0.8 ‰ $\delta^{13}C$ (PDB) (Hannah & Stein, 1984).

Different hydrothermal dolomite generations were analyzed to determine the fluid sources responsible for deposition of main stage mineralization (Lohmann & Frank, 1982; Keller *et al.*, 2000). Each dolomite generation was progressively more enriched in ^{13}C and ^{18}O (i.e., higher $\delta^{13}C$ and $\delta^{18}O$ values, respectively), while the last generation of cement (Type 4) had much lower $\delta^{13}C$ and $\delta^{18}O$ values. They suggested that these isotopic variations were caused by a single evolving fluid, followed by a distinct, second pulse of fluid which formed hydrothermal dolomite with lower $\delta^{13}C$ and $\delta^{18}O$ values (Lohmann & Frank, 1982; Keller *et al.*, 2000).

Strontium, carbon and oxygen isotope data were used to characterize the relationship between ore fluids and hydrothermal dolomite in a basal dolostone bed from the Viburnum Trend. This basal bed is not directly associated with mineralization and lies at the contact between the underlying LaMotte Formation and the Bonneterre Formation, approximately 200 ft. below the main ore bearing horizons. These studies established that the mineralized fluids were sourced from basinal waters, which primarily affected the lower part of the Bonneterre Formation. In addition, different generations of mineralizing fluids within the Bonneterre Formation had complex fluid mixing histories and distinct sources for metals and sulfur (Gregg, 1985; Shelton *et al.*, 2009).

Overall, while significant work has been completed on analyzing different colors of sphalerite from the Viburnum Trend, no comprehensive work has been completed on either the blanket zones, or the Stratiform Replacement Zones. Blanket zones are areas

where galena mineralization occurs on a single horizon within the upper Bonneterre Formation, while Stratiform Replacement Zones (SRZ) are areas where sphalerite mineralization (with minor galena) has replaced dolostone on a single horizon within the upper Bonneterre Formation. Both of these zones are described in Sections 2.3.3 and 2.3.3.1.

1.3 Purpose and Scope of Study

While several paragenetic, stable isotope and trace element studies have been completed on the Viburnum Trend, very little focus has been directed at understanding the paragenesis, ore controls or isotope characteristics of the fluids associated with the SRZ. In addition, no attempt has been made to utilize the C and O isotopic values of carbonate in hydrothermal dolomite veinlets as an exploration tool in this mineral district.

As the Viburnum Trend nears its sixth decade of continuous production, there is a need to develop improved exploration strategies to discover new ore resources of sufficient grade and tonnage. This method has the potential within blanket areas of the Viburnum Trend, particularly in the Stratiform Replacement Zone (Clendenin, 1993; Schott, 2015, Personal Communication).

Therefore, the overall goal of this work is to determine whether bulk carbon and oxygen isotopic analysis can be used as a supplement to traditional exploration methods to assist in the exploration of the SRZ. To achieve this goal my objectives are: (1) paragenetically characterize the different dolomite textures associated with the Stratiform Replacement Zone; (2) analyze the carbon and oxygen isotopic composition of both host dolostone and hydrothermal dolomite veinlets, within the deposits and at increasing distances from the

deposits; (3) Evaluate trends in the data at increasing distances from the deposits to determine if there are vectors that can be used to guide exploration; (4) complete oxygen isotope *in situ* micro-analysis of the dolomite textures in order to understand the source of the bulk isotope values; and (5) characterize the sphalerite mineralization from the SRZ and compare its mineral paragenesis to the rest of the Viburnum Trend, including its sulfur isotopic composition.

Samples were obtained from the SRZ from four different mines along the Viburnum Trend. These include the Casteel, Buick, Fletcher and Sweetwater mines. Underground samples and drill core were obtained. Due to the lack of outcrop exposure, no samples were taken from the surface. Paragenetic studies were completed on mineralized and barren samples, with a particular focus on the relationship between sphalerite and hydrothermal dolomite zones as well as the paragenetic sequence of the different sphalerite generations. In addition, *in-situ* sulfur and oxygen isotope work was completed to help link different stages of mineralization to representative dolomite textures found in the SRZ.

Chapter 2: **Geologic Setting**

2.1 Regional Geology

2.1.1 General Geology

Southeast Missouri is located on the margins of the Ozark Uplift. This is part of the central stable interior of the North American Craton. The region is southwest of the Illinois Basin, to the North of the Arkoma Basin, and is located several hundred miles northwest of the Reel foot Rift. The Ouachita mountain chain is located to the south of the Arkoma Basin and forms an E-W belt that extends from Texas to Louisiana (Shelton *et al.*, 2009). Figure 2.1 shows the location of the Southeast Missouri Lead District compared with other regional basins and the Ouachita Mountains.

(Removed Due to Copyright)

Figure 2.1: Regional geologic setting of the Viburnum Trend (Shelton *et al.*, 2009).

The ore deposits in southeast Missouri are hosted in the Bonneterre Formation. This unit consists of limestones and dolostone (in the vicinity of ore zones all carbonates are dolomite in composition) with shaly interbeds (Gerdemann & Myers, 1972). The formation reaches a cumulative thickness of up to 300 ft. and has been dated to the Late Cambrian (Thacker & Anderson, 1977). A significant period of erosion produced a large unconformity between the Precambrian and the Early Cambrian marine sediments. Carbonate shelf and platform deposition followed, beginning in the Early Cambrian and continuing to the Middle Ordovician. Uplift and subsequent erosion occurred, which produced significant karst events during the Mississippian (Thacker & Anderson, 1977).

The Viburnum Trend is cut by several sets of regional scale faults, all of which saw multiple periods of activation. Many of these fault systems penetrate the underlying Precambrian basement. Major regional structures include the northeast striking Ellington, Black, St. Genevieve and Simms Mountain fault systems. Smaller scale, but still important structures include the Northeast striking Greenville and Big River Fault systems, which merge into a broad trending west-east fault zone known as the Palmer fault system. The Ellington fault system in the southern portion of the Viburnum Trend shows evidence of three distinct periods of movement, with changing block directions from different periods of reactivation. Some periods of this fault system resulted in normal movement, others resulted in strike-slip movement. The Simms Mountain fault system shows the most offset of any of the fault systems with at least two periods of movement, including a normal faulting phase which was followed by a shallow angle thrust fault phase which has been linked with certain mineralization structures, including transpressional duplex "flower" structures (Clendenin *et al.*, 1989; Clendenin, 1993). For a description of transpressional duplex "flower" structures, see Section 2.3.3 (p. 34). The St. Genevieve faults systems has been linked with major strike-slip faults in Illinois and Kentucky. Two periods of movement have been identified, including a Late Devonian extension period, which was followed by reactivation sometime after the Carboniferous period (Clendenin *et al.*, 1989, 1994).

Figure 2.2 shows the major fault systems in Southeast Missouri and their relation to the mining districts in the region.

(Removed Due to Copyright)

Figure 2.2: Major regional structures of southeast Missouri (Clendenin, 1993)
Red box is the location of the Viburnum Trend. V.T.= Viburnum Trend, O.L.B = Old Lead Belt, S.F.T = St. Francois Terrane, S.M.D.B = Southeast Missouri Barite sub district. Numbers correspond to the different mines and the stippled pattern is the location of known ore deposits in the region.

These major structures have been interpreted to be the site of tectonic activity during the following periods (Clendenin *et al.*, 1989):

1. Late Cambrian-Early Ordovician (Basin development)
2. Late Carboniferous (Ouachita Orogeny)
3. Late Carboniferous -Early Permian (Alleghenian Orogeny)

4. Late Cretaceous (Reelfoot Rift)

Hydrothermal dolomite was deposited in vugs, open spaces, fractures and has resulted in recrystallization of the original dolostone. The hydrothermal dolomites were produced by a large scale hydrothermal system associated with several periods of sulfide fluid pulses, which interacted with rocks in Kansas, Arkansas, Missouri and Illinois. (Voss *et al.*, 1989).

2.1.2 Precambrian Rocks

The Precambrian basement suite of rocks unconformably underlies all Paleozoic rocks and is composed of rhyolite, granite, diabase and ash flow tuff. They date from roughly 1.5 billion years ago and are part of an anorogenic sequence of rocks which stretch from Oklahoma to Ohio (Kisvarsanyi, 1977). Approximately 900 million years of exposure resulted in erosion and weathering of the Precambrian surface before deposition of sediments in the Early Cambrian (Thacker & Anderson, 1977). Erosion created steep relief on this paleosurface, which approached a maximum of 2,000 ft. in a northeast-trending, uplifted platform. During the time of the deposition of the LaMotte and Bonneterre Formations, these Precambrian knobs stood out as partially submerged highlands and governed depositional facies in the area (Larsen, 1977).

2.1.3 Paleozoic Stratigraphy

Southeast Missouri is covered by hundreds of feet of carbonate and shaly rocks, with dolostone rocks dominating the lithology of the section. Figure 2.3 shows a stratigraphic column detailing the Upper Cambrian and Lower Ordovician strata, which comprise all the Paleozoic rocks in southeast Missouri.

(Removed Due to Copyright)

Figure 2.3: Stratigraphic column for southeast Missouri (Shelton *et al.*, 2009).
Only Cambrian-aged rocks are preserved along the Viburnum Trend. The red square indicates stratigraphy found along Viburnum Trend. The remainder of the stratigraphic column has been eroded away in this area.

2.1.3.1 Stratigraphy

Seven formations define the Cambrian section in southeast Missouri, including the LaMotte Formation, the Bonneterre Formation, the Davis Formation, the Derby-Doerun, the Potosi Formation and the Eminence Formation.

The LaMotte Formation is composed of well-rounded and sorted medium to coarse grained quartz sandstone, which varies from an arenite to arkosic sand, based on its relationship to Precambrian paleo-islands (Shelton *et al.*, 2009). The cement varies from quartz to calcite and tends to coarsen upwards through the section. Red hematitic shale partings occur in the lower part of the formation. This unit represents a transgressive sequence of marine sand which filled the irregular and variable geometry of the basin caused by extensive weathering of the Precambrian rocks (Lyle, 1977; Thacker & Anderson, 1977). The LaMotte Formation varies in thickness from 0 meters where it pinches out over top of Precambrian knobs to 150 m in thickness and can become partially dolomitized in the upper part of the section near the contact with the Bonneterre Formation. Laminated shale partings occur closer to the contact of the overlying Bonneterre Formation. The LaMotte Formation forms a conformable contact with the overlying Bonneterre Formation and is unconformable with the underlying Precambrian rocks (Gerdemann & Myers, 1972).

The Bonneterre Formation represents a marine limestone that has been variably dolomitized in different parts of Missouri. Five distinct carbonate facies have been identified and described in the literature. These faces include a lime micrite, an oolite package, a digitate stromatolite package, a planar stromatolite package and a sandy transition zone. This package of rocks is representative of an epeiric sea model with fluctuations caused by rising and lowering sea levels (Lyle, 1977).

Continued subsidence during the deposition of the Bonneterre Formation resulted in a distinct pattern of transgressive facies across southeast Missouri (Figure 2.4). The

Bonneterre Formation thickens from northwest to southeast and its thickness was locally controlled by the underlying Precambrian highlands (Larsen, 1977).

(Removed Due to Copyright)

Figure 2.4: Facies Variations and Regional thickening of the Bonneterre Formation (Larsen, 1977). The red box is the approximate location of the Viburnum Trend. Contours represent the net thickness of the Bonneterre Formation, the stippled pattern represents mineralization and the black represents Precambrian outcrop.

.

Throughout the period of sedimentation, the partially eroded Precambrian highlands continued to influence the depositional facies of the Bonneterre Formation, despite being

partially buried by the underlying LaMotte Formation. Changes in slope and depth of the shallow sea imparted a ring-like distribution of the facies. The creation of very well developed and digitate stromatolite reef further influenced the depositional characteristics of sediments deposited later. The digitate stromatolite facies represent intertidal facies composed of distinctive digitate fingers of digitate stromatolites with associated channel fill in between these digitate structures. The digitate stromatolite facies are separated into two sub-types: biostromes and bioherms. Bioherms are associated with the digitate stromatolite fingers and are very distinctive. The biostromes, on the other hand, tend to occur in distinct vertical cycles and often have continuous, traceable channels which cross cut them. The planar and digitate stromatolite reef record a high energy environment, with the oolitic facies representing a medium energy zone. The lime micrite mud facies record low energy environments (Larsen, 1977).

In most parts of Southeast Missouri, the Bonneterre Formation is dominantly oxidized with calcite cement filling pores and vugs. In addition, evidence of sub aerial bleaching is common throughout much of the state. This is evidenced by a visually distinct white coloration change (appearing bleach-white) along with hematitic staining (Larsen, 1977).

Relationships among facies types across Southeast Missouri can be complex and difficult to correlate. Figure 2.5 shows the unconformity in the lower-middle Bonneterre Formation, which is part of the sub-aerial exposure event, and is related both to widespread oxidation and bleaching. This unconformity is also observed in the Southern Viburnum Trend where it truncates the digitate stromatolite facies of the Middle Bonneterre Formation (Mouat &

Clendenin, 1977). More detailed information on the Bonneterre Formation within the Viburnum Trend can be found in the following section.

(Removed Due to Copyright)

Figure 2.5: Generalized Facies relationships in the Bonneterre Formation in the Viburnum Trend (Larsen, 1977)

The Davis Formation is distinguished by an abundance of shale relative to the other units, although dolostone and limestone beds make up a significant proportion of the formation. The unit is variably dolomitized and varies from a minimum 0 ft. to a maximum of 270 ft. in the thickest sections. The lower 30-90 ft. of the unit generally contains the highest shale content, whereas the upper sections contain thick dolostone and limestone beds, often with glauconite and thin conglomerate beds. The Davis Formation has a conformable surface

with the underlying Bonneterre Formation in most areas (Gerdemann & Myers, 1972; Thacker & Anderson, 1977).

The Derby-Doerun Formation conformably overlies the Davis Formation and is composed of bedded to medium crystalline dolostone with silty interbeds. Much of the Derby Doe Run Formation contains glauconite pellets and small amounts of silt. This unit is 30-210 ft. in thickness and is one of the most consistent stratigraphic markers in southeast Missouri (Thacker & Anderson, 1977; Shelton *et al.*, 2009).

The Potosi Formation is composed of medium to coarse crystalline dolostone, which conformably overlies the Derby Doe Run and is commonly oxidized and vuggy. Drusy quartz and partial rock sillicification are common as are openings, fractures and clay zones. Reef facies dominate the original rock lithology, as do back reef (oolitic) sections. Some areas are burrowed (Thacker & Anderson, 1977; Shelton *et al.*, 2009).

2.2 Viburnum Trend Stratigraphy & Facies

2.2.1 Bonneterre Formation

The Bonneterre Formation along the Viburnum Trend, though it sits directly on top of the LaMotte Formation, contains facies which are strongly affected by the underlying Precambrian knobs. These Precambrian knobs, despite being heavily eroded were still high enough to have pinched out the LaMotte Formation as well as other units above it in limited areas (Snyder & Odell, 1958; Gerdemann & Myers, 1972).

2.2.1.1 The Lower Bonneterre Formation

The lower portion of the Bonneterre Formation consists of a sequence of bleached, sandy and digitate reef material along with erosional sections, which formed in a regressive basinal setting within a shallow sea. This part of the Bonneterre Formation formed directly on top of the LaMotte Formation and exposed Precambrian highlands, except where the LaMotte Formation sits over the underlying Precambrian knobs. Depending on the proximity to underlying Precambrian knobs, the lithology can vary from crystalline dolostone with strong glauconite to lime mud to shaly and sandy dolostone. In general, the glauconite lithology occurs along the western part of the Viburnum Trend. The middle Viburnum Trend contains a fine grained tuffaceous bed, which is very thin (0.01-1.0 ft.) and records an explosive volcanic event that occurred approximately 3-6 miles east of the Viburnum Trend and is unconnected to mineralization (Gerdemann & Myers, 1972; Lyle, 1977; Thacker & Anderson, 1977).

2.2.1.2 The Middle Bonneterre Formation

The Middle Bonneterre Formation generally contains two different facies, based on the relative position of the paleo-sea with the Precambrian highlands: a well-developed algal stromatolite reef with grainstones and micrite in between the stromatolite mounds and an oolitic grainstone which represents an offshore shelf facies. In general, this section records a transgressive sequence within the Bonneterre Formation, with the position of the reef changing based on proximity to the knobs as well as changing water depths as a result of subsidence. The reef algal stromatolites contain numerous digitate finger morphologies with a vertically stacked and branching morphology in cross section. Grainstones in between the digitate stromatolite structures contain fragments of trilobites, algal pellets

and echinoderm fragments. Portions of the digitate stromatolites are bleached with small sections of clay and some minor shale bands. The bleached zones, combined with truncated digitate stromatolite fingers, provide evidence for subaerial exposure. On a larger scale, the reef forms complex but frequently connected networks of channels which diverge and converge in broadly North-South directions. An important marker in the middle Bonneterre Formation is the gray beds. These are consistent across most of the Viburnum Trend and are a series of thin micrite beds which alternate with oolitic grainstones. These gray beds measure one to two inches in thickness, and the overall unit is generally ten to fifteen feet in thickness (Gerdemann & Myers, 1972; Lyle, 1977; Gregg *et al.*, 1993).

2.2.1.3 The Upper Bonneterre Formation

The Upper Bonneterre Formation consists of alternating sections of oolitic grainstones which are interpreted to have formed in a subtidal depositional zone on a basin slope. The oolitic grainstones occur both proximally and at increasing distances from the underlying Precambrian highlands. A silty quartz unit, called the Sullivan Siltstone is situated near the top of the upper Bonneterre Formation and is a relatively consistent marker zone across Missouri, though it is only found in portions of the Viburnum Trend. In addition, a dark green, thin (2-5 ft.) shale unit, called the False Davis is located approximately 50 ft. below the top surface of the Bonneterre Formation. This unit overlies the Sullivan Siltstone and in intra-cratonic shelf areas can truncate the Sullivan Siltstone (Larsen, 1977; Lyle, 1977; Thacker & Anderson, 1977). These zones, while generally reliable as stratigraphic markers, can be variable. In some areas they are inconsistent in their vertical distribution and relationship with each other (Gerdemann & Myers, 1972; Lyle, 1977; Thacker & Anderson, 1977; Gregg *et al.*, 1993).

2.2.1.4 Post Lithification Features

The Bonneterre Formation contains a sharp, but irregular interface of limestone and dolostone. This contact of limestone and dolostone cuts facies in many areas, though the limestone sections do preferentially occur in specific lithologies of the Bonneterre Formation, including the reef, offshore shelf, back reef and fore reef areas. Even in sections of Bonneterre Formation which contain abundant limestone, calcite and dolomite are prevalent as pore and vug filling cements. Based on the fact that the contact between limestone and dolomite cuts various facies of the Bonneterre Formation, the dolomitizing fluids have been identified as post-deposition. Isotopic evidence and cathodolumience comparison of hydrothermal dolomites from the Viburnum Trend and other areas in Southeast Missouri further support an outside, hydrothermal source for the dolomitizing fluids (Lyle, 1977; Voss *et al.*, 1989; Gregg *et al.*, 1993; Shelton *et al.*, 2009).

An additional post lithification feature common to the Bonneterre Formation is a rock coloration zone, locally termed “white rock”. This is a bleached zone which represents sub-aerial exposure and is almost always barren of mineralization. It generally is strata bound within the stromatolite reef zone. In general this zone occurs on the east side of the Viburnum Trend and forms an eastern edge to mineralization. The west side of the Viburnum trend is bounded by basinal limestone facies in the Bonneterre Formation and is completely barren of mineralization (Gerdemann & Myers, 1972; Lyle, 1977; Thacker & Anderson, 1977).

Different facies and vertical sections of the Bonneterre Formation have been dolomitized with varying levels of intensity. Oolites were the first and most susceptible to

dolomitization, followed by pellets, lime mud and algal stromatolite material, trilobite fragments and others. Hydrothermal dolomite crystals occasionally cross cut earlier calcite cement. They can also preferentially grow on particular sides of styolites, which indicates that dolomitizing fluids interacted with the rock both before and after styolite development (Lyle, 1977).

The textural evidence indicates that areas along and adjacent to styolites and early calcite cements were dolomitized first with successive periods of dolomitizing fluids controlled largely by limestone grain size and lithology. In addition, evidence for several stages of de-dolomitization have been identified. Evidence for de-dolomitization consists of high iron within dolomite crystals, silicified and clay-rich zones (Lyle, 1977).

Dolomite cements are generally post-lithification, not related to diagenesis, but are intricately related to sulfide mineral zonation. Four distinct types of dolomite cement have been identified along the Viburnum Trend. In addition, at least two periods of dissolution have been identified within the specific zones. These cements are generally only visible under a cathodoluminescent (CL) microscope (Voss *et al.*, 1989).

Figure 2.6 shows a simplified paragenesis with an emphasis on the dolomite cements, whereas Figure 2.7 displays a more detailed paragenesis that shows the relationship between each generation of sulfide minerals and dolomite cement. The following are descriptions of each dolomite cement zone and their relationship to the sulfide minerals (from Voss *et al.* 1989):

Type 1: Earliest cement, pre-dates earliest disseminated sphalerite.

Type 2: Precipitated after early disseminated sphalerite, but pre-dates octahedral galena.

Type 3: Pre-dates cubic galena, occasionally overprints type 2 dolomite cement. Post-dates main stage Pb-Zn ore deposition.

Type 4: Post-dates pyrite, chalcopyrite and cubic galena. Includes pink saddle dolomite as well as an opaque, white iron-rich cement. It may contain minor late crusts of marcasite, pyrite or even chalcopyrite in some areas.

(Removed Due to Copyright)

Figure 2.6: Simplified paragenesis of cements from SE Missouri (Voss *et al.*, 1989).

Figure 2.7 shows the five types of dolomite cement and their relationship to sphalerite from the Viburnum Trend. Five distinct stages of sphalerite have been identified across the district, with only one identified as late stage.

(Removed Due to Copyright)

Figure 2.7: Complete mineral paragenesis of sulfides (Voss *et al.*, 1989).
The red box outlines sphalerites, while the green box outlines the late stage sphalerite observed in the SRZ and its relationship with late stage dolomite cement.

These cement types correlate across the district and are common across all of southeast Missouri. The paragenetic relationship of hydrothermal dolomite and calcite with the sphalerites is similar to many other MVT districts, including the Tri-State District and Central Tennessee District, though calcite preceded sphalerite deposition in the Central Tennessee Zinc District (Voss *et al.*, 1989).

2.2.2 Ore Deposition & Fluid Sources

Common sulfide textures include colloform banding, open space filling, framboids, exsolution and replacement. Galena, sphalerite and chalcopyrite can occur as open space filling in vugs, fractures and voids as well as massive replacement of the host rock. Other sulfides, which occur in trace concentrations include fletcherite ($Cu(Ni,Co)_2S_4$) (discovered on the Viburnum Trend at the Fletcher Mine), bornite (Cu_5FeS_4), bravoite ($(Fe,Ni)S_2$), siegenite $(Ni,Co)_3S_4$, gersdorffite (NiAsS) and chalcocite (Cu_2S). Hydrothermal dolomite and calcite are the most widespread gangue minerals, whereas quartz is only found in isolated locations. Nearly all sulfides were deposited in multiple stages, with some sulfides showing evidence of five or more stages (Gerdemann & Myers, 1972; Craig & Carpenter, 1977; Voss *et al.*, 1989; Hagni, 1995).

Fluids that formed the main stage galena and sphalerite came from the Arkoma basin during the Ouachita Orogeny. They were driven north by fluid compaction up dip and were influenced by topographic relief caused by the uplift of the Ouachita Mountain belt. These fluids rose up through the LaMotte Formation once arriving at the Viburnum Trend. (Gerdemann & Myers, 1972; Goldhaber *et al.*, 1995; Appold & Garven, 1999; Shelton *et al.*, 2009). Some authors have suggested that the source of some of the main stage fluids was the Reelfoot rift and proposed other basins as potential fluid sources, including the Black Warrior Basin (Clendenin & Duane, 1990; Viets & Leach, 1990; Clendenin *et al.*, 1994).

Fluids associated with late stage cubic galena and sphalerite mineralization have trace element signatures which indicate a separate source that did not interact with the underlying LaMotte Formation. These late stage fluids interacted with impure carbonates

rich in organic material, such as shale beds and share geochemical characteristic across several mineral districts, including the Viburnum Trend, the Tri-State area, Central Missouri, and the Upper Mississippi Valley Deposits in Wisconsin. (Viets & Leach, 1990; Viets *et al.*, 1992; Appold & Garven, 1999).

Ore deposition ages have been calculated using both paleo magnetization and Rb-Sr dating along the Viburnum Trend. Paleomagnetic data indicate an ore deposition age of Late Pennsylvanian, while Rb-Sr dating of glauconites indicates ore formation during the Mississippian (Stein & Kish, 1985).

Northwest striking faults, which are dominantly strike-slip, acted as regional conduits and in some cases barriers to ore forming fluids. For main stage Pb-Zn mineralization, they provided a pathway for the fluids flowing from the Arkoma Basin via uplift from the Ouachita mountains which then ascended upwards, leaching Fe, Pb and Zn from the red beds in the underlying LaMotte Formation. In addition, they acted as conduits for late stage Pb-Zn mineralizing fluids which migrated laterally to the area from different basins that share trace element similarities among the Pb and Zn fluids with other regional MVT districts (Clendenin *et al.*, 1989, 1994; Clendenin & Duane, 1990; Goldhaber & Mosier, 1990; Viets & Leach, 1990; Appold & Garven, 1999).

The mechanism of precipitation was fluid mixing between highly saline sulfate fluids and metal rich fluids. Mixing occurred on a timescale of only a couple of hundred thousand years (Appold & Garven, 1999; Shelton *et al.*, 2009). Temperatures during ore deposition varied from 90 to 150 °C, with a pH of 4-5. Based on fluid inclusion work, salinities ranged from 20-30% NaCl (Gerdemann & Myers, 1972; Hagni, 1995). Some parts of the Viburnum

Trend show evidence of much higher temperatures (200-250 °C), though the regional extent of these high temperature fluids is unknown (Cavender, 2015).

Locally, mineralized fluid movement varied depending on proximity to Precambrian knobs and their overall position within the Viburnum Trend. Based on the overall distribution of the ore bodies and analysis of metal zonation patterns, it is likely that ore fluids entered the Viburnum Trend near the Casteel and Buick Mine areas and flowed north and south to the distal parts of the Viburnum Trend. Fluid flow deviated from this pattern in some locations, including Magmont West. (Hagni, 2006).

At the Casteel mine, the fluid flow was complex, and but in most areas flowed to the north and later to the west. At the Fletcher mine, the fluids flowed from the west, where they began to encircle the Precambrian knob. At Sweetwater, the fluids flowed from north to south, and where guided and modified by regional-scale SE-NW faults and Precambrian knobs (Hagni, 2006).

Mineralizing fluids were channeled locally by positions of Precambrian knobs and LaMotte Formation pinch outs as well as localized pinch outs of important dolostone marker beds within the Bonneterre Formation. They were also influenced by general proximity to bleached dense dolostone (locally referred to as “white rock”), sedimentary facies sequences and overall proximity to the limestone-dolomite contact. These units influenced mineralization because of porosity variations connected with the different facies (Gerdemann & Myers, 1972; Hagni, 1995).

2.3 Mineralization Description

2.3.1 District Mineralization

The elongated, relatively narrow part of the Viburnum Trend is due to three major factors: 1) The formation of a regional scale algal barrier reef around topographic highs in the underlying sand influenced heavily by the elevation of the underlying Precambrian highs, 2) the presence of a well-developed back reef, which is distinctive in drill core and is bleach white in color (marking the eastern boundary of the Viburnum Trend) and 3) the presence of a limestone "edge", marking the western boundary of the Viburnum Trend (Gerdemann & Myers, 1972; Larsen, 1977; Leach *et al.*, 2010).

The architecture of the algal reef, while complicated in many areas, generally grew on localized topographic highs of the underlying sand and Precambrian highs. While the Viburnum Trend has multiple, discrete "knobs" which pinched out the sand and are erratically distributed, in general they are highest locally within a forty mile trend where the Viburnum Trend is situated. These "knobs" favored the growth of a complex algal reef facies, which channeled and localized fluids in the area. This reef is impermeable in many areas, but did contain highly permeable channels which are thought to permit mineralizing fluids to work their way upwards (Gerdemann & Myers, 1972; Larsen, 1977; Leach *et al.*, 2010).

The location of the back reef facies marks the eastern edge of the Viburnum Trend. This unit is somewhat porous and is composed of coarsely crystalline dolostone. Dolomitizing processes have obscured most of the original depositional textures of the rock. It is not entirely clear why this zone is not mineralized, but the fact that it generally lacks the

presence of any significant hydrothermal dolomite is an indicator that mineralizing fluids never interacted with this zone. While this zone marks the eastern boundary of the mineralization, it is not a vertically straight boundary, but instead is a highly irregular, complex contact that is still not fully understood (Gerdemann & Myers, 1972; Larsen, 1977; Leach *et al.*, 2010, Schott 2015, Personal Communication, Palmer 2017, Personal Communication).

The western boundary of the Viburnum Trend is marked by the fore-reef zone. This zone is composed of limestone which represents basin ward, deeper water environments. The limestone in this area suggests that little interaction with dolomitizing fluids, some of which likely had a role in ground-preparation, were not available. This section of rocks is distal to the pinch out of the sand and the buried Precambrian knobs, which is likely the main reason why it is not mineralized (Gerdemann & Myers, 1972; Larsen, 1977; Leach *et al.*, 2010, Schott 2015, Personal Communication, Palmer 2017, Personal Communication).

2.3.2 Breccia Mineralization

There are two types of mineralization on the Viburnum Trend: breccia and blanket. Breccia style mineralization is further subdivided into two styles: dissolution and submarine slides. Dissolution breccias are formed by circulating ground waters, which dissolved permeable portions of the rock. This dissolution caused the rocks to collapse at the site of dissolution. These collapsed areas were permeable pathways for successive generations of ore fluids. Submarine slides formed when different sized carbonate particles accumulated on the flanks of Precambrian knobs, before diagenesis and sedimentation. As build-up on the slope of the sediment occurs, the pile eventually collapses. Slide breccias are distinct from

solution collapse features because the mechanism for the creation of the breccia occurred during sedimentation, rather than after. Solution collapse breccias on the other hand are related to post-depositional karst events and are frequently filled with hydrothermal dolomite. Both styles are readily identifiable in drill core and can be inferred using gravity geophysical surveys. In addition, simple contouring of formation elevations often reveals a "slumping" or change in elevation, which is indicative of a breccia zone (Snyder & Odell, 1958; Gerdemann & Myers, 1972; Clendenin, 1991).

Solution collapse breccias generally are more vertically extensive, with down-dropping of beds from the overlying Davis Formation down into the Bonneterre Formation being common. These solution collapse breccias vary, but can reach vertical thickness of one hundred to one hundred fifty feet in certain areas. Slide breccias on the other hand, are limited in their vertical thickness, and rarely reach thicknesses of fifty feet. Regardless of the breccia type, the ore mineralogy of the breccias is primarily galena, though they can have minor amounts of copper if they occur lower in the section. Some breccia zones have sub-economic quantities of zinc. The exact cause of the solution collapse breccias is unknown, but likely they formed from nearby pre-existing weakness in the rock, especially where these weakness intersected each other, including but not limited to faults, fractures, and bedding planes. These zones also contain variable amounts of gangue minerals, including quartz, yellow calcite and hydrothermal dolomite. At the Buick mine, each breccia zone had a distinctive zonation and ore mineralogy. In addition, the authors noted the presence of fractures along the outer boundaries of the breccia zone. This, combined with the known relationship of caves and large vugs with solution collapse breccias in other

deposits, suggests that these had a strong influence on post-lithification karsting, solution-collapse and slide breccias on the Viburnum Trend (Rogers & Davis, 1977; Ohle, 1985).

2.3.3 Blanket Mineralization

Blanket mineralization forms occupy the upper Bonneterre Formation and are composed of stratiform replacement mineralization. Mineralization is partially controlled by the vertical thickness variation of both the gray beds and the gray silt, especially where these units pinch out. Precambrian knobs exert variable control over this zone by forcing ascending mineralizing fluids upwards and by governing the formation of the algal reef zone, which channels these mineralizing fluids into favorable areas. Ore zones are horizontal to sub-horizontal and occur as layers, which range from 1 to 5 ft. in vertical thickness. Galena and sphalerite are the most common minerals within these zones, with minor or trace chalcopyrite and bornite. Faults and fractures acted as both conduits and barriers for mineralizing fluids within this zone (Gerdemann & Myers, 1972; Clendenin, 1991, 1993).

Localized "flower" structures associated with strike-slip faults have been identified as an important mineralizing control within the blanket zones. Underground mapping and field relationships indicate that northwest striking horizontal braided bands of sphalerite and galena mineralization, which are directly related to northwest striking faults, are an important control on mineralization. These braided mineralized bands are difficult to identify because while they are related to regional faulting, they are usually separated from the faults by 150-180 ft. of unmineralized rock. In addition, they usually overprint younger unrelated, syn-sedimentary slide breccias (which can also be mineralized), and themselves

are overprinted and offset by even later strike-slip and normal faults. While major regional scale faults are unmineralized and therefore not related to these structures, small-scale, pre-mineralization strike-slip faults are directly related to these mineralized, horizontal braided mineralized bands. While detailed study of these braided mineralized bands was completed at the Sweetwater Mine, similar structures have been identified and reported at the No. 29, Buick and Casteel Mines (Dunn & Grundmann, 1989; Clendenin, 1993). Figure 2.8 shows a diagrammatic representation of these structures.

Figure 2.8: Horizontal Braided Band Structure (Clendenin, 1993).
This is part of a localized "flower structure" with mineralization occurring above the down thrown side of the left-lateral strike-slip fault. Numbers in center of diagram refer to different generations of splay structures. 1 = oldest, 4 = youngest

Blanket mineralization shares some characteristics with controls on breccia mineralization. These commonalities include: relative proximity to Precambrian knobs and the fact that

these zones are so often found very close to each (often directly adjacent or separated by 1,000 to 2,000 ft. of unmineralized rock) (Gerdemann & Myers, 1972; Clendenin, 1991; Leach *et al.*, 2010).

2.3.3.1 Stratiform Replacement Zone

A sub-type of blanket mineralization, is a separate classification called the Stratiform Replacement Zone (SRZ). This zone shares most of the geologic features and controls on mineralization as the blanket zone, but is distinguished by higher concentrations of sphalerite than blanket areas and contains sphalerite rich layers which replace sections of the host dolostone. The Stratiform Replacement Zone is strongly influenced by certain early faulting and fracturing, is vuggy and has a strong association with bitumen and organic matter. Discrete, narrow (50 – 100 ft.) sections of dolostone that are tilted up to 15 degrees are strongly associated with these zones. Sphalerite rich bands show an association with the downdip, most distal parts of the blanket zones and tend to concentrate above dark shale bands, in bedding planes and within permeable sections of dolostone (Mouat & Clendenin, 1977; Clendenin, 1993; Niewendorp & Clendenin, 1993).

The SRZ varies in vertical thickness, horizontal width and strike length throughout different parts of the Viburnum Trend. While its general location is known, the full extents of this zone have never been mapped or fully delineated by drilling.

2.3.4 Stratiform Replacement Zone Mineralization

The following descriptions describe mineralization within the Blanket and Stratiform Replacement Zones at each mine, and do not include descriptions of breccias or other mineralization types.

2.3.4.1 Casteel Mine

The main mining portion of the Bonneterre Formation is made up of a significant amount of reef and oolitic dolomite. Gray beds are located in between the oolitic dolomite zones; these are a gray and gray/tan dense microcrystalline mottled dolomite with irregular thin shale beds. This unit is usually 14 feet thick at Casteel, but can be as thin as 2 ft. The reef varies in thickness from 0 to over 100 ft. near the mine. Locally, bleached sections are found below the gray beds in the underlying reef in the eastern section of the mine, generally in the vicinity of the SRZ (Dunn & Grundmann, 1989).

The mineralization that comprises the Stratiform Replacement Zone at Casteel is approximately 2,000 ft. east of the main breccia zones. It has a mottled appearance, with an abundance of small, hydrothermal dolomite veinlets which infill vugs, faults and fractures and has mineralization that is dominated by galena and sphalerite. The width of the main ore trend in these areas is variable, with horizontal widths from 30 to 1,000 ft. (Koob, 2014).

North Casteel contains the highest density of fractures and faults along the Viburnum Trend. Mineralization in the SRZ is controlled by three main geologic features (Koob, 2014):

1. Variable geometry of the top of the digitate stromatolite reef zone

2. Thinning of the gray bed unit

3. Fractures & Faults

Fracture sets have a variety of directions. The fracture sets are multi-generational and can be difficult to trace. According to Dunn & Grundmann (1989) in certain parts of the Casteel mine, fault and fracture networks control the intensity of mineralization, and some are filled with ore. While there are numerous fracture sets at Casteel, most of them are unrelated to mineralization. Generally, only specific fractures with an azimuth ranging from 345 to 015 degrees which are sub vertical and have evidence of gangue or sulfide mineralization are related to mineralization (Dunn & Grundmann, 1989).

2.3.4.2 Buick Mine

The Buick Mine, much like the Casteel Mine directly to the North, has a substantial breccia trend with multiple levels and a pronounced parallel trend where the SRZ is situated. It is located 1,500 ft. to the east of the main breccia trend and is separated by barren dolostone. The mineralization is approximately 700 ft. wide and 6,500 ft. long, and ranges from 10 to 20 ft. in vertical thickness. This is considerably smaller than the main breccia trend and is relatively well defined due to the dense drilling (Rogers & Davis, 1977).

The LaMotte Formation underneath Buick contains minor amounts of bitumen, along with trace zinc, copper and lead sulfides. A pronounced high in the elevation of the top of the LaMotte Formation occurs underneath most of the mine workings and is approximately 800 ft. wide and 30 ft. tall (Rogers & Davis, 1977).

Mineralization stair-steps upwards and follows the undulating surface of the top of the reef. This stair-step pattern reflects the increase in elevation of the underlying Precambrian topography and creates a vertical mineral zonation, with galena on top, sphalerite on the bottom and chalcopyrite on the flanks of the mineralization (Rogers & Davis, 1977).

2.3.4.3 Fletcher Mine

The mineralization at Fletcher is located in close proximity to a buried uplifted portion of the Precambrian which dramatically affected facies patterns during the Upper Cambrian. Once the underlying LaMotte sand was deposited, local highs caused by the underlying surface of the Precambrian became the site of large networks of algal reefs. This reef complex caused different carbonate environments to form, including offshore, reef and open marine environments (Paarlberg & Evans, 1977).

Mineralization follows a pronounced north-south trend with horizontal sphalerite and galena bands closely surrounding the underlying Precambrian ridge. In addition to facies control, mineralization follows certain early stage fractures and breccia structures (Paarlberg & Evans, 1977).

The mineralization at Fletcher averages 1,000 ft. long, 300 ft. wide and 20 ft. thick. The mineralization conforms to the changing strike and dip of the beds as they drape over the Precambrian knob. Sphalerite replaces dolomite beds and is associated with minor galena mineralization (Paarlberg & Evans, 1977).

2.3.4.4 Sweetwater Mine

The Sweetwater mine extends over a total length of 7.2 miles. The mine is cut by two faults, the Suses Branch Fault and Sweetwater Fault. Both faults show evidence of both normal and strike-slip movement (Clendenin, 1991).

The Suses Branch Fault is located several thousand feet to the south of the main mine workings. It is a west-northwest striking, vertical normal fault with vertical displacement of 40 ft. The main development drift which connects the northern and southern portions of the mine cuts this fault. Over 90% of the mineralization within the South Mine is located within the Middle Bonneterre Formation, within a porous brown oolitic grainstone with local inter bedded burrowed mottled wackestones. The orebody is constrained at the top by the False Davis (Walker, 1977).

Mineralization is widespread and is contained with a specific horizon of mottled dolostone. This unit is more permeable than other units above and below it and contains abundant hydrothermal dolomite veinlets and vugs. Bedding plane shear fractures are common, as are East-West fractures. Some faulting is pre-ore, with mineralization filling fault planes (Walker, 1977).

Mineralization is relatively continuous and extends for several miles with zones that range from 1,000 to 3,000 ft. long, 800 ft. in width and 10-15 ft. in height. Both structural and stratigraphic controls affect the distribution and grade of mineralization. Mineralization has been localized along the flanks of buried Precambrian highs or stromatolitic mounds in the reef (Mouat & Clendenin, 1977).

Chapter 3: **Methodology**

3.1 Sampling

Samples were taken from underground exposures on multiple sampling campaigns from September 30th, 2015 to January 12th, 2016. Each mine was sampled within the Stratiform Replacement Zone in the Upper Bonneterre Formation and was restricted to the oolitic grainstone lithology. A total of 32 samples were collected from underground and drill core for bulk carbon and oxygen isotope and SIMS analysis and for polished thin section examination. All available stopes within the SRZ were sampled. Some areas were not accessible due to active mining activities or flooding.

In addition a total of 24 samples were taken from drill cores associated with the SRZ at each mine targeted for underground sampling. The overall objective for the drill core sampling was to obtain samples at progressively greater distances from each underground area to evaluate the potential for a trend in oxygen or carbon isotopes, which could be related to the mineralization.

Drill core sampling criteria were:

- Samples had to be completely unmineralized
- Samples had to be from the same stratigraphic horizon as subsurface samples (as determined by geologic logs)
- Samples had to be within the same approximate elevation as underground samples (+/- 30 ft.)

- Samples had to be taken from progressively greater distances from the mine workings at any direction
- Samples could not be within 1,000 ft. of any known mineralized occurrence (other than mine workings)

During the drill core sampling campaign, an emphasis was placed on strictly sampling drill cores which were completely barren of mineralization. This was done so that the results would be representative of a real-world application of stable isotopes to an exploration campaign.

In total, 56 samples were taken from 5 areas of the SRZ along the Viburnum Trend, all of which are hosted within the same stratigraphic horizon. Figure 3.1 shows the sample locations for underground and drill hole samples within the Stratiform Replacement Zone. More detailed maps showing sample locations and stable isotope results within each project area are included in Section 4.4.1.3 on pages 113 - 117.

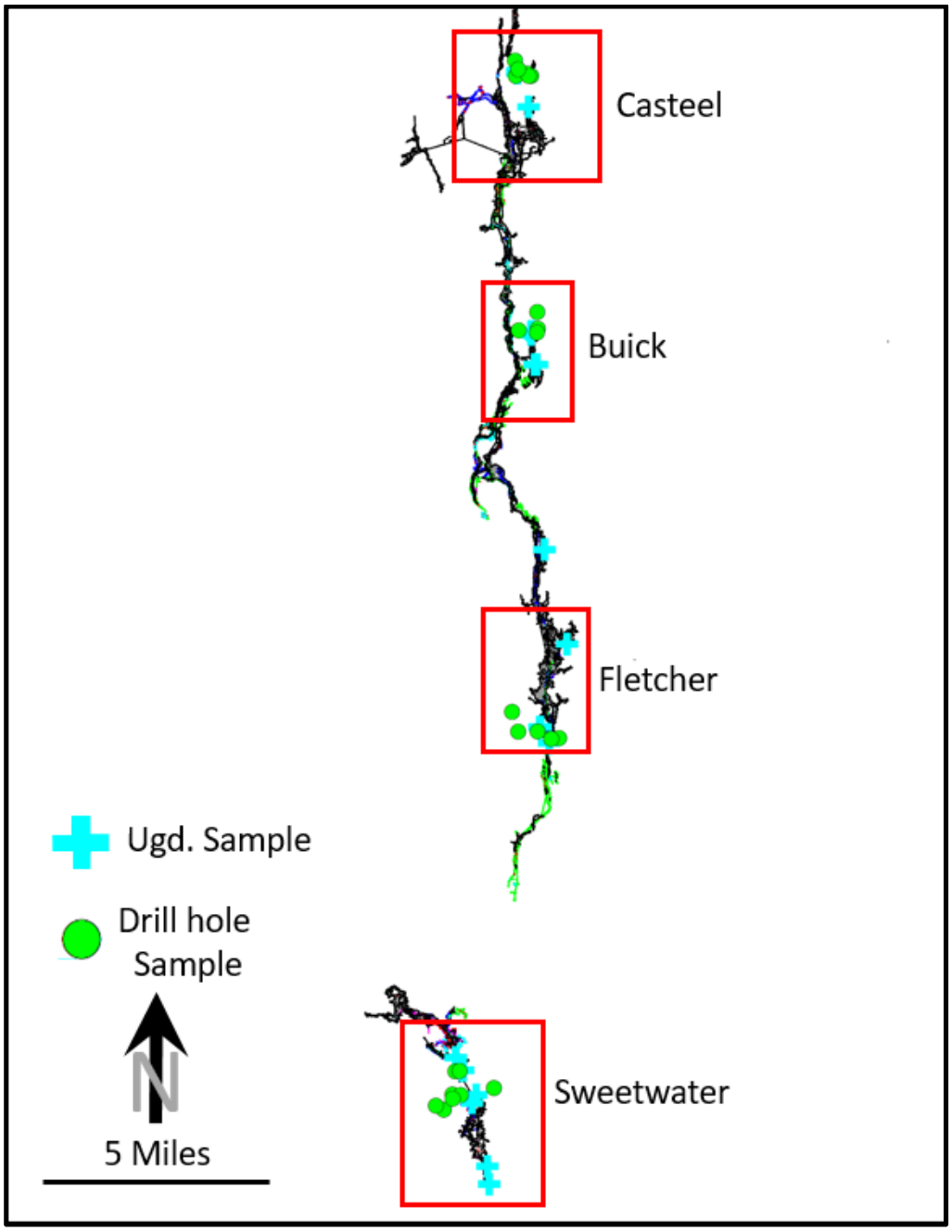

Figure 3.1: Sample location map for the Stratiform Replacement Zone.

3.2 Optical Microscopy

All samples were examined using transmitted and reflected microscopy with a Nikon Eclipse 50i POL polarizing microscope to determine the overall gangue and sulfide paragenesis. Attention was given to the relationship between sphalerite and galena as well as its relationship to the hydrothermal dolomite cements. Reflected and transmitted microscopy was used to identify areas for scanning electron microscopy (SEM), cathodoluminescence, electron microprobe (EM) and secondary ion mass spectrometry (SIMS). Images of samples were collected using Nikon NIS Elements F 3.0 software.

3.3 Scanning Electron Microscopy (SEM)

Selected samples were analyzed on an FEI Inspect S50 SEM. The SEM is computer controlled and contains a backscatter electron detector and an energy dispersive x-ray spectrometer, which permitted semi-quantitative elemental analysis. Samples were carbon coated to ensure conductivity during analysis and were placed under vacuum. The SEM was used to identify textures, definitively identify select sulfide and gangue minerals and was also used to identify additional areas for further analysis with the electron microprobe and SIMS.

3.4 Cathodoluminescence

Selected samples were analyzed with cathodoluminescence to refine the relationship between sphalerite and the distinct hydrothermal dolomite cements described by Voss *et al.*,(1989). Analysis was completed using a Nikon optical microscope with a technosyn cold cathode luminescence model 8200 Mk II, with both 5x and 10x objectives used for analysis.

3.5 Electron Microprobe

Selected sphalerite rich samples were analyzed with a Cameca SX100 Microprobe with five wavelength spectrometers and a Princeton Gamma-Tech (PGT) energy dispersive spectrometer. Analysis of 20 elements in sphalerite was carried out using a beam size of 20 nA and a 15 keV acceleration voltage. These elements were Mn, Fe, Cu, Cd, In, Sb, Ag, Sn, Pb, Bi, Cu, Zn, As, Ge, Se, Mg, Co, Ni, Hg, and Ga. Compositional data for these elements from sphalerites exclusively was obtained using the microprobe. Detection limits which were <750 ppm include Mn, Fe, Cd, In, Sb, Ag, Ge, Mg, Co, Ni, S and Sn, while detection limits for elements were <1,500 ppm include Bi, Cu, As, Hg, and detection limits for elements were < 2,500 ppm for Zn, Se and Hg. Standards used in the final microprobe analysis are listed in Appendix B.

3.6 Carbon & Oxygen Isotope Analysis – Gas Source Mass Spectrometry

To prepare samples for analysis using gas source mass spectrometry, all 56 samples from underground and drill core were micro drilled. Some samples were micro drilled with a Foredom Model TXH Micro drill press with drill bit sizes that ranged from 0.5 to 0.9 mm in diameter. Due to mechanical issues with the micro drill press, a Dremel electric tool was used for the majority of the samples. A 1.2 mm tungsten carbide drill bit was utilized in the Dremel Tool. During sampling, acetone was utilized to thoroughly clean the drill bit and the immediate work area in between each sample to eliminate contamination.

Each powdered sample, which ranged from 10-20 mg in weight, was placed in a small plastic vial. This amount of material allowed for multiple sample runs during analysis with the gas spectrometry. Nearly all samples were dolomite or ferroan dolomite. The samples

were extracted from host dolostone in all samples and from dolomite veinlets when available.

For analysis, an aliquot of powdered sample was weighed out onto a small piece of weigh paper. The weighed sample was then transferred into a specialized borosilicate vial which was kept at a consistent temperature of 70 °C. This vial has a lid which is connected to a He gas source and was flushed for 10 minutes. After flushing is completed, anhydrous phosphoric acid was added by hand to each borosilicate vial and left to react for approximately 4 hours in a Thermo Finnigan GasBench II.

The CO_2 gas generated by the reaction of the dolomite with the phosphoric acid was analyzed by a Delta V plus Isotope Analyzer. Isotope data are reported in parts per mil (‰) relative to VPDB (*Vienna Peedee Belemnite*) for $\delta^{13}C$ and VSMOW (*Vienna Standard Mean Ocean Water*) for $\delta^{18}O$. δ is defined as:

$$\delta_X = \left(\frac{R_X - R_{std}}{R_{std}} - 1\right) \times 1000 \quad [1]$$

where

$$R_x = (C^{13}/C^{12})_X \text{ or } (O^{18}/O^{16}) \quad [2]$$

for the sample and R_{std} is the isotope ratio of the reference standard.

Two international standards, NBS18 and NBS19, were analyzed at the beginning, middle and end of each sample run to calibrate the instrument. A least squares regression line was calculated by plotting the known and measured isotope values of the international calibration standards. To verify analysis performance on the dolomite samples, isotopic

values of a Tytri Dolomite sample were analyzed. This dolomite standard has the following values:

$\delta^{13}C$ = +0.78±0.01‰ VPDB

$\delta^{18}O$ = +7.07±0.04‰ VSMOW

This Tytri Dolomite standard was analyzed as an unknown, and the difference in oxygen isotope values, which were measured against the international standards were used to correct the oxygen isotope values. The analytical errors for the analysis are as follows:

- $\delta^{13}C$: ≤ ±0.1‰
- $\delta^{18}O$: ≤ ±0.2‰

Out of a total of 115 micro drilled samples that were analyzed, 33 (28.6%) did not contain enough dolomite or had too much iron within the dolomite for an accurate analysis. These samples were removed from the dataset.

An attempt was made to sample the different dolomite cement zones described by Voss *et al.*(1989) using the micro drill. The drill bits currently available, however make it challenging to separate each dolomite cement zone. Figure 3.2 shows typical dolomite cements found within the SRZ with a diameter of a small micro drill bit drawn to scale (blue circle) on the figure for comparison. To isolate any of the distinct isotopic signatures of these cement zones with a micro drill would be impossible.

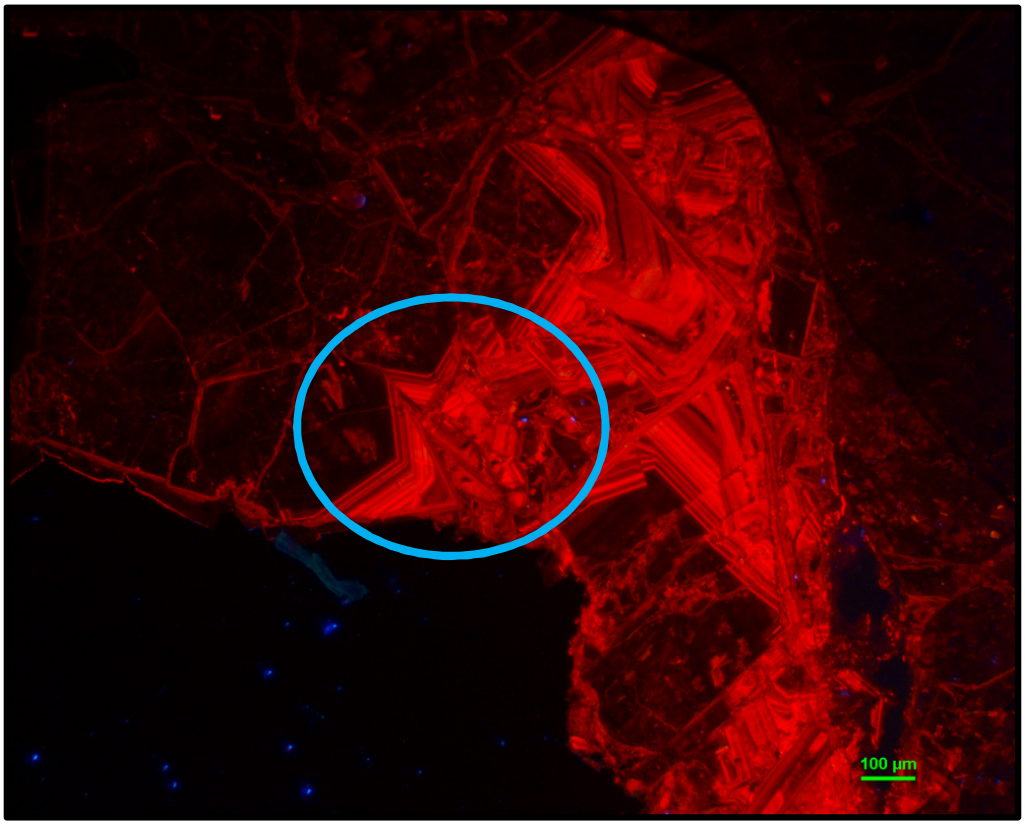

Figure 3.2: Example of typical dolomite cement with CL Zoning (sample Sweetwater 04, Sweetwater mine).
Blue circle represents the size of the smallest drill bits that can be used to sample for carbon and oxygen isotope analysis (0.5 mm).

3.7 In Situ Secondary Ion Mass Spectrometry

Sample analysis by secondary ion mass spectrometry (SIMS) was completed on a CAMECA IMS 7f secondary ion mass spectrometer. To prepare samples for SIMS, polished thin sections were cut into circular 1 inch diameter round samples around the points of interest which were previously selected by petrography, SEM and microprobe. The samples were then taken through a series of cleaning stages to remove the carbon coating from SEM and microprobe study, as well as provide a good surface for the later coating process required for SIMS.

First, a diamond polishing compound was utilized to remove the carbon coating. The sample was then cleaned with a multi-stage process in an ultrasonic cleaner, first with a dilute dish soap solution, then distilled water and finally with ethanol. Each sample spent approximately 15 minutes in each solution in the ultrasonic cleaner. After cleaning, the cut and cleaned samples were coated with a thin layer of gold to ensure a conductive surface during the analysis. Samples were placed into a vacuum chamber and let sit until the needed vacuum was achieved (5-10 minutes).

During SIMS analysis, isotopes are fractionated by the instrument, which is known as instrumental mass-fractionation (IMF). The most important factors that contribute to IMF are preferential ionization of the lighter isotopes and the composition of the sample, commonly referred to as a "matrix effect". To correct for both the IMF and matrix effect, standards that have a similar matrix (e.g., calcite) to the unknown sample are analyzed during the same session as the unknown samples. The correction factor calculated from the chemically similar standard during the same analytical session is then applied to the samples being analyzed, (Riciputi *et al.*, 1998; Fayek *et al.*, 2002).

The equation used to correct for IMF during SIMS is:

$$\alpha_{SIMS}=R_{SIMS}/R_{STD} \quad [3]$$

R is the measured isotopic ratio (e.g., $^{34}S/^{32}S$), while R_{SIMS} refers to the unknown sample being analyzed, and R_{STD} refers to the standard value. To determine the true isotopic ratios, the equation below is used:

$$R_{True} = \alpha * R_{SIMS} \quad [4]$$

Sulfur and oxygen isotopes in sphalerite and dolomite, respectively, were analyzed during different sessions using similar conditions. To obtain an analysis by SIMS for sulfur and oxygen isotopes, a primary beam of cesium ions with a current of 3nA for oxygen and 2nA for sulfur were accelerated at 10kv onto the sample surface with a sputtering diameter of ~20 μm. The instrument operated at a 300V offset and a negative secondary voltage of -8.7 kV with a mass resolving power of 347. An e-gun was used for charge compensation for the oxygen isotope analysis. Typical analyses lasted 10 minutes for oxygen, with 70 cycles, while sulfur only took 7 minutes with 50 cycles.

For the analysis of sphalerite, the Balmat sphalerite standard was used, which has a $\delta^{34}S$ value of 14.3 ± 0.3 ‰. Spot to spot reproducibility (1σ) for sphalerite was 0.3 ‰. For oxygen isotopes within dolomite, a calcite standard was used with a $\delta^{18}O$ value of 5.7 ± 0.6 ‰. Spot to spot reproducibility (1σ) was 1.2 ‰.

For the analysis of dolomite, the average oxygen isotope value determined by Gas Source Mass Spectrometry was used to standardize the SIMS values for each sample. This method was used because there were significant variations in iron content within the different dolomite samples. Small (< 1 wt. %) quantities of iron within a dolomite crystal can significantly affect the accuracy of the analysis during SIMS (Claire & Carbonne, 2011).

For a thorough discussion of SIMS instrument operating conditions during oxygen isotope analysis, see Fayek *et al.*, (2002) and Riciputi *et al.*, (1998) for sulfur isotope analysis operating conditions. Isotope data for sulfur and oxygen are expressed in δ notation in units of per mil (‰) relative to VSMOW for oxygen isotopes and Cañon Diablo Troilite (CDT) for sulfur isotopes.

Oxygen analysis by SIMS was completed on selected hydrothermal dolomite cements. However, differentiating the precise regionally correlatable cements (e.g. Type 1 vs Type 4) was not possible. This is because the SIMS navigation window does not have cathodoluminescence, which is required to be able to definitively identify the specific dolomite cement types during analysis.

Chapter 4: **Results**

4.1 Paragenesis

Petrography was completed on all 56 samples, with an emphasis on the relationship between sphalerite, other sulfides and hydrothermal dolomite cements for underground samples. For drill core samples, the focus was on studying the hydrothermal dolomite generations present. The paragenesis was determined by a combination of thin section petrography, CL petrography and SEM. Textures and relationships for minerals were compared with petrographic reference guides which provided representative mineral photographs and general guides on identification and interpretations of textures. These petrographic reference guides include the following: (Ramdohr, 1969; Barton, 1970; Craig & Vaughan, 1994; Craig, 2001). Electron microprobe and sulfur isotope work was completed on selected sphalerite samples for comparison to previous microprobe, trace element and sulfur isotope work on sphalerites. This was completed to further constrain the relationship of the sphalerite compared with previous studies. Figure 4.1 shows the mineral paragenesis for the SRZ, including important gangue minerals and sulfides.

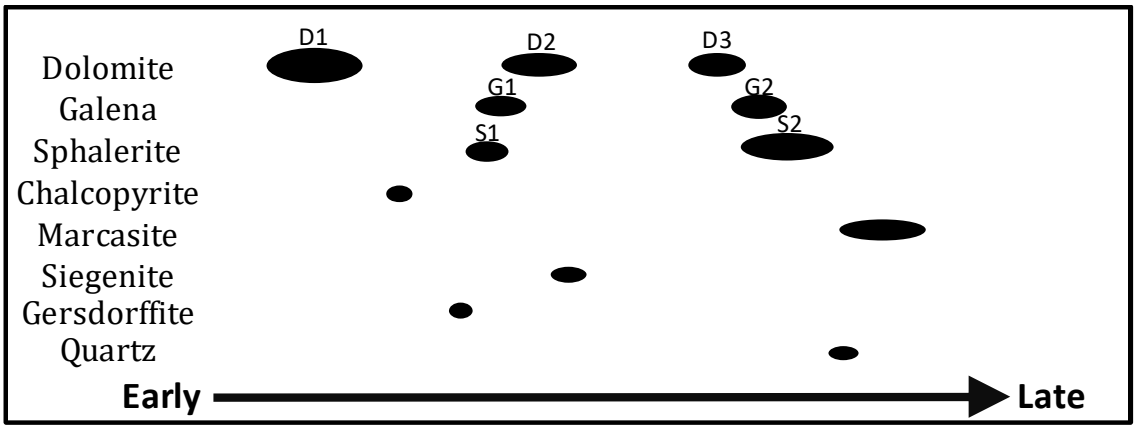

Figure 4.1: Mineral paragenesis for the Stratiform Replacement Zone.
Length of ovals indicates relative duration of mineral occurrence or event, while oval width indicates relative abundance of mineral. Abbreviations: D1 = host dolomite, D2 = recrystallized dolomite, D3 = recrystallized dolomite in vugs and veinlets, G1 = early stage galena, G2 = late stage galena, S1 = early stage sphalerite and S2 = late stage sphalerite.

4.2 Stratiform Replacement Zone Geology

Limited mapping and descriptions of mine faces were done underground during several mapping trips from February 18th, 2016 through August 16th, 2016. The objective was to place the samples in as much geologic context as possible and to better understand the structural geology. In most areas, mapping quality and detail was severely limited by a thick covering of dust on the faces. Where possible, pillars and faces were cleaned to expose the geology. Some stopes where samples had been originally taken in Fall 2015 were not available for mapping due to flooding or production activities.

4.2.1 Casteel Mapping

The northern part of Casteel which was analyzed as part of this study is heavily faulted and fractured, with multiple generations of movement. Some of the faults are normal, while others are strike-slip. The faulting is multi-generational, with some faulting showing evidence for activation prior to mineralization, while other faults postdate the mineralization and displace it. The Black Fault, which strikes NW, is located approximately 600 ft. to the SW of the mapped stopes. It is the largest and most important fault in the area, with multiple fault splays having been identified. Only one stope from the two which were originally sampled was available for mapping due to production related activities. Figure 4.2 shows the location of the mapped stope and the approximate extents of the Stratiform Replacement Zone compared with the rest of the Casteel and the Viburnum Trend.

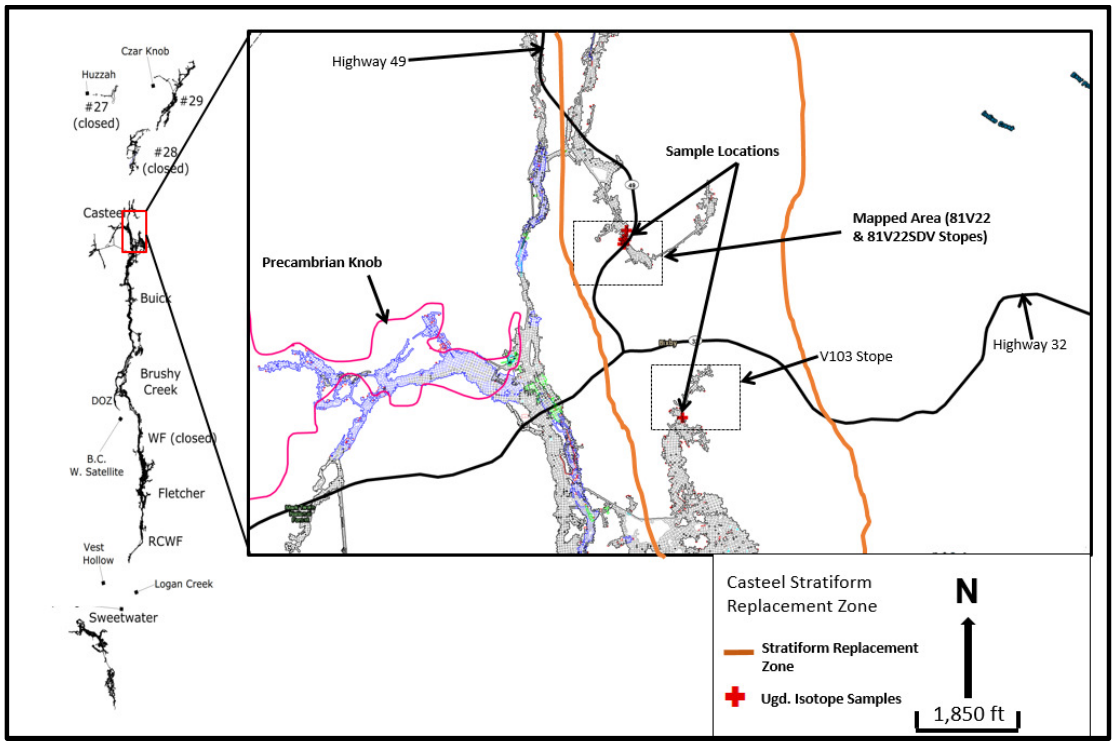

Figure 4.2: Casteel Stratiform Replacement Zone & Study Areas.

Mapping in the 81V22 and 81V22SDV stopes, shown in Figure 4.3 and Figure 4.4 has confirmed that faulting and fracturing are intense. The faulting consists of NE striking, near vertically dipping faults with evidence for normal and strike-slip movement. Slickensides were identified on several of the fault surfaces, and one of the fault surfaces contains idiotopic hydrothermal dolomite growth on the fault place along with marcasite. Two pronounced north striking vertical fractures cut through the stope. Mottled bedding is variable and occurred in the upper 2/3 of the stope, with tight crystalline dolostone present in the rest of the stope. Sphalerite in vugs from this zone contain a complex intergrowth relationship with subhedral to euhedral quartz. In addition, etching of several samples within this area was observed. The pre-mineralization fault zone occurs as dense

swarm of NE striking structures which are splays from the main feeder fault shown in Figure 4.6.

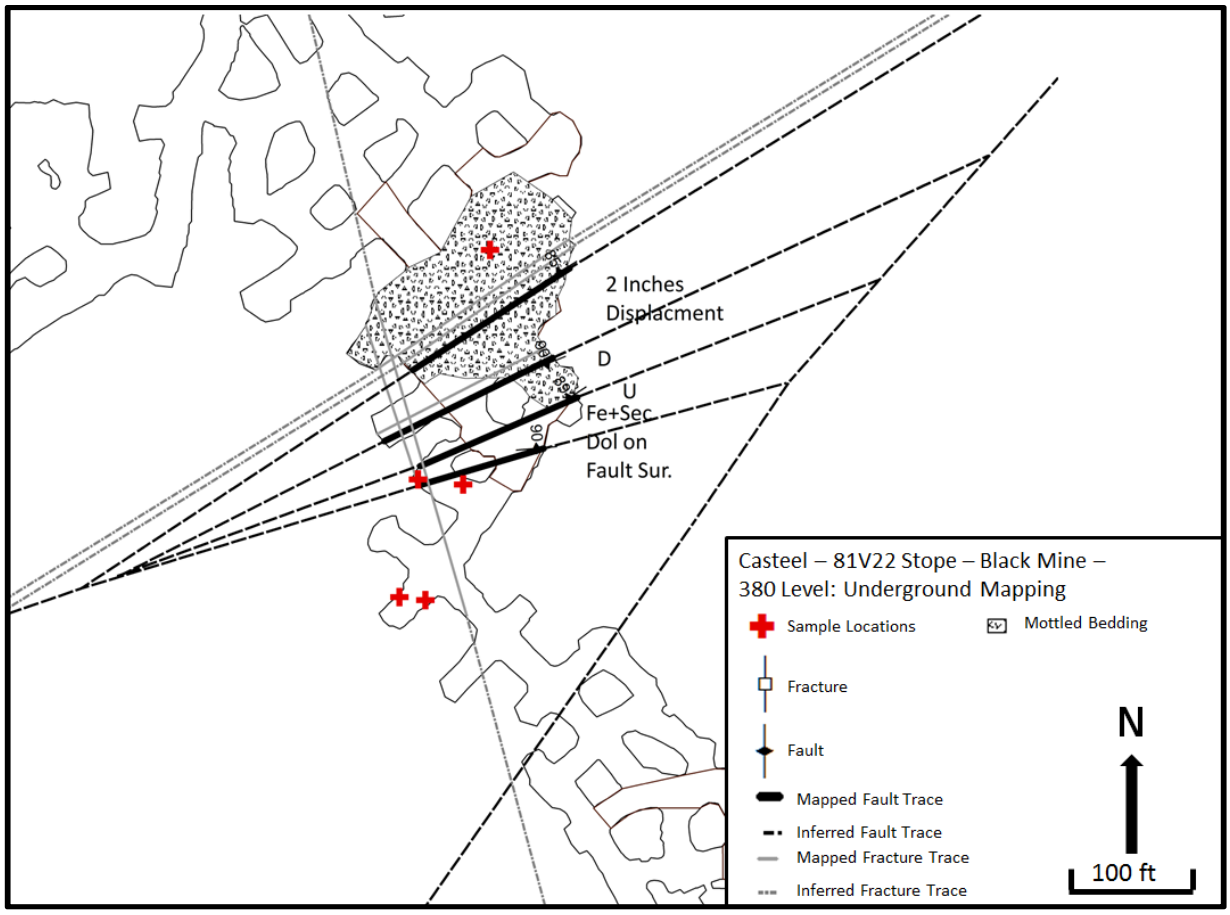

Figure 4.3: 81V22 Stope Mapping.

The 81V22SDV stope, which is situated to the South of the 81V22 stope contains abundant faulting and fracturing. The faulting in this area is even more intense, with some faulting vertically offsetting horizontal galena and sphalerite bands in the face. Slickensides indicate both normal and strike slip faulting was present in this stope. Strike slip movement is indicated on the fault projecting to the NE by visible slickensides. This fault offsets sphalerite and galena bands in this stope and cuts off sphalerite mineralization in adjacent stopes (not shown) to the east of this zone (Figure 4.4).

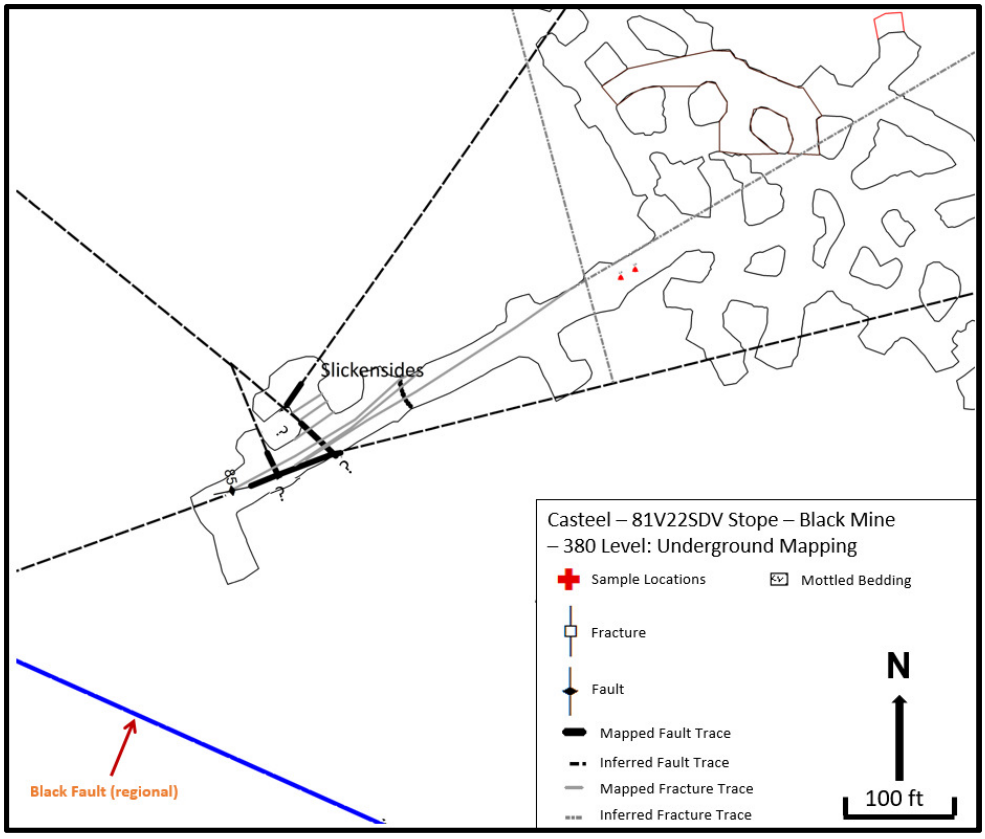

Figure 4.4: 81V22SDV Stope Mapping.

Stratiform replacement mineralization is generally horizontal or gently dipping (2-3 deg), with the mineralized sphalerite bed bounded on top and below by less porous, finely crystalline dolostone beds. The mineralized bed is usually "mottled" in appearance from the increased frequency of vugs, hydrothermal dolomite veinlets and other secondary porosity (Figure 4.5). The bedding can steepen to upwards of 10-12 degrees locally, but this generally does not persist for more than a few hundred feet along strike.

Figure 4.5: Casteel Stratiform Replacement Mineralization – 81V22SDV Stope

Figure 4.6 shows one of the faults underground which controls the sphalerite mineralization in this area, with mineralized rock (left side of photo) being cut by the fault, with barren dolostone on the other side (right side of photo). This is one of several N-NE striking faults that were identified as pre-mineralization and contains hydrothermal dolomite and marcasite growth on the fault surface.

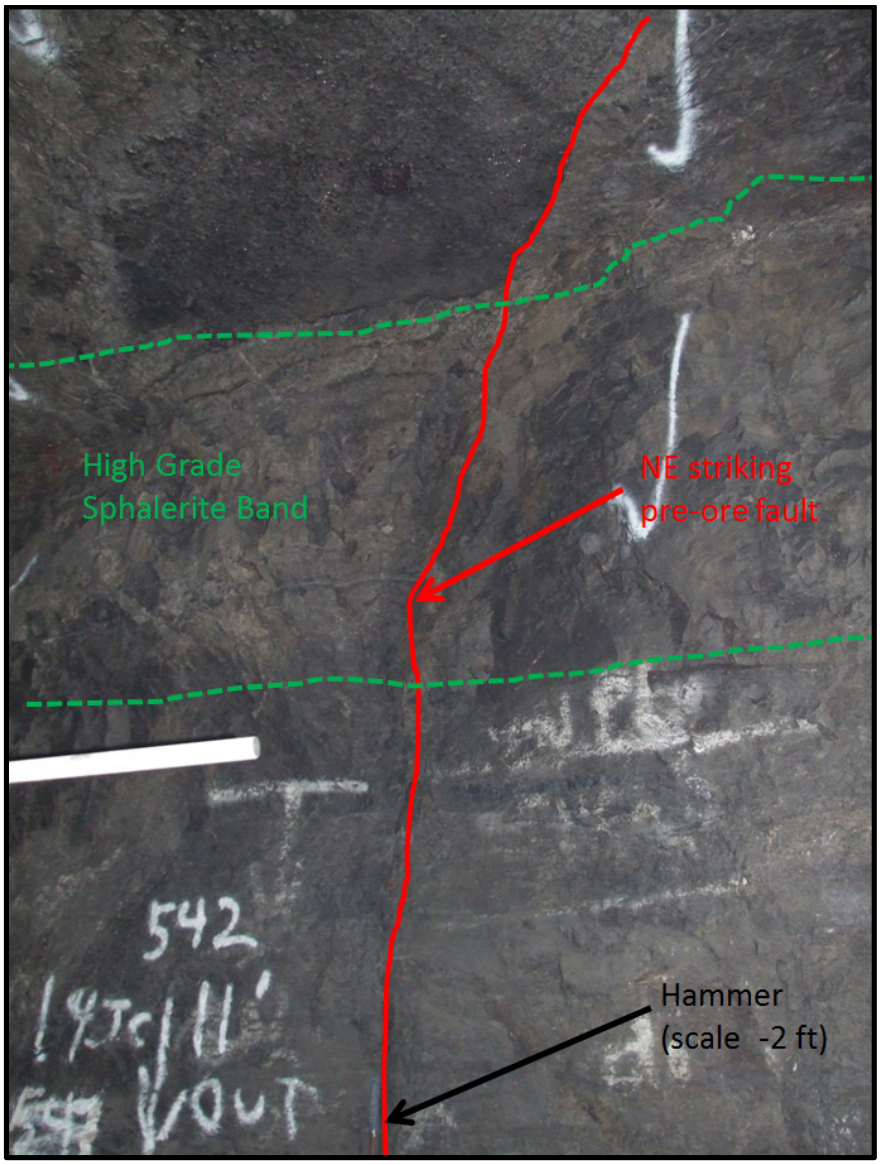

Figure 4.6: Casteel Stratiform Replacement Zone -81V22 Stope – Pre-Mineralization Faulting – 81V22 Stope.

Mapping and geologic observations from this part of the SRZ at Casteel has confirmed that the intensity and distribution of sphalerite is strongly controlled by the following features:

- Specific early stage faults & fractures

- Facies changes within the stratigraphically lower reef complex (not seen in stope or photos)
- Local porosity variations within the host dolostone horizon (potentially related to faulting)

4.2.2 Buick Mapping

The Buick Mine has a substantial breccia trend with multiple levels and a pronounced "parallel trend" to the East. This parallel trend is the location of the SRZ and contains strong sphalerite and galena bands replacing dolostone. It is situated 1,500 ft. to the east of the main breccia trend and is separated by barren dolostone in between the two zones. The zone is approximately 700 ft. wide and 6,500 ft. long. This is smaller than the main breccia trend, but is relatively well defined due to the dense drilling.

The first area mapped (93DRV stope) is located 324 ft. directly north of a major Precambrian knob. The second area mapped (A11 SE) is situated directly above a Precambrian knob and LaMotte Formation pinch out (Figure 4.7).

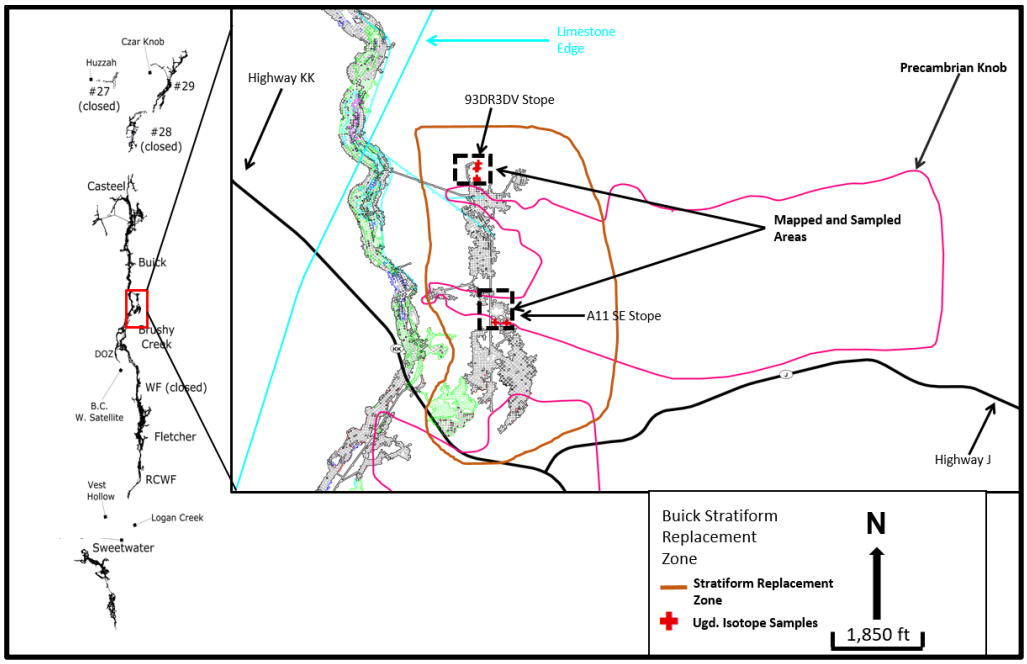

Figure 4.7: Buick Stratiform Replacement Zone & Study Areas

Underground mapping was completed in two stopes in the SRZ at Buick. Mapping in the A11 SE, shown in Figure 4.8 reveals strong fracture-faulting, though not as intense as Casteel. Mottled bedding is spatially related to a major N-NE striking fault and associated fractures, all with vertical dips. The distribution of sphalerite is erratic, with substantial overlap with the galena zone. The northern-most fault is associated with the highest grade sphalerite values, as well as mottled bedding. Bedding dips to the NE away from the Precambrian knob from 9 to 12 degrees.

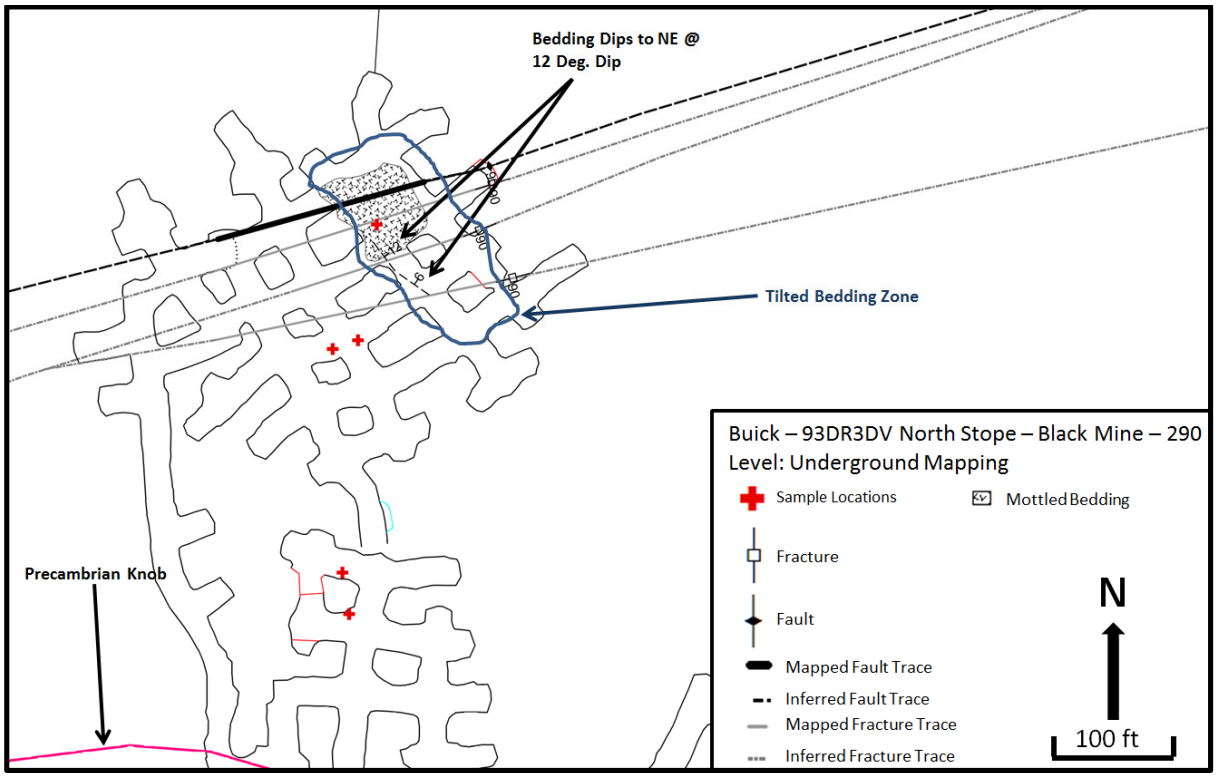

Figure 4.8: Buick Stratiform Replacement Zone– 93DR3DV Stope- Underground Mapping

Figure 4.9 shows mapping in the A11SE stope (3,700 ft. south) and a similar pattern to the geology in the 93DR3DV stope. In this area, no pinch outs or contacts of the gray beds, white rock or mottled bedding were identifiable in the stope. Fractures, however, were prominent and all were steeply dipping. Bedding is clearly defined, with strong undulation present. Overall, the rocks had a similar dip to the rocks from the stope to the north. This stope contains a discrete tilted bedding zone which forms a northwest boundary to the sphalerite mineralization. Abundant etching of samples was observed throughout the stope.

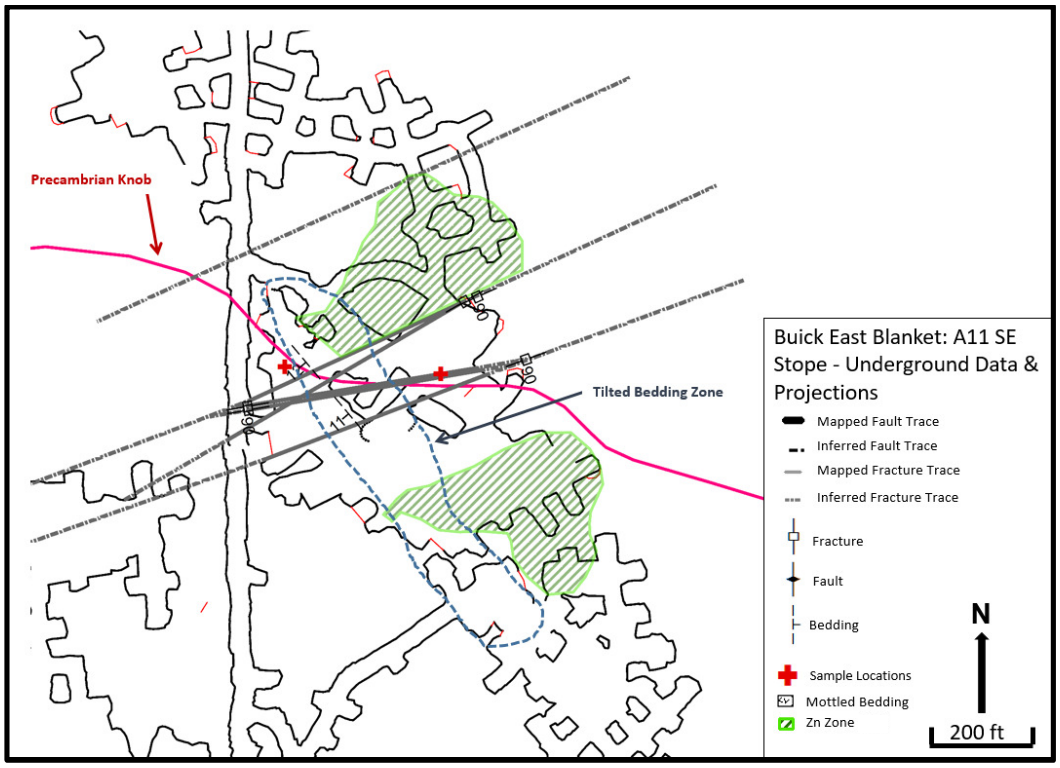

Figure 4.9: Buick Stratiform Replacement Zone – A11 SE Stope – Underground Mapping

The photographs shown below are from the Buick A11 stope and show brown sphalerite in bands on top of galena as well as sphalerite growing in vugs around galena (Figure 4.10). This location contains a high density of vugs which are situated within the tilted bedding zone. This zone contained a dark black shale bed (6" thick) directly beneath the bands of sphalerite and galena, and the stope was heavily fractured.

Figure 4.10: Buick A11 Stope: Sphalerite & Galena Bands in Fractured and Tilted Beds.

4.2.3 Fletcher Mapping

Mapping and underground sample collection took place in two stopes from Fletcher, one at the north end of the mine and one at the south end of the mine. The north end of the mine (99BC5 stope) was mapped and studied to better understand mineralization, but no samples were available from nearby drill cores for isotope geochemical sampling. The second location, in the south end of the mine (J3UC stope) was sampled for isotope geochemical analysis.

4.2.3.1 99BC5 Stope

Figure 4.11 shows the location of the studied and mapped stope along with the approximate extents of the SRZ. This part of the SRZ is unusual because it is distal from Precambrian knobs.

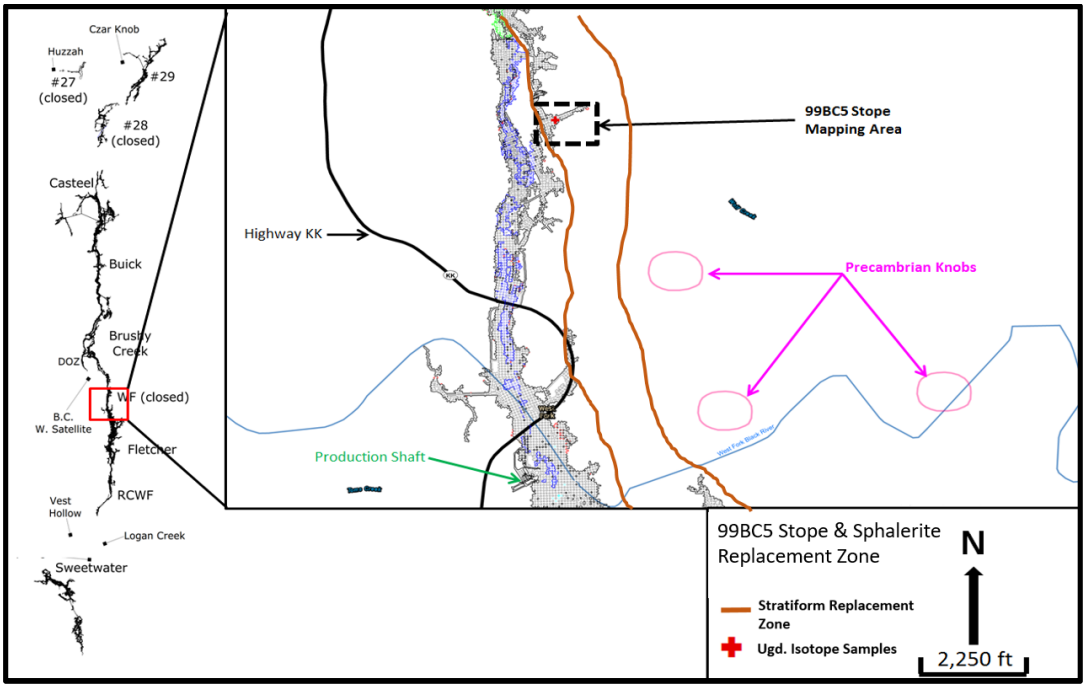

Figure 4.11: Fletcher – 99BC5 Stope

Mapping was completed in most of the 99BC5 stope. Some of the stope, however, was not available due production related activities. Mapping shown in Figure 4.12 reveals a complex network of fractures and faults, some of which formed conjugate fracture sets. Tilted bedding was also present, as were synforms and antiform structures within the dolostone beds between the heavy fracture-faulting. Two directions of faulting and fracturing were mapped; a N-NW set and a NE-E set. All structures were vertically oriented. The NE-E fracture on the north end of the stope coincides with a tilted bedding zone. This fracture is offset laterally approximately 10 ft. by the major NW striking fault.

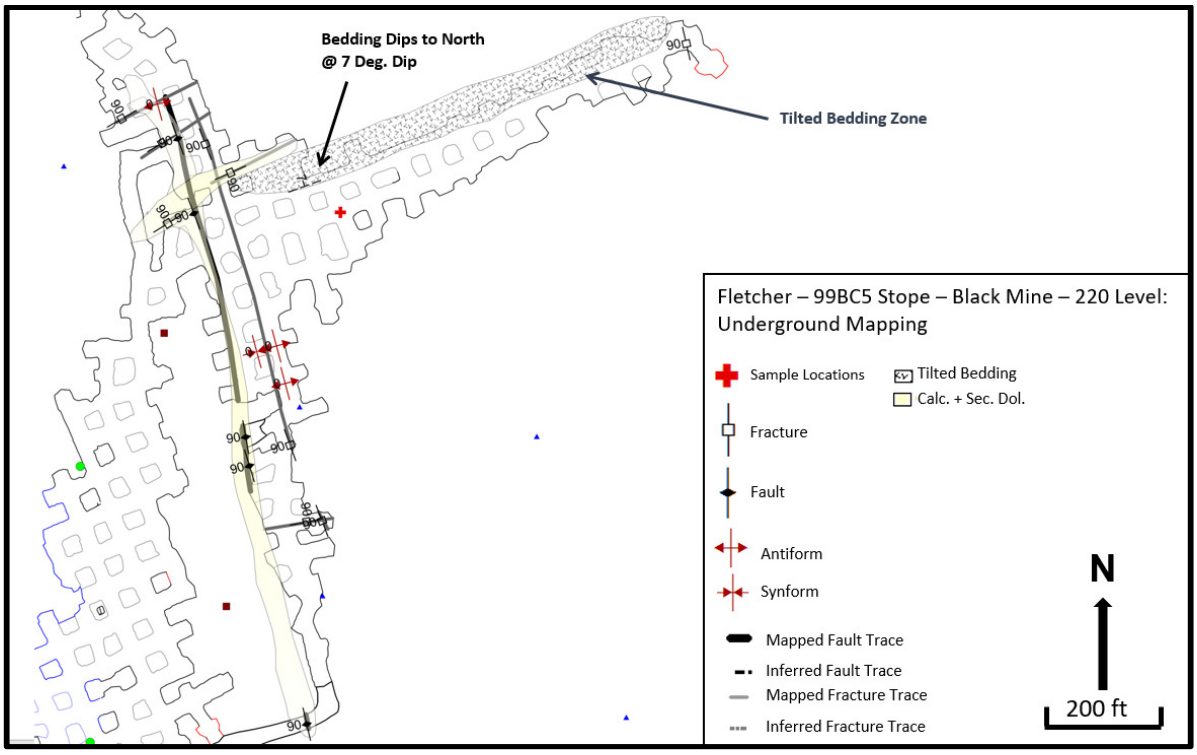

Figure 4.12: Fletcher Location 1- 99BC5 Stope Mapping.

Figure 4.13 illustrates the metal zoning of the stope. Fault and fracture relationships indicate that much of the metal zoning is controlled by different stages of faulting and fracturing. In addition, calcite and hydrothermal dolomite in fill two major structures, both the NW and NE bearing structures.

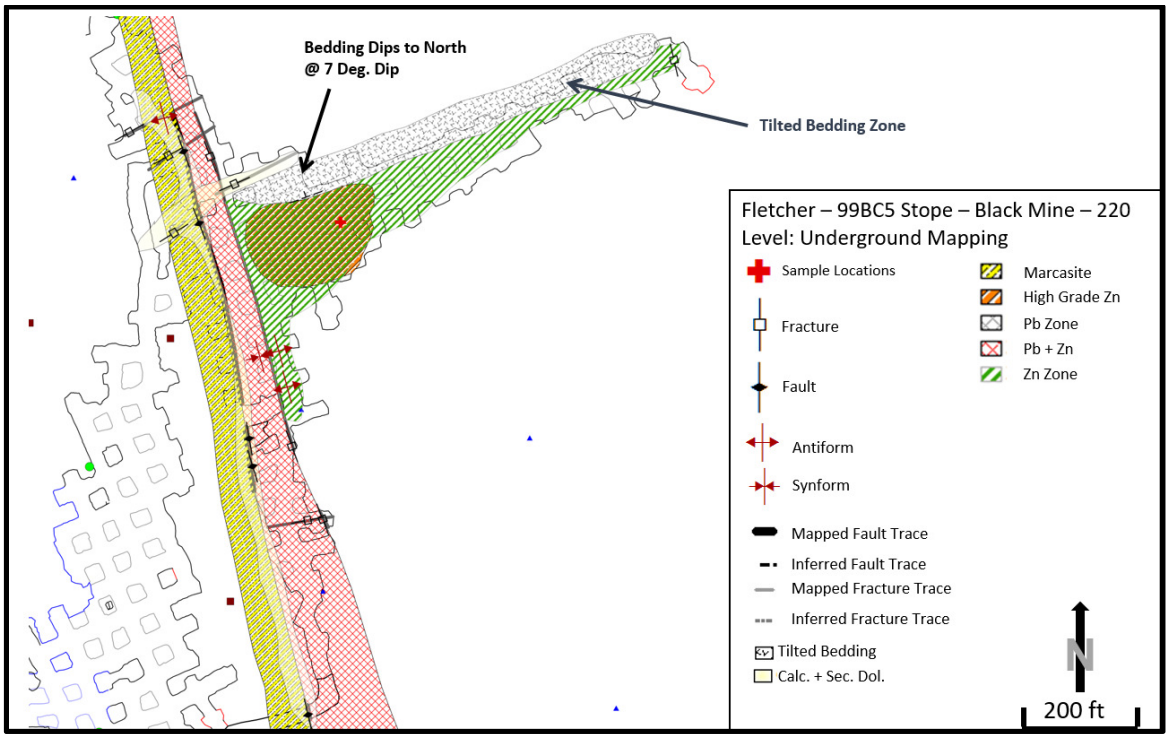

Figure 4.13: Fletcher 99BC5 Stope Mapping with Metal Zoning. Dip readings removed (all structures vertical).

4.2.3.2 J3UC Stope

Figure 4.14 shows the location of the second stope which was studied. This part of the SRZ is unusual, because it contains mineralization on multiple levels. The nearest Precambrian knob is located approximately 2,000 ft. to the North.

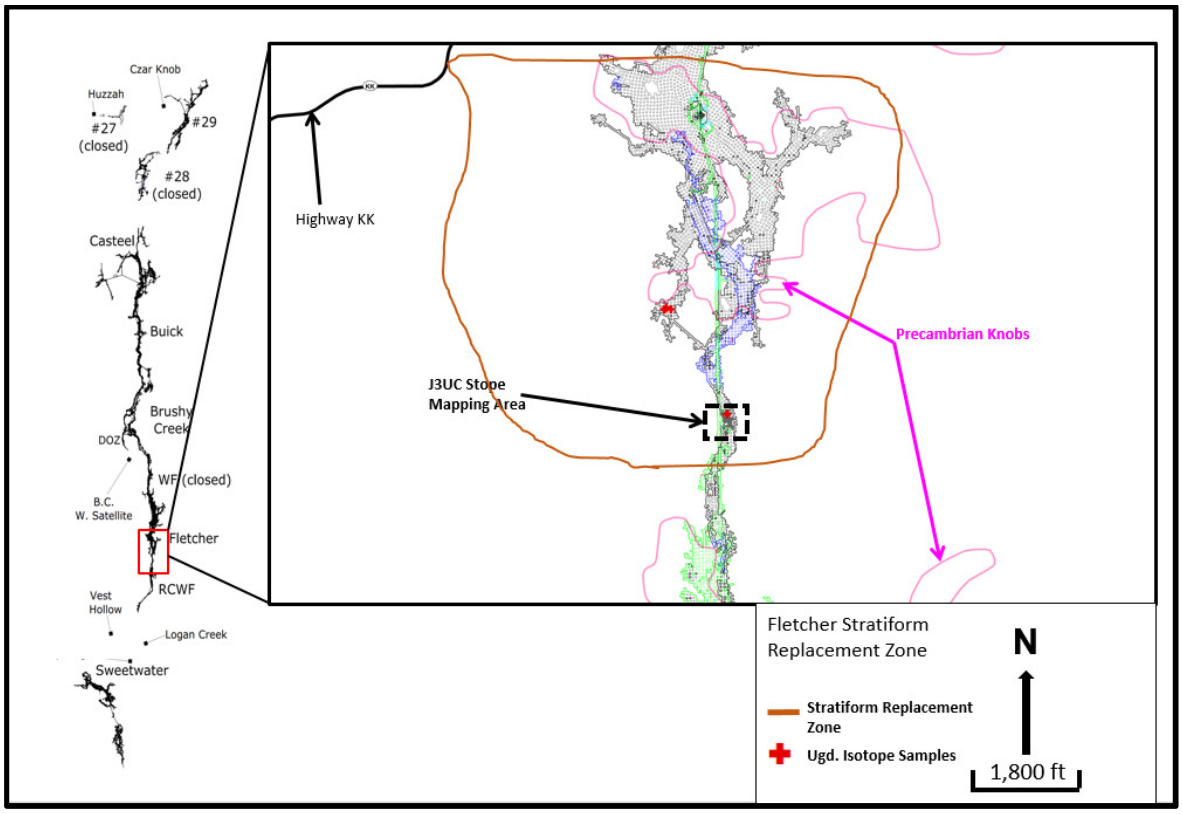

Figure 4.14: J3UC Stratiform Replacement Zone & Study Areas.

Figure 4.15 shows the mapping from the upper level of the stope. Due to production related activities, this was the only level available. This stope is characterized by strong fracturing with fractures forming conjugate sets in certain areas. There is oil, fractures and mineralization throughout the stope. The intense fracturing shows a spatial relationship with the mottled bedding zone, which consists of dolostone which is visibly more permeable than the surrounding rock and contains abundant hydrothermal dolomite. The bedding has no appreciable dip, unlike the other areas mapped. Euhedral galena and sphalerite are found growing in the NE bearing fractures

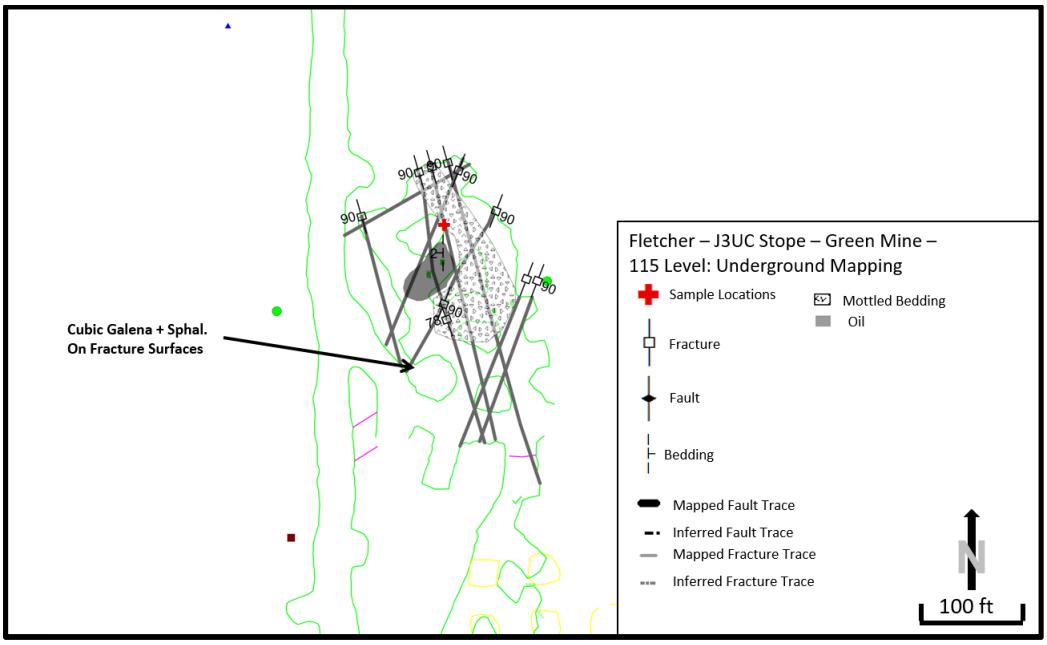

Figure 4.15: Fletcher - J3UC: Underground Mapping Data

Figure 4.16 shows cubic galena growing in the fracture from the J3UC stope. While not in the photograph, spahlerite was observed in growing in fractures in this and several other fractures within the stope.

Figure 4.16: Cubic galena growing in fracture – Fletcher J3UC Stope.

Figure 4.17 shows an example of mottled bedding that was common in the J3UC stope, as well as multiple other stopes. The mottled bedding is associated with higher zinc and lead grades throughout all parts of the SRZ.

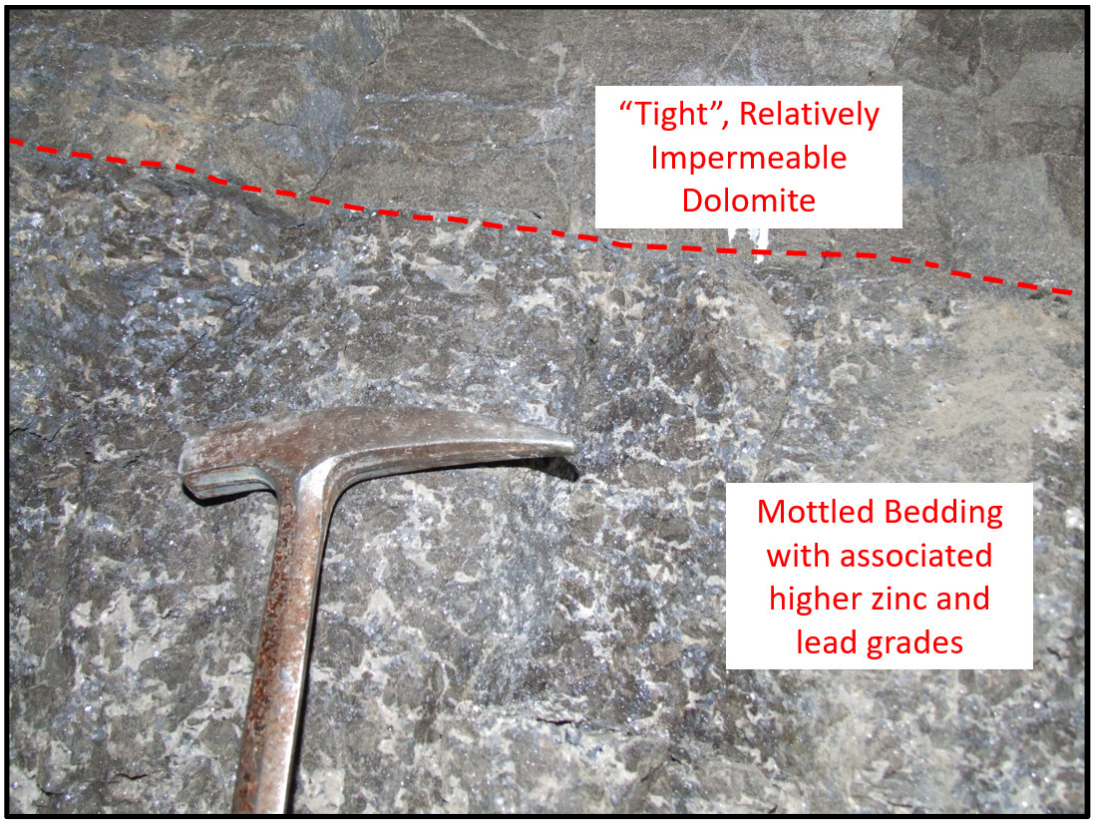

Figure 4.17: Mottled Bedding in the SRZ.

Abundant vugs within this part of Fletcher showed abundant galena with subhedral to euhedral sphalerite growing on top of the galena cubes.

4.2.4 Sweetwater Mapping

Figure 4.18 shows the location of the Sweetwater study areas. Of all the areas where samples were taken, only one had enough exposure to map. Other exposures were unavailable due to flooding or production activity. The detail and quality of mapping in these areas, however was hindered by poor exposures due to dust on mine and pillar faces.

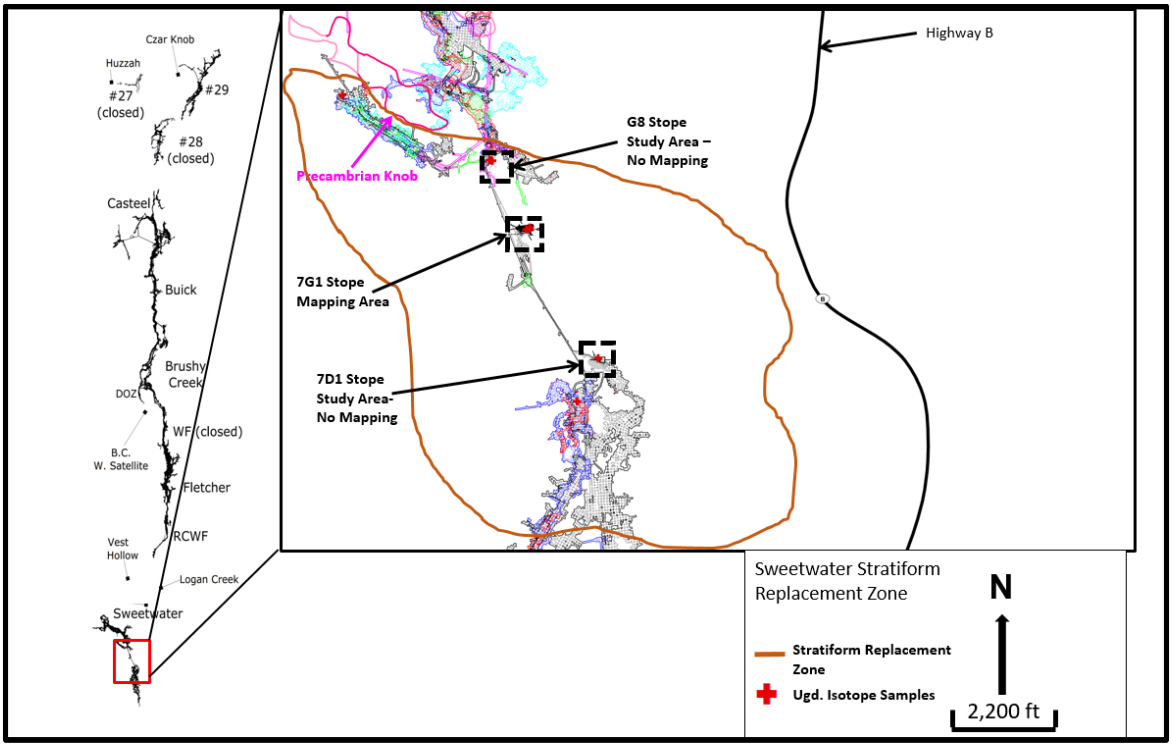

Figure 4.18: Sweetwater Stratiform Replacement Zone & Study Areas

4.2.4.1 G8 Stope

Exposures were poor in the G8 stope, but some information was gathered on the general geology. This zone has particularly high sphalerite grades, with mineralization being controlled by the architecture of the underlying reef as well as vertical fractures.

In addition, organic material demonstrates a strong spatial relationship with the grade of sphalerite mineralization. These organic zones are dark, occur in small pockets the size of a softball, and typically contain subhedral to euhedral sphalerite crystals (Figure 4.19). This organic material is a form of liquid or tacky bitumen which has been described previously in multiple locations throughout the Viburnum Trend (Marikos *et al.*, 1986; Henry *et al.*, 1992; Niewendorp & Clendenin, 1993).

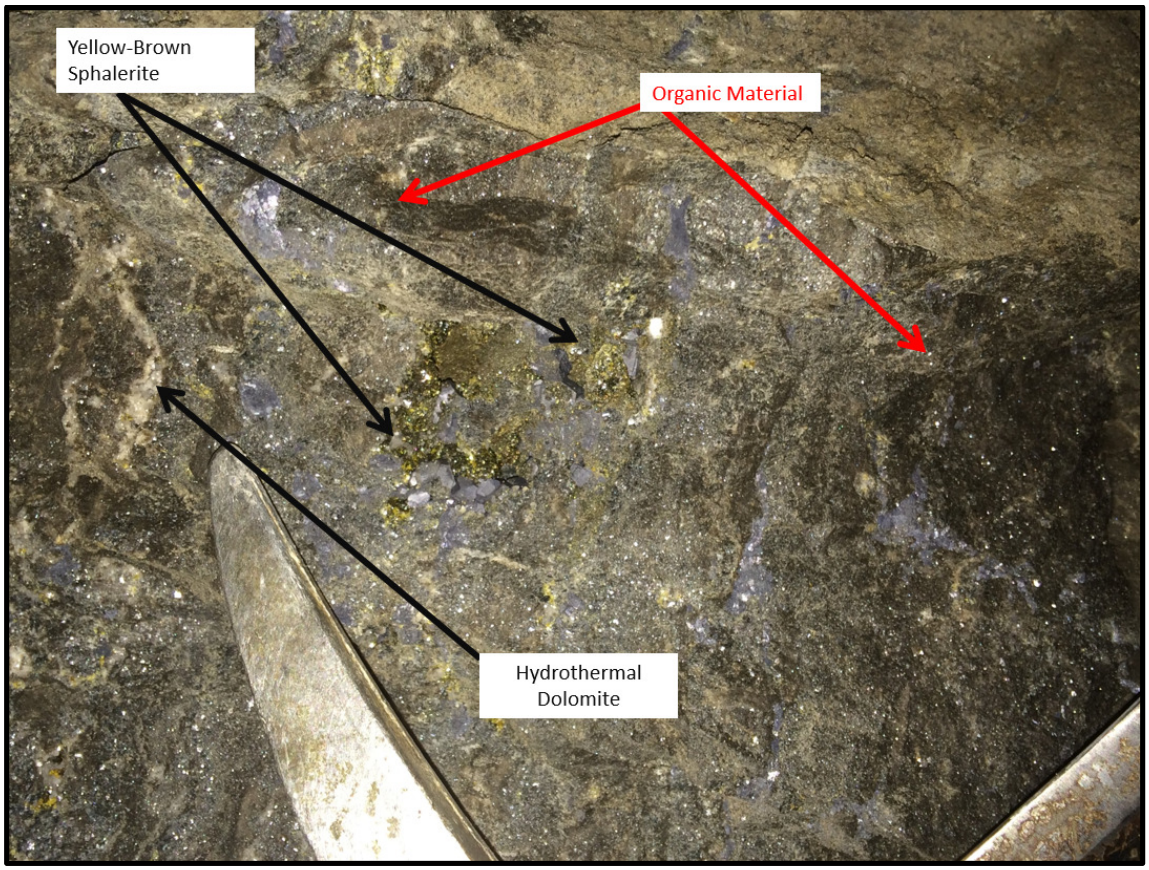

Figure 4.19: G8 Stope – Stratiform Replacement Zone.

Samples from this part of Sweetwater have abundant vugs with a complex intergrowth texture between euhedral quartz and sphalerite crystals. Moderate etching of host dolostone is present throughout the stope.

4.2.4.2 7G1 Stope

This area is heavily faulted, with a major bedding-plane thrust fault cutting through the middle of the stope. The faulting in this stope is closely related to regional faulting that post-dates mineralization. Thick liquid bitumen was identified and mapped where it traveled along beddings planes and seeped into the stope. Sphalerite occurs as yellow-brown vug fill and as horizontal replacement bands. Figure 4.20 shows the regional-scale thrust fault which thrusts mineralized zones on top of barren zones.

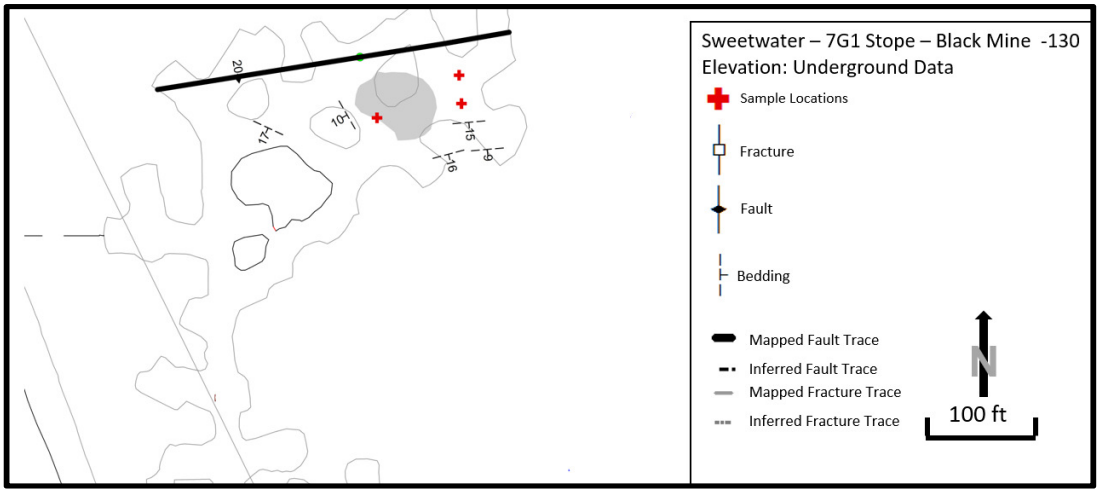

Figure 4.20: Sweetwater 7G1 Stope - Underground Mapping

4.2.4.3 7D1 Stope

The 7D1 stope contains abundant liquid bitumen and strong E-W fracturing. The fractures are lined with sphalerite, cubic galena, marcasite, hydrothermal dolomite and yellow calcite. Sphalerite occurs as euhedral open space fillings growing directly on top of the euhedral hydrothermal dolomite crystals and marcasite.

Figure 4.21 shows liquid bitumen coming out of the mine face in this stope. The bitumen also occurs as tacky blebs and visibly impregnates the dolostone. The bitumen in this stope is broadly associated with higher sphalerite concentrations.

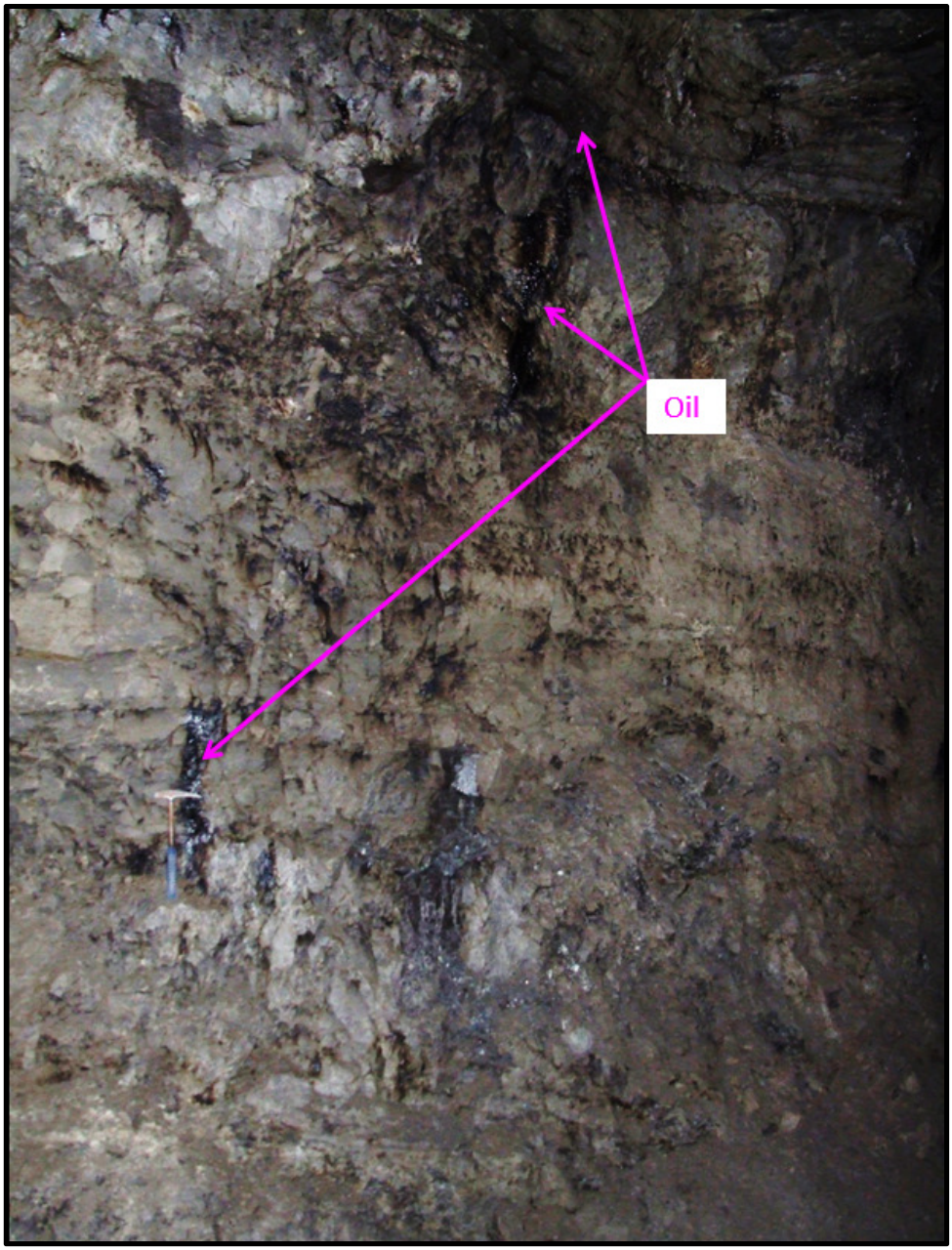

Figure 4.21: Liquid Bitumen – 7D1 Stope.

4.3 Petrography

4.3.1 Dolomite Textures

4.3.1.1 Host Dolomite (D1)

The host rocks of the Viburnum Trend are composed of dolostones with variable degrees of dolomitization. This variable dolomitization is indicated by the degree of destruction of the original carbonate fragments and textures, as well as the relative degree of recrystallization and replacement of the dolostones by subsequent hydrothermal dolomite cements.

Ferroan, xenotopic dolomites (D1) are the most abundant type of dolomite in the within the SRZ. This generation of dolomite is distinct from other dolomites because it represents the original dolomite which has not been recrystallized or altered by hydrothermal events, such as those which are recorded by the D2 and D3 generations of dolomite. This zone does contain evidence of recrystallization, but this recrystallization is related to the original compaction and dolomitization of the rock which is not associated with mineralization or any hydrothermal fluid events, and is therefore distinct from the D2 and D3 dolomite. The dolomite grains are 50-200 um in size, tightly interlocking and contain relict microfossils in unmineralized samples. Grain size decreases in proximity to styolites in most samples. Dolomite near styolites is typically iron rich, idiotopic and has a noticeably smaller crystal size compared with dolomite further away from a styolite (Figure 4.22 A- B). Original sedimentary features from the deposition of the limestone are sometimes preserved and can be identified in thin section (Figure 4.22 C). The degree of recrystallization of dolomite related to styolites varies, and can be significant in some cases (Figure 4.22 D).

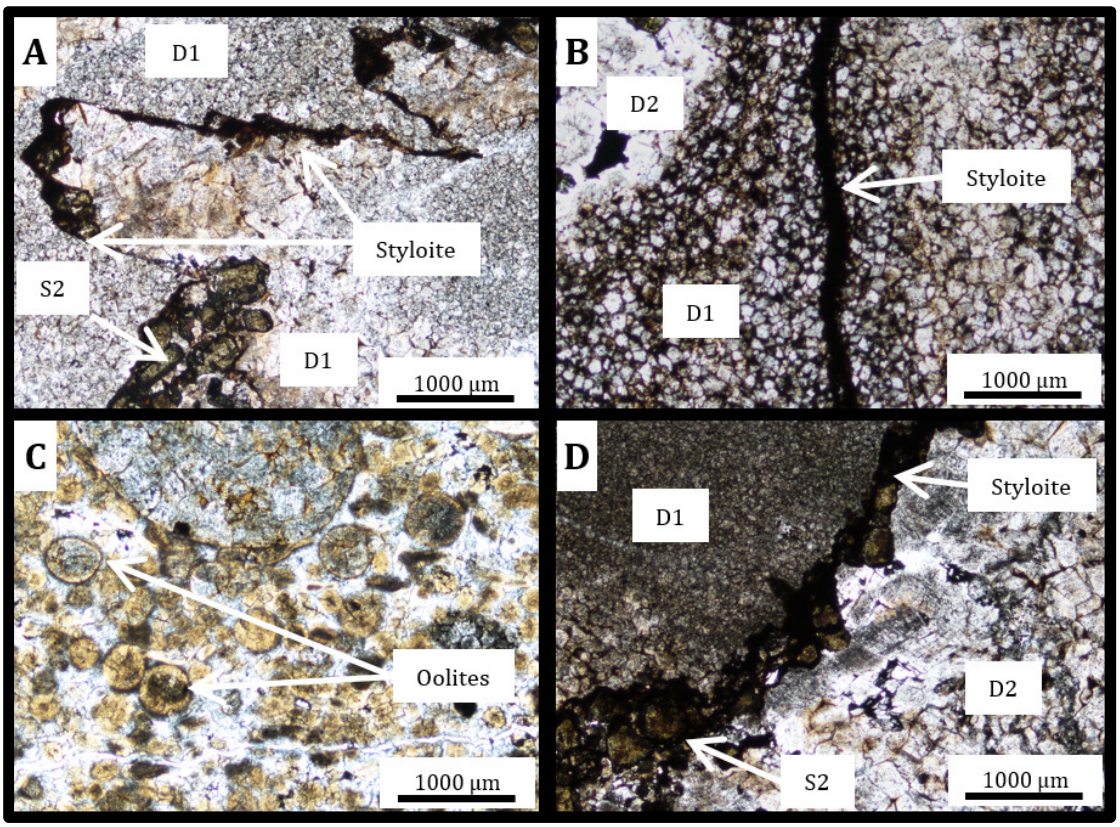

Figure 4.22: Plane polarized light (PPL) images of Stratiform Replacement Zone host dolomite textures.
A) Medium amplitude styolite with early stage dolomite (D1) and late stage sphalerite (S2) (sample Sweetwater 02, Sweetwater mine). B) Low amplitude styolite adjacent to D1 dolomite. D2 dolomite in upper left of image (sample Buick 03, Buick mine). C) Well preserved dolomite oolites with original depositional texture from distal parts of the ore zone (sample 59W28, Buick mine). D) Early stage dolomite (D1), with a styolite marking the boundary between host dolomite (D1) and recrystallized later stage (D2) dolomite. Late green sphalerite (S2) grains near styolites (sample Casteel 06, Casteel mine).

Different stages of dolomite are often identifiable in hand samples, with styolites marking the boundaries between host dolomite (D1) as well as recrystallized dolomite (D2) and late dolomite veinlets (D3) (Figure 4.23 A & B).

4.3.1.2 Recrystallized Dolomite (D2 & D3)

This study did not use the same grouping as Voss *et al.* (1989) (Types 1- 5) for dolomite cements, because many of the cement types identified in that study were absent in the SRZ.

Recrystallized dolomites (D2) have variable, but generally larger (200-400 um) crystals and frequently contain cathodoluminescent cement. Recrystallized dolomite (D2) frequently cross-cuts the ferroan xenotopic dolomites (D1) and is broadly related to main stage mineralization events (G1 & S1). The recrystallized dolomite (D2) occur in nearly all stratigraphic horizons of the Bonneterre Formation. D2 dolomite is interspersed with D1 dolomite (Figure 4.23 A, upper center).

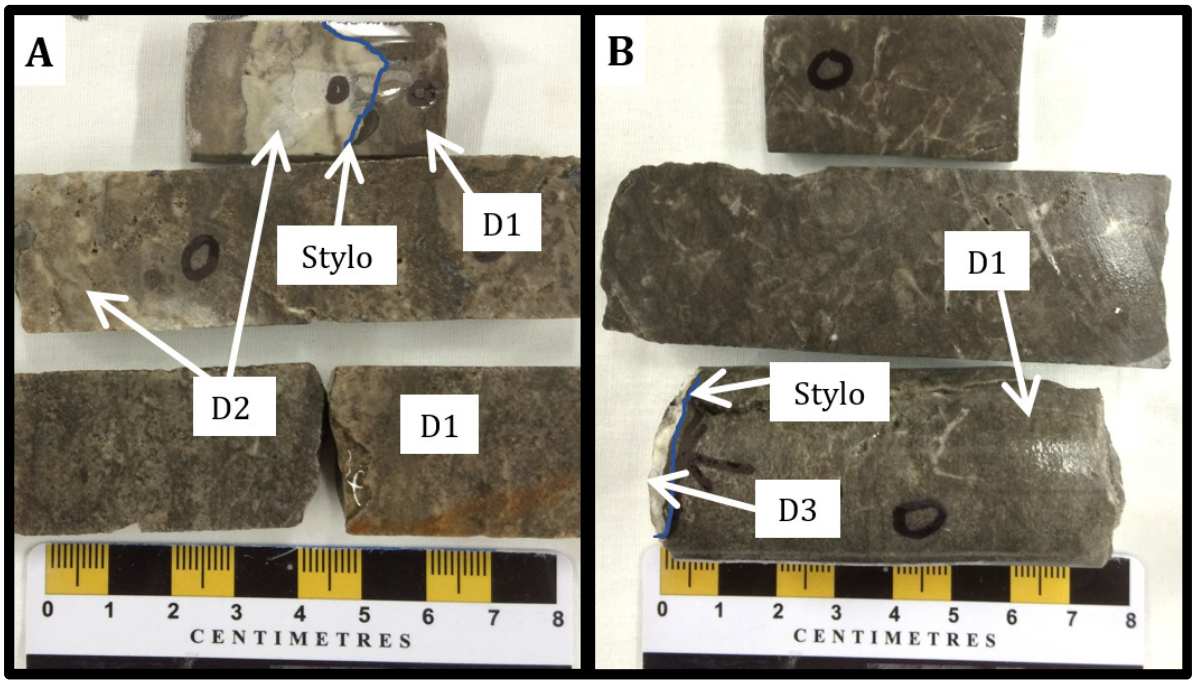

Figure 4.23: Drill core samples of host dolomite (D1) and recrystallized dolomite (D2). A) Recrystallized dolomite (D2) in thick section and drill core with a styolite (blue line, Stylo) marking the boundary between host dolomite (D1) and recrystallized dolomite (D2) (sample 89DR3, Buick mine). B) Styolite (blue line, Stylo) marking the boundary between late stage recrystallized dolomite veinlet (D3) and host dolomite (D1) (sample LC-499, Sweetwater mine).

Dolomite veinlets (D3) cut all other dolomite generations. D3 dolomite veinlets are typically 1-3 mm in thickness, 10-50 cm in length and have a random orientation. They are almost always white, though a pale pink variety has been observed. These veinlets are usually barren though galena and sphalerite do occur within these veinlets in select samples. These veinlets often replace styolites and are usually connected to open space and vug networks within the Bonneterre Formation. The hydrothermal dolomite veinlets in the SRZ have a similar texture to calcite veinlets studied by other researchers (Hannah & Stein, 1984). However, the hydrothermal dolomite veinlets in the SRZ are composed of dolomite cements that are paragenetically distinct from the calcite veins at Magmont West that was studied (Hannah & Stein, 1984). The relative concentration of recrystallized dolomite veinlets is often associated with other ore controlling structures and the frequency generally increases with proximity to mineralized areas in the Stratiform Replacement Zone. In thin section, D3 dolomite contains the largest range (400-950 um) of idiotopic dolomite crystals.

Figure 4.24 shows barren drill core samples and mineralized underground hand samples with representative dolomite veinlets and vug filling cements (Figure 4.24 A & C) from the Stratiform Replacement Zone. The veinlets in the SRZ, while having variable strike and dip (Figure 4.24 B), often follow bedding, and in some replace nearby horizontal styolites (Figure 4.24 D).

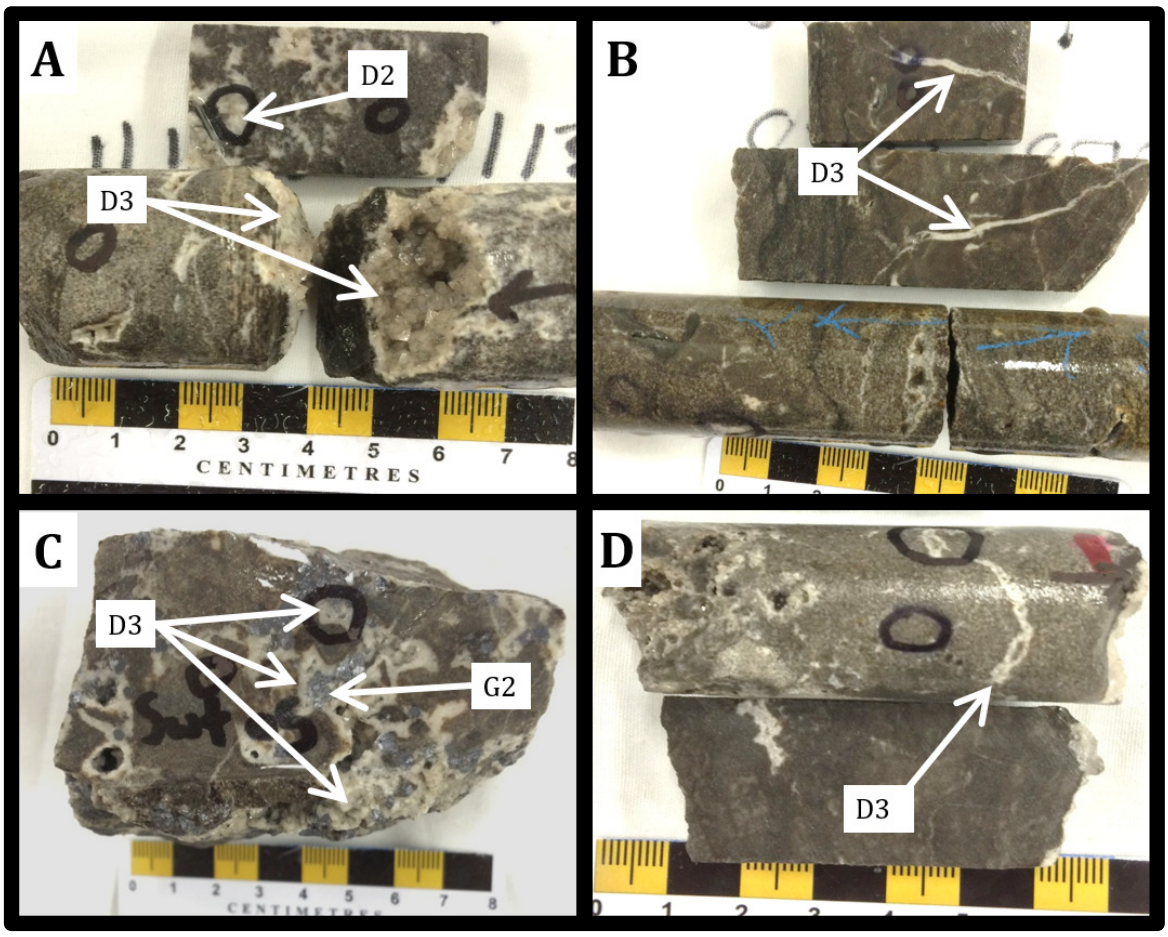

Figure 4.24: Drill core & hand samples of hydrothermal dolomite cements within the SRZ. A) Vug-filling (D3) idiotopic dolomite on core ends with small rasps of recrystallized (D2) dolomite. (sample 61W104, Casteel mine). B) Late stage dolomite (D3) (sample 89V64, Casteel mine). C) Recrystallized dolomite veinlet (D3) with early galena (G1) (Sweetwater 05, Sweetwater mine D) Bedding-parallel recrystallized dolomite veinlet (D3) replaced a pre-existing styolite (sample LC-710, Sweetwater mine).

The cathodoluminescence banding shown in Figure 4.25 (A) is an example of a zoned dolomite crystal. Figure 4.24 (B) shows the microstratigraphy of a zoned dolomite crystal that is found regionally throughout SE Missouri, as described in detail by Voss *et al.*, (1989). Distinguishing recrystallized dolomite (D2) from the host dolomite (D1) can be difficult in hand samples.

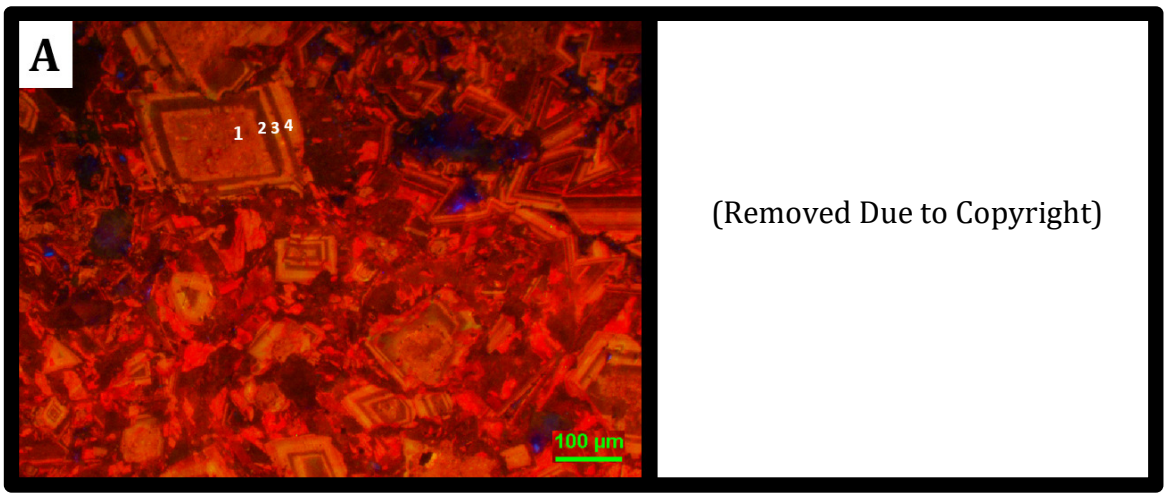

Figure 4.25: Example of Dolomite Crystal Zoning
A) CL image of zoned dolomite. Numbers correspond to the crystal zoning identified by (Voss *et al.*, 1989) and illustrated to the right B) (sample 61W104, Fletcher mine). While the one crystal in this sample has an identifiable crystal zoning, most of the other crystals have a different dolomite crystal zones, or none at all. B) Zoned dolomite crystal. This "micro-stratigraphy" of crystal variation is found regionally throughout SE Missouri, from Voss *et al.*, 1989.

Figure 4.26 shows several different variations of recrystallized dolomite cements within the SRZ. Late stage styolites can cut and offset recrystallized dolomites (Figure 4.26 A-B) while dolomite cement can occur in any dolomite fabric (Figure 4.26 C-D). Recrystallized dolomite veinlets, which almost always hydrothermal dolomite cement, often only show two or three cement types instead of all four types as described by Voss *et al.* (1989) (Figure 4.26 E-F).

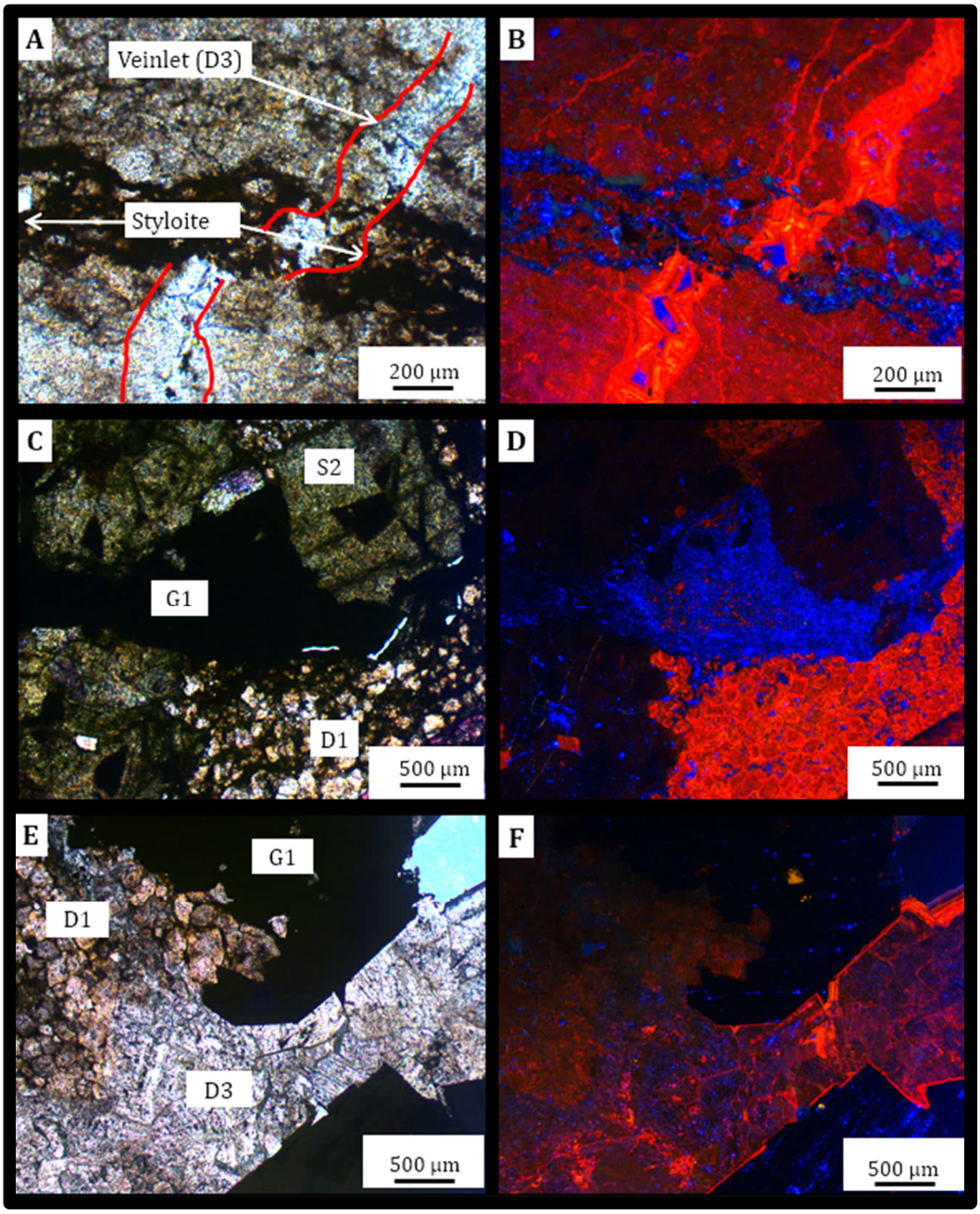

Figure 4.26: Thin section images (PPL) with corresponding CL images of D1 & D3 Dolomites. A-B) Styolite cutting and offsetting a late recrystallized dolomite veinlet (D3) (D3; sample LC-617, Sweetwater mine). C-D) Host dolomite (D1) with late stage sphalerite (S2) and early stage galena (G1) (sample 82V45, Casteel mine). E-F) Host dolomite (D1) cross cut by a late stage recrystallized dolomite veinlet (D3) overgrowing early stage galena (G1) (sample Sweetwater 05, Sweetwater mine).

Figure 4.27 A-B show late stage recrystallized dolomite (D3) with sphalerite in PPL and CL respectively. The sphalerite in this sample cross-cuts dolomite cements (D3) and shows evidence of replacement of these zones of dolomite. While the dolomite cement is easy to recognize with cathodoluminescence microscopy, the exact correlatable dolomite cements (Types 1-4) for most samples are challenging to identify. Identification of the specific hydrothermal dolomite cement zones identified by Voss *et al.* (1989) (e.g. Type 1 vs Type 4) was difficult to determine in most samples from the SRZ due to complicated cement intergrowths (Figure 4.27 B).

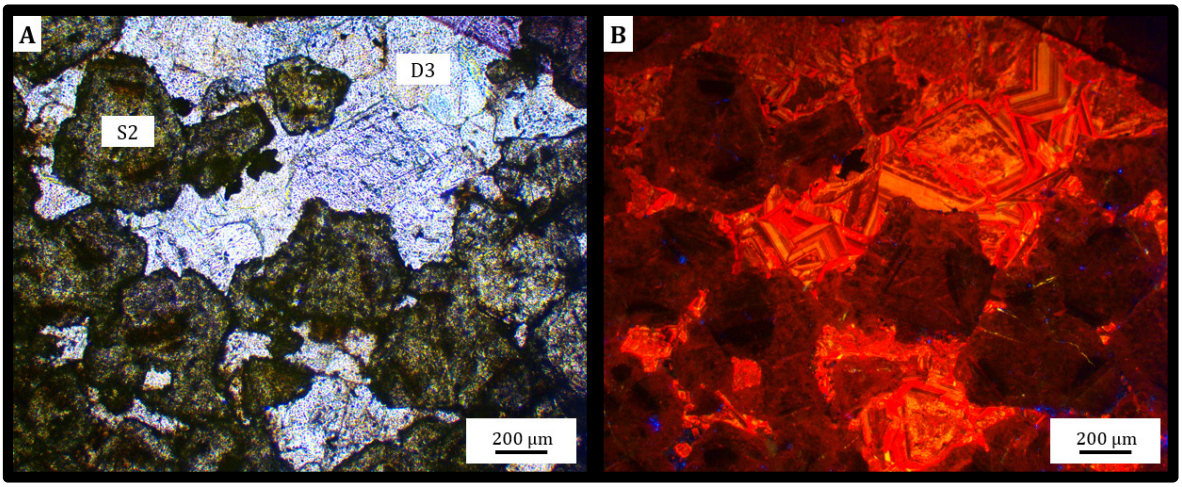

Figure 4.27: Late sphalerite (S2) replacing recrystallized vug filling dolomite (D3) A) PPL image. B) Corresponding CL image (sample Casteel 04, Casteel mine).

4.3.2 Sulfides and Associated Gangue Minerals

Two stages of sphalerite have been identified in the stratiform replacement zones: S1 and S2. For S1 (Figure 4.8 A), color ranges from pale brown to light green, and occurs as disseminated sphalerite. S2 colors range from yellow (Figure 4.28 B) to light green (Figure

4.29 B). Based on observations from mineralized areas underground and analysis in thin section, S2 is the most widely distributed and abundant generation.

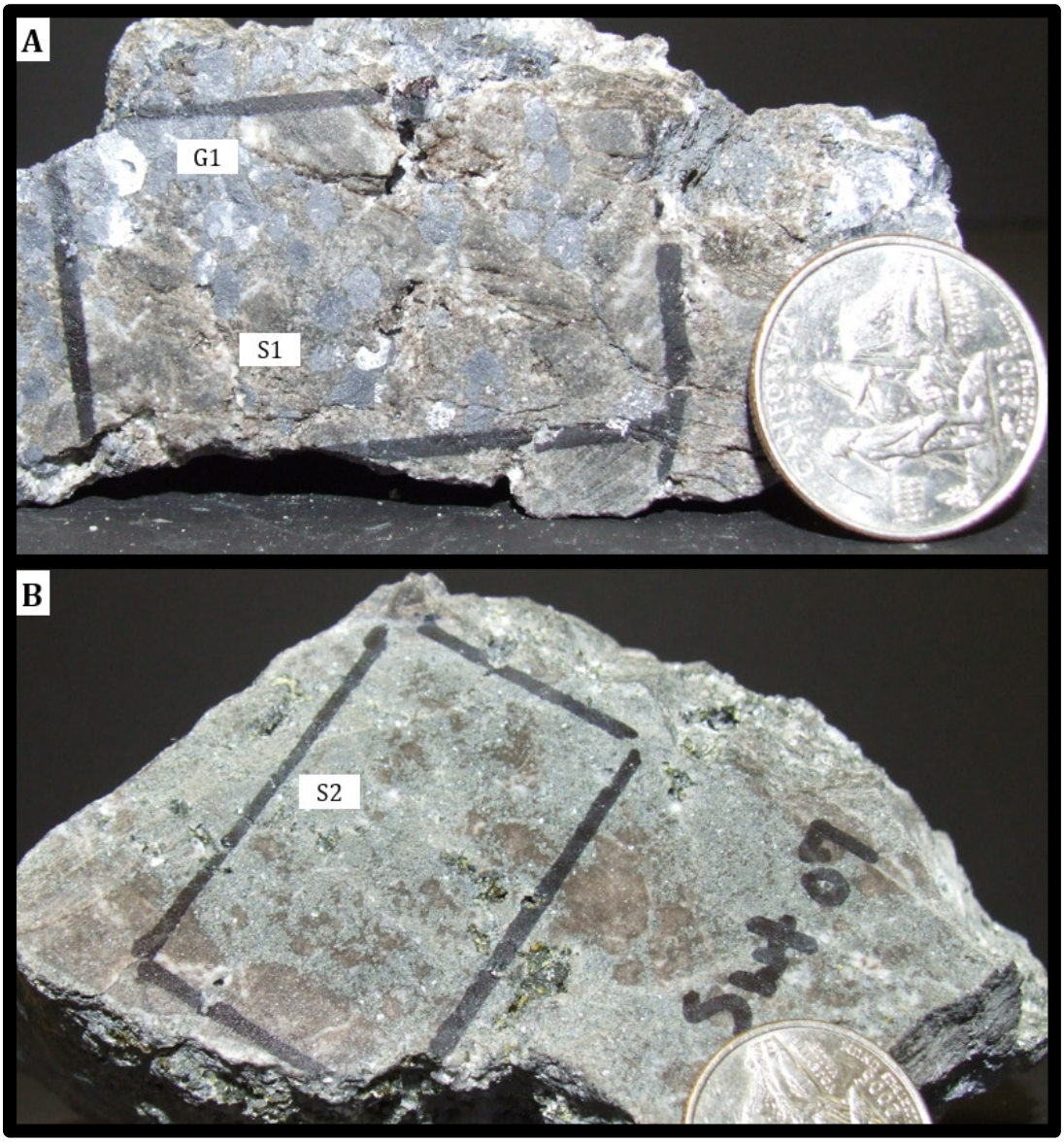

Figure 4.28: Stratiform Replacement Zone hand samples
showing: A) early brown sphalerite (S1) with early stage galena (G1) (sample Sweetwater 09, Sweetwater mine and B) late stage sphalerite (S2) (sample Sweetwater 07, Sweetwater mine).

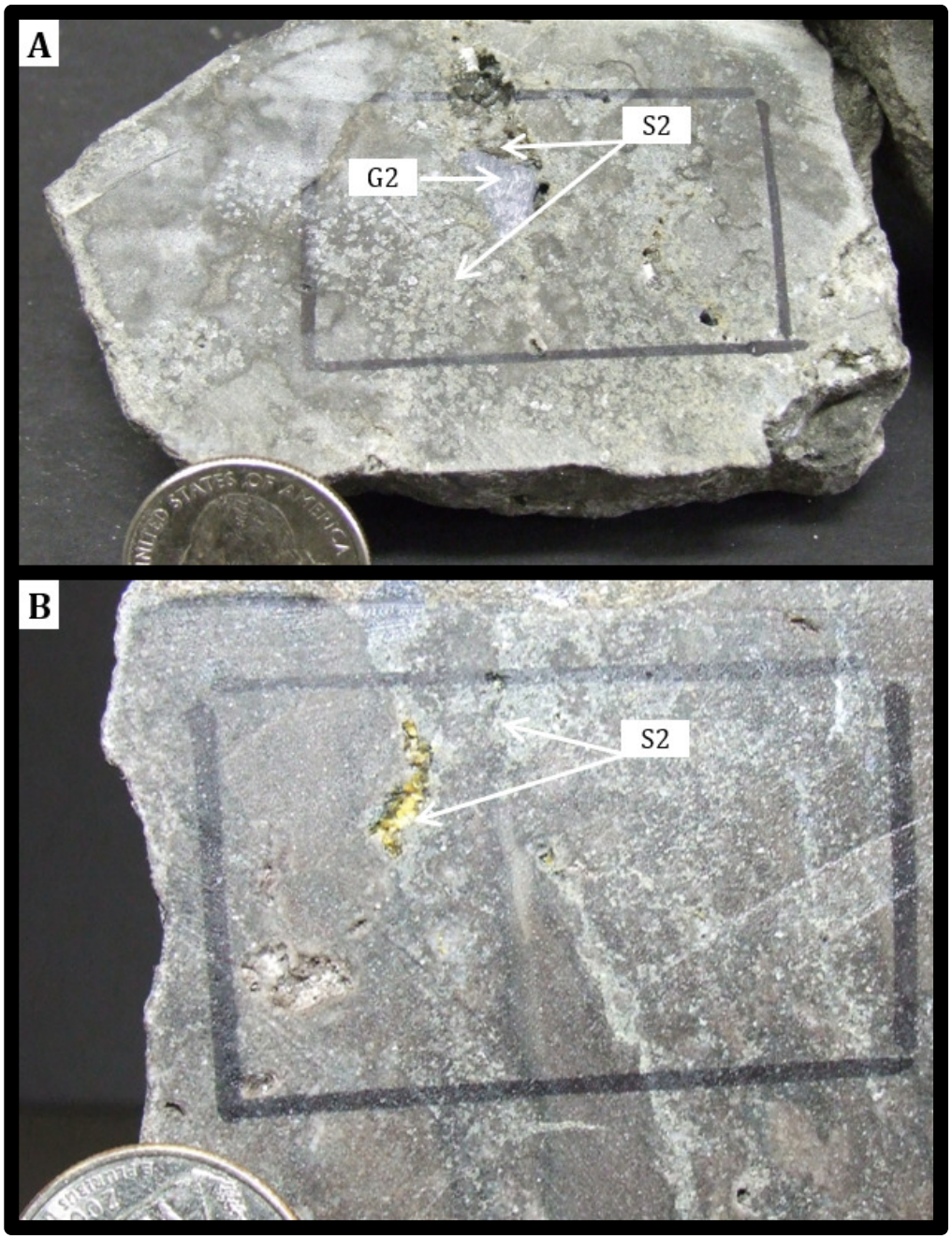

Figure 4.29: Stratiform Replacement Zone hand samples.
A) Green vug filling & disseminated sphalerite (S2) with cubic galena (G2) (sample Casteel 08, Casteel mine). B) Yellow vug filling sphalerite (S2) (sample Fletcher 04, Fletcher mine).

Sphalerite is the most abundant sulfide in the areas studied. Sphalerite occurs as colloform (Figure 4.30 A), replacement (Figure 4.30 C) and large masses of subhedral aggregates of

crystals within the host and hydrothermal dolomites (Figure 4.30 D), which can be fractured (Figure 4.30 B).

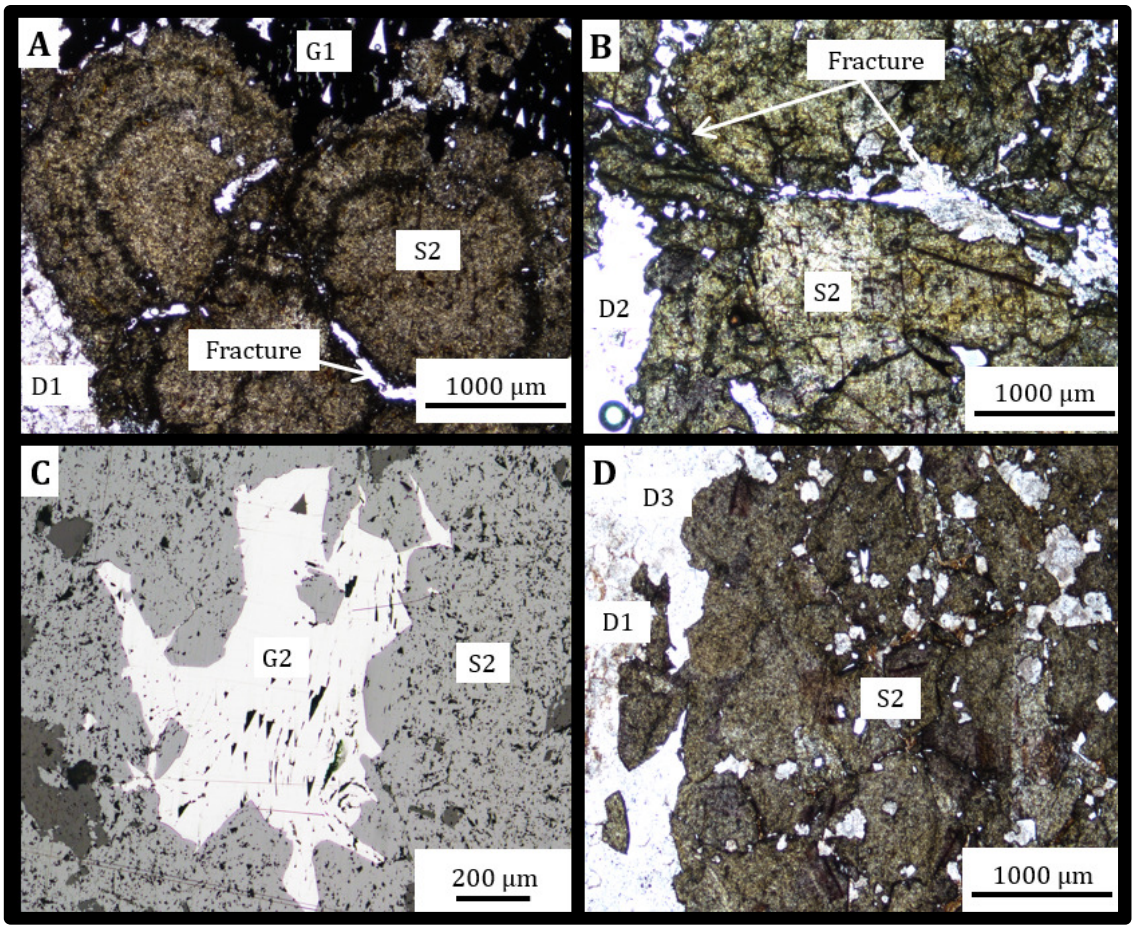

Figure 4.30: Sphalerite textures in the Stratiform Replacement Zone.
A) PPL image of colloform growth texture of late stage sphalerite (S2) with dolomite (D1) and early galena (G1) from the Buick Mine (sample Buick 06). B) PPL image of fractured late stage sphalerite (S2) with dolomite (D2) from the Casteel Mine (sample Casteel 05). C) Reflected light image of cusp/carrie textures indicating that sphalerite (S2) is replacing galena (G2) from the Fletcher Mine (sample Fletcher 06). D) PPL image of subhedral to annhedral sphalerite (S2) replacing dolomite (D1 & D3) from the Casteel Mine (sample Casteel 07).

Sphalerite from certain parts of the SRZ displays color zonation, which is visible in PPL, especially at the Casteel mine (Figure 4.31 A-D). Sphalerite is cut by fractures in samples from the Casteel mine (Figure 4.31 C), with mottling and color variation (Figure 4.31 D).

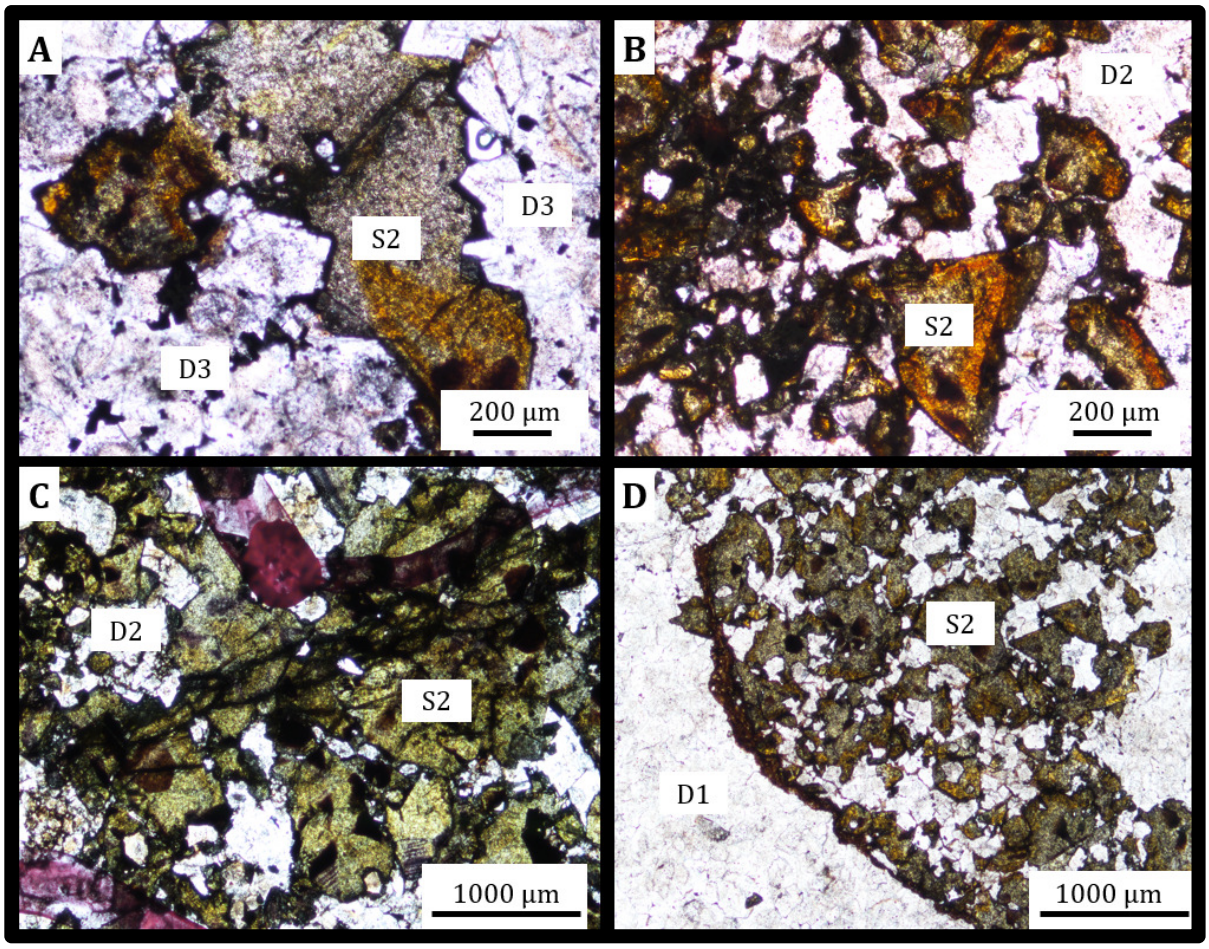

Figure 4.31: PPL images of thin sections of late stage sphalerite (S2) with different dolomite generations (D1, D2, D3). A) Irregular color variations in sphalerite from the Casteel mine with late dolomite (D3) (sample 60W117). B) Color zonation in sphalerite (S2) crystals from the Casteel mine with recrystallized dolomite (D2) (sample 60W117). C) Fractures cutting sphalerite from the Casteel mine with recrystallized dolomite (D2) (sample 82V45). D) Sphalerites with color variation in early stage dolomite (D1) near a styolite from the Casteel mine (sample 60W117).

SEM back scattered electron (BSE) imaging of samples from the Buick and Sweetwater mines revealed that fractures frequently cut sphalerite (Figure 4.32 A-B) and other sulfides (Figure 4.32 C-D). Within these zones, tiny fragments of kaolinite are associated with the areas immediately surrounding the fractures. These fractures are distinct from large scale fracturing mapped in stopes and only occur within close proximity to styolites, and are only visible at the thin section scale.

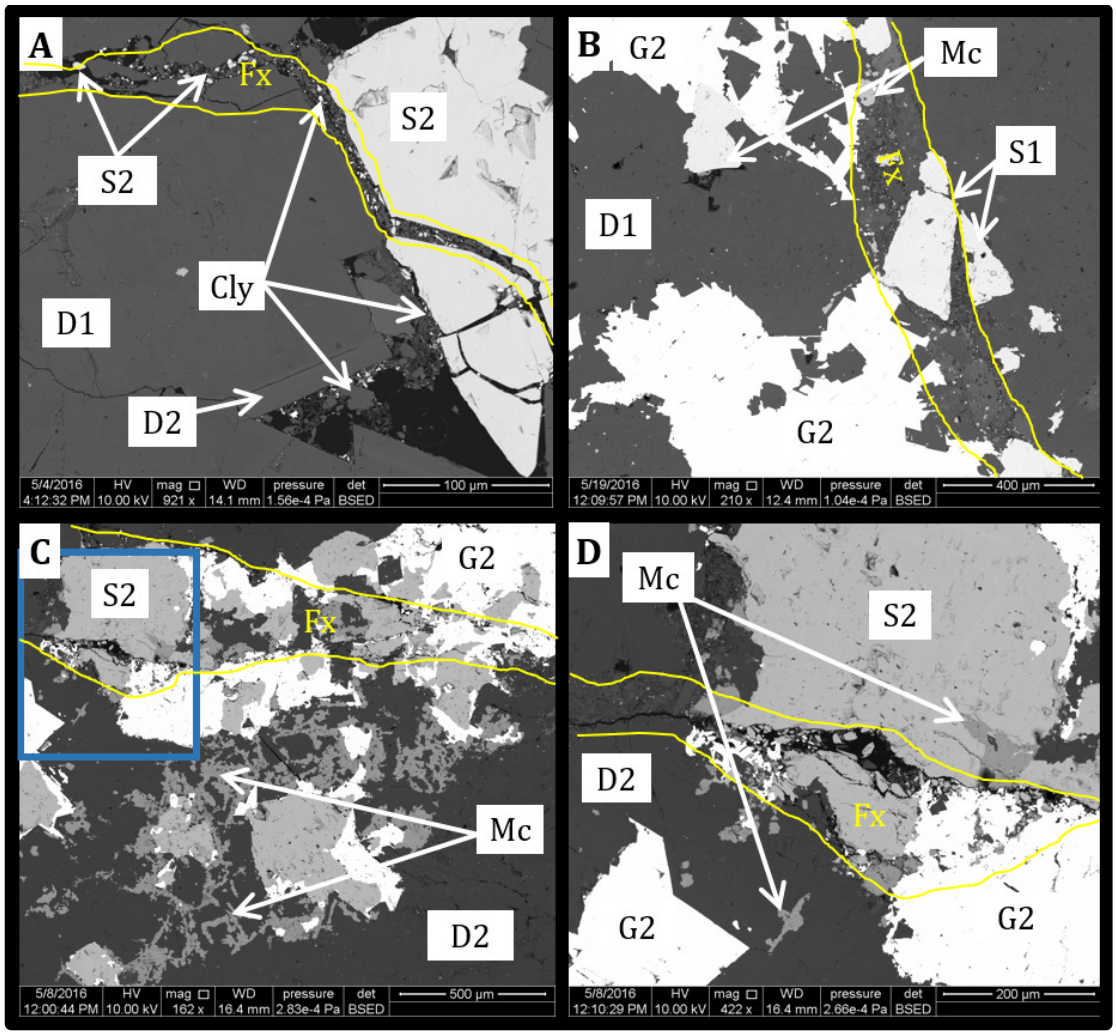

Figure 4.32: Back-scattered electron (BSE) images of fractures.
A) Fracture (Fx) cuts sphalerite (S2) grain. Abundant clay (Cly) is observed within the styolite zone, along with small, rotated and transported grains of sphalerite (S2) (sample Buick 03, Buick mine). B) Fracture cuts sphalerite (S1) grain with early stage dolomite (D1) texture being cut by marcasite (Mc) which is cutting early stage sphalerite (S1) (sample 93DR7, Buick mine). C) Fracture (Fx) cross-cutting galena (G2) and sphalerite (S2) with late marcasite (Mc) (sample Sweetwater 04, Sweetwater mine). Blue box is enlarged in (D). D) Enlargement of C showing fracture (Fx cutting sphalerite (S2), galena (G2) and marcasite (Mc). Marcasite cuts sphalerite.

The Stratiform Replacement Zone contains many sulfides in addition to sphalerite. The most abundant sulfide in the zone after sphalerite is galena followed by marcasite. Siegenite occurs in very small quantities only in limited areas. Fractures cut and mechanically rotate galena and marcasite in some areas (Figure 4.33 A). Spongy pyrite is surrounded by sphalerite (Figure 4.33 B), siegenite replaced galena (Figure 4.33 C) and

sphalerite and dolomite surrounds early chalcopyrite in a sample from the Casteel mine (Figure 4.33 D).

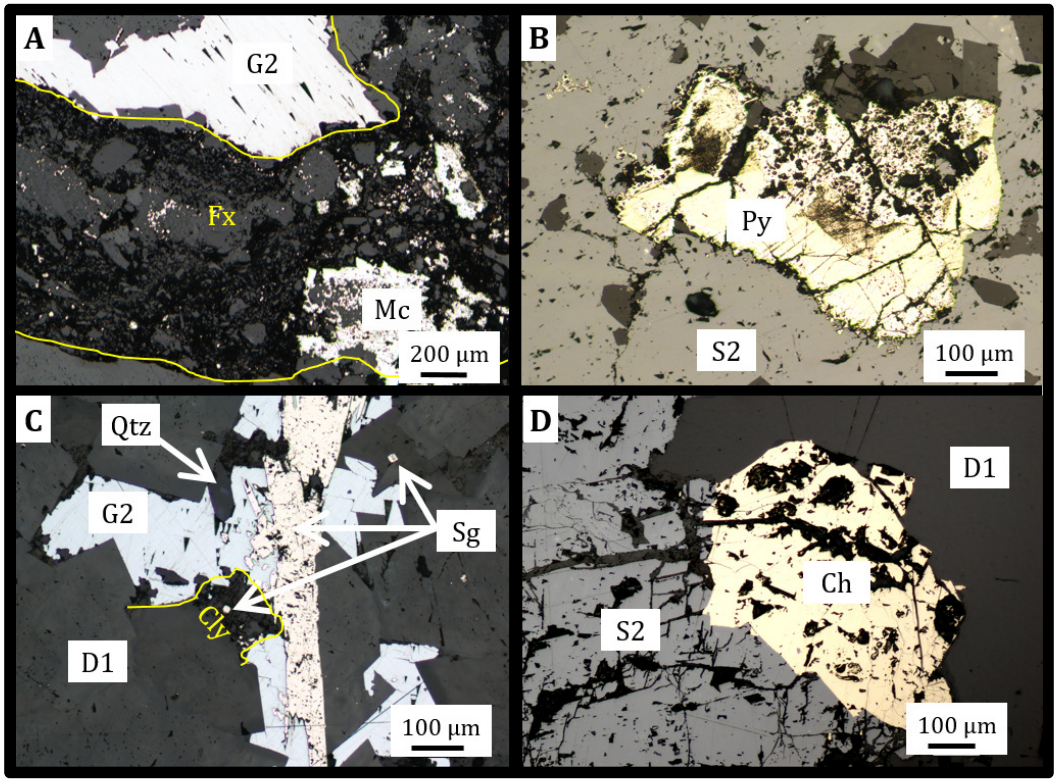

Figure 4.33: Reflected light photographs of sulfides.
A) Late cubic galena (G2) and marcasite Mc) being cut by a fracture with visible rotated fragments throughout (sample 89DR13, Buick Mine). B) Spongy pyrite (py) surrounded by sphalerite, sample 82V45, Casteel Mine. C) Late galena (G2) replaces siegenite (Sg) and euhedral siegenite crystals are scattered throughout. Quartz crystal (Qtz) grows inward towards galena crystals (sample Buick 03, Buick Mine). D) Late stage sphalerite (S2) growing on chalcopyrite (Ch) and surrounded by early stage dolomite (D1) (sample Casteel 05, Casteel Mine).

Replacement, cement and over growth relationships among sulfides are also common (Figure 4.34 A and B).

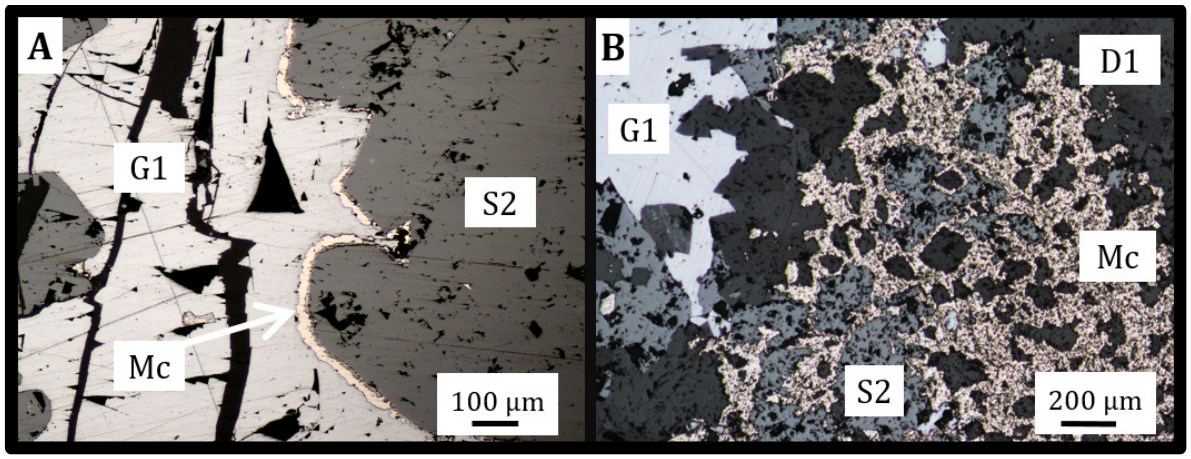

Figure 4.34: Reflected light images of replacement textures.
A) Marcasite (Mc) overgrows late sphalerite (S2) with cusp and carrie textures, indicating replacement of the galena (G1) (sample Buick 07, Buick mine). B) Marcasite (Mc) cement texture: marcasite fills in the matrix in between dolomite (D1) and late stage sphalerite (S2) (sample Buick 04, Buick Mine).

Multiple samples contained etching of all generations of sphalerite and galena, and in several areas there are molds of octahedral sulfides. In some samples, dolomite cement infilled voids with a spatial relationship to etching whereas in other samples there is void space where the etching occurred. Figure 4.35 (A) is a sample from the Casteel mine showing etching and pitting textures in early galena (G1) with associated dolomite infilling voids, whereas Figure 4.35 (B-C) shows a hand sample and associated thin section photo from the Sweetwater mine of etching and pitting in early stage brown sphalerite (S1). Figure 4.35 (D) shows etching of galena, and later infilling with clay, which is surrounded by D3 dolomite from the Sweetwater mine.

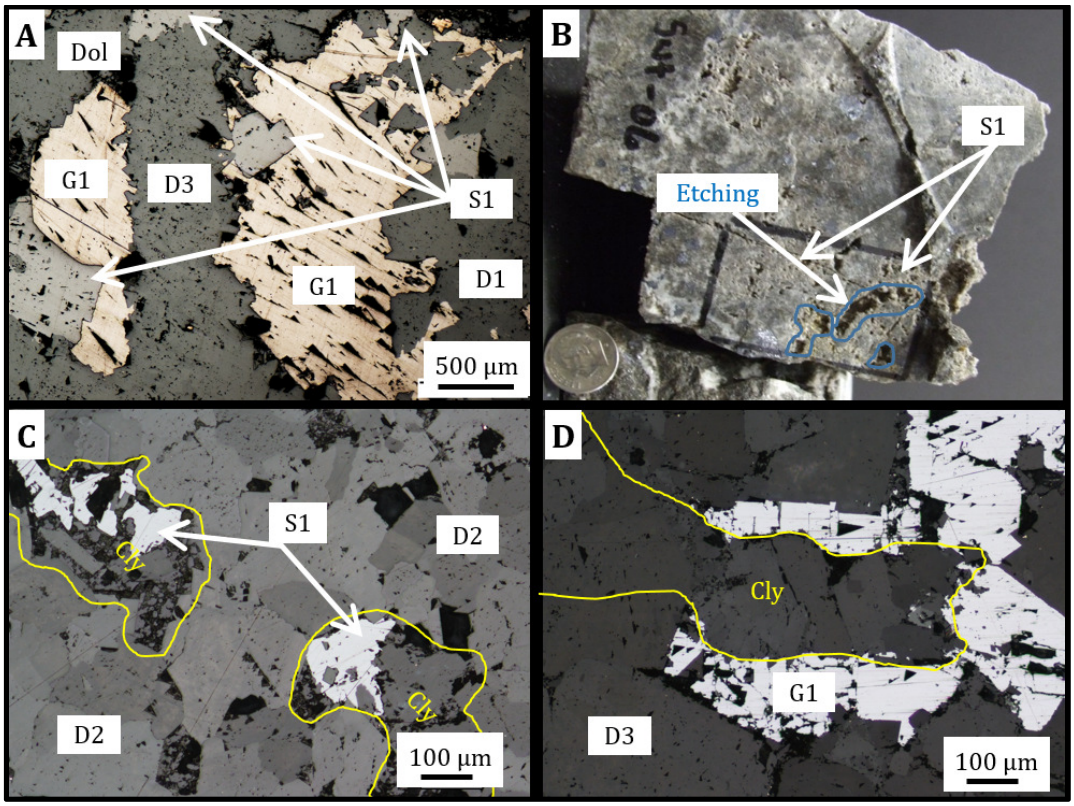

Figure 4.35: Galena and sphalerite etching textures.
A) Early galena (G1) and early sphalerite (S1) replacing early dolomite (D1) and being cut by etching with subsequent infilling by late dolomite (D3), sample 93DR7, Buick mine. B) Hand sample from the Sweetwater Mine showing etching of early sphalerite (S1), sample Sweetwater 06. C) Reflected light photomicrograph of the same Sweetwater sample showing clay (Cly) in proximity to early sphalerite (S1) and dolomite (D2). D) Clay (Cly) in filling a void within galena (G1) which is surrounded by late dolomite (D3), Sweetwater 05, Sweetwater mine.

In Figure 4.36, late galena is replaced by chalcopyrite, which in turn is replaced by sphalerite. Sphalerite is cut by a fracture associated with marcasite, which is infilling the fracture and surrounding void space.

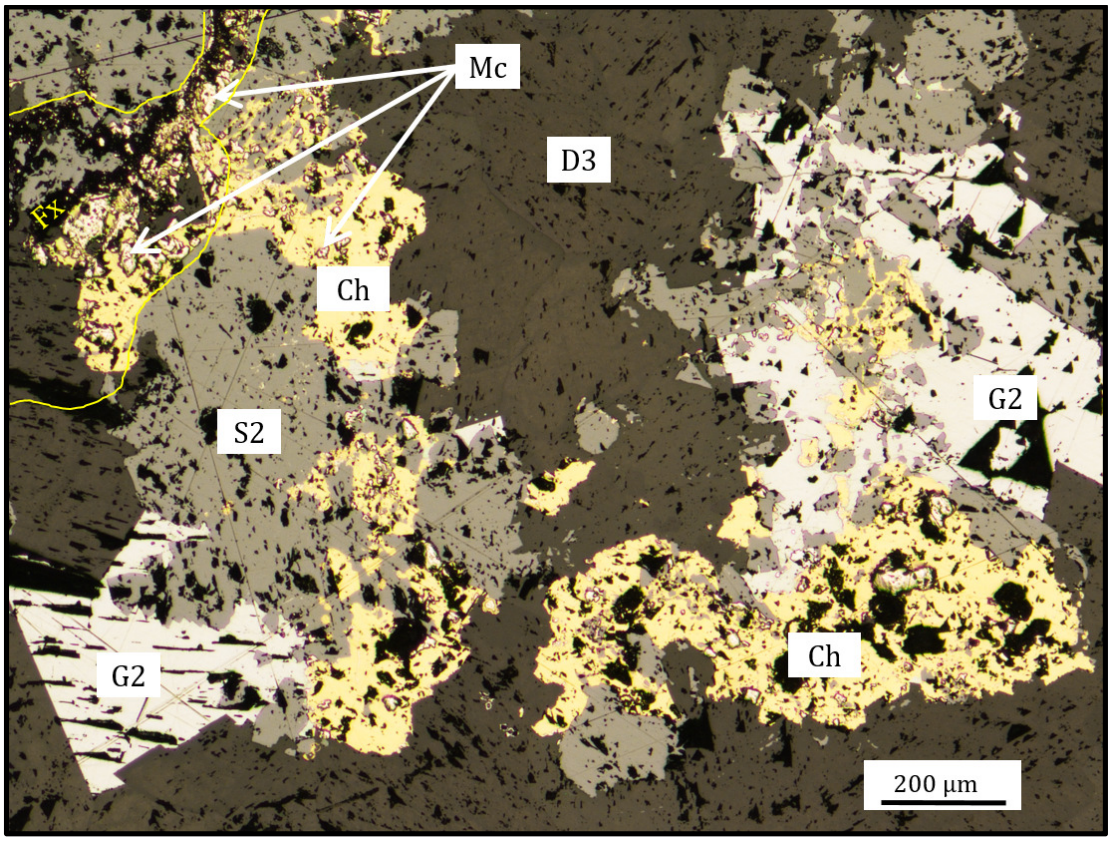

Figure 4.36: Reflected light image of sulfide textures from the Fletcher mine Showing early stage chalcopyrite (Ch) as inclusions within late stage galena (G2), being cut by late stage sphalerite (S2).). These sulfides are cut by a fracture (Fx) which with associated marcasite (Mc). These sulfides are surrounded by a D3 dolomite (sample Fletcher 03).

Siegenite, while only found in the Buick Mine samples forms tiny euhedral crystals (Figure 4.37 A). Gersdorffite, also only occurring at the Buick mine, shows an interlocking texture with galena (Figure 4.37 B). Apatite, while only identified in one sample, is likely a detrital grain (Figure 4.37 C-D). Quartz was identified in multiple samples in different mines and is associated spatially with fractures. Quartz forms euhedral grains which grow within voids of sphalerite (Figure 4.37 D).

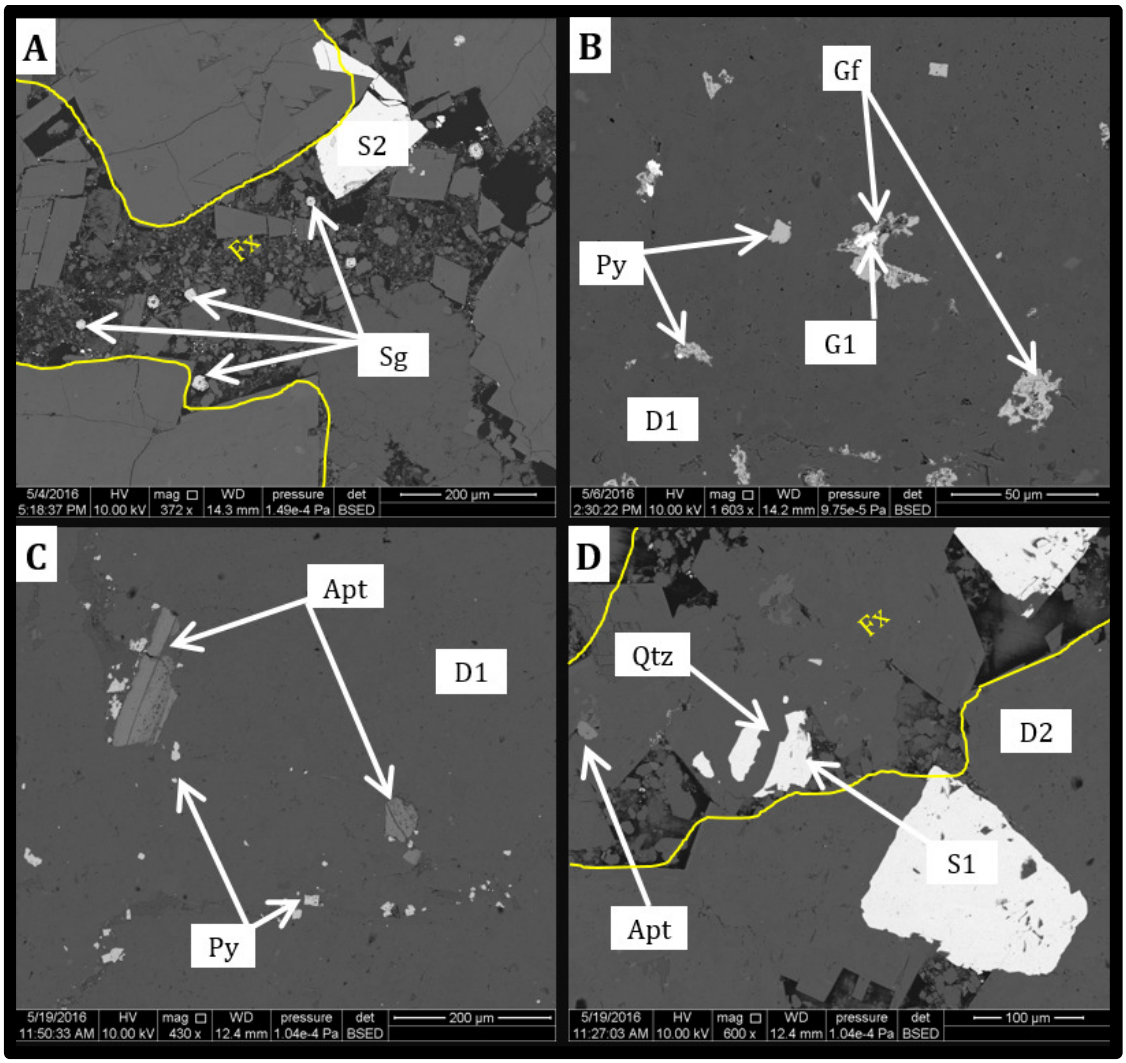

Figure 4.37: BSE images of gangue minerals.
A) Euhedral siegenite (Sg) growth in a fracture zone (Fx) that is cutting late stage sphalerite (S2) in sample Buick 03, Buick Mine. B) Gersdorffite (Gf) enclosing early stage galena (G1) which is surrounded by host dolomite (D1) in sample Buick 06 Buick Mine. C) Apatite (Apt) fragments within host dolomite (D1) with tiny pyrite fragments (Py) in sample 93DR7, Buick Mine. D) Euhedral quartz (Qtz) grain grows in a void space of a sphalerite (S1) from sample 93DR7, Buick Mine.

4.3.1 Electron Microprobe Data

In thin section (PPL), green sphalerite from these samples has less <0.5 wt.% Fe or Cd, while orange and purple sphalerite have higher concentrations (> 1.0 wt. percent) of Fe and Cd. The data displayed in Table 4.1 shows selected microprobe point data for the Stratiform Replacement Zone samples which showed noticeable color and textural variation in petrography.

Table 4.1: Electron microprobe point data for sphalerite from the Stratiform Replacement Zone. All other elements were below detection limits and excluded from this table.

Sample - Analysis Point	Zn	Fe	Cd	S	Total
Buick 06 Spot 1 Pt 1	65.97	0.86	1.03	33.15	101.22
Buick 06 Spot 1 Pt 2	66.67	0.73	0.41	33.18	101.06
Buick 06 Spot 1 Pt 3	67.48	0.09	0.33	31.41	99.51
Buick 06 Spot 1 Pt 4	64.86	1.22	1.22	32.62	100.01
Buick 06 Spot 1 Pt 5	65.85	0.83	1.01	32.99	100.81
Buick 06 Spot 1 Pt 6	64.61	1.25	1.24	32.51	99.8
Buick 06 Spot 1 Pt 7	64.73	1.03	1.32	32.71	99.98
Buick 06 Spot 1 Pt 8	65.67	0.67	0.99	33.11	100.54
Buick 06 Spot 1 Pt 9	66.05	0.86	0.98	32.58	100.54
Buick 06 Spot 1 Pt 10	66.83	0.48	0.56	33.35	101.32
Buick 06 Spot 1 Pt 11	65.68	0.91	0.89	32.98	100.62
Buick 06 Spot 1 Pt 12	66.76	0.38	0.60	32.92	100.86
Buick 06 Spot 1 Pt 13	65.78	0.85	1.00	32.94	100.75
Buick 06 Spot 1 Pt 14	65.81	0.73	0.84	33.04	100.54
Buick 06 Spot 1 Pt 15	65.75	0.94	0.90	32.91	100.69
Buick 06 Spot 1 Pt 16	66.90	0.42	0.53	33.40	101.4
Fletcher 06 Spot 2 Pt 1	66.30	0.43	0.74	32.97	100.56
Fletcher 06 Spot 2 Pt 2	64.96	0.59	1.02	33.02	99.74
Fletcher 06 Spot 2 Pt 3	65.57	0.70	0.98	32.71	100.11
Fletcher 06 Spot 2 Pt 4	65.43	0.72	0.87	32.70	99.85
Fletcher 06 Spot 2 Pt 5	64.67	0.80	1.52	31.76	98.80
Casteel 09 Spot 1 Pt 1	66.08	0.22	0.52	32.93	100.03
Casteel 09 Spot 1 Pt 2	66.14	0.43	0.90	33.35	101.03
Casteel 09 Spot 1 Pt 3	66.79	0.26	0.71	33.43	101.37
Casteel 10 Spot 3 Pt 1	66.69	0.43	0.67	32.99	100.96
Casteel 10 Spot 3 Pt 2	63.70	3.32	0.97	33.34	101.45
Casteel 10 Spot 3 Pt 3	63.88	2.52	1.03	32.87	100.52

The images below show analysis point locations that correspond to geochemical data found in the previous table (Table 4.1). Sphalerite with open space textures (Figure 4.38 A and B) has variation in Fe, Cd and Zn throughout the crystal. Subhedral sphalerite (Figure 4.38 C

and D) shows chemical variations in sphalerite grains, which are associated with the color of sphalerite observed in PPL microscopy.

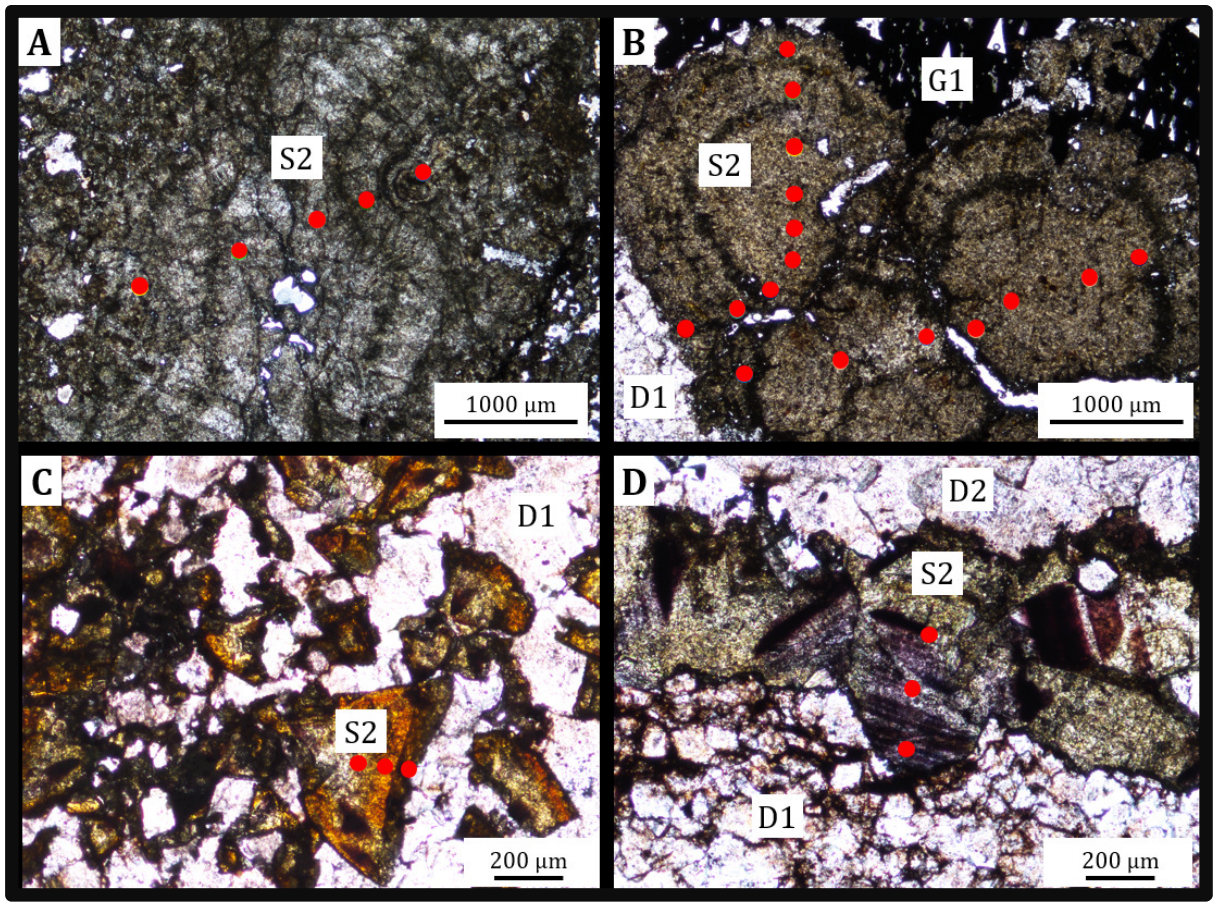

Figure 4.38: Plane polarized light images (PPL) of sphalerite showing the location of electron microprobe analysis points.
EMP analysis points correspond to data in Figure 4.39. A) Analysis points for sample Fletcher 06, Fletcher mine, showing compositional changes in the late stage (S2) green sphalerite. B) Analysis points for sample Buick 06, Buick mine, with open space filling textures of late stage (S2) sphalerite. C) Analysis points of color variation in sphalerite from sample Casteel 09, Casteel mine. D) Analysis points of sphalerite with purple color variation from sample Casteel 10, Casteel mine.

Figure 4.39 show plots of Cd + Fe vs. Zn for the selected samples at the Buick, Fletcher and Casteel mines respectively. Traverses across zoned sphalerite grains shows that there is an inverse correlation between Cd+Fe and Zn concentrations. This correlation does not vary systematically from core to rim within a single sample or grain.

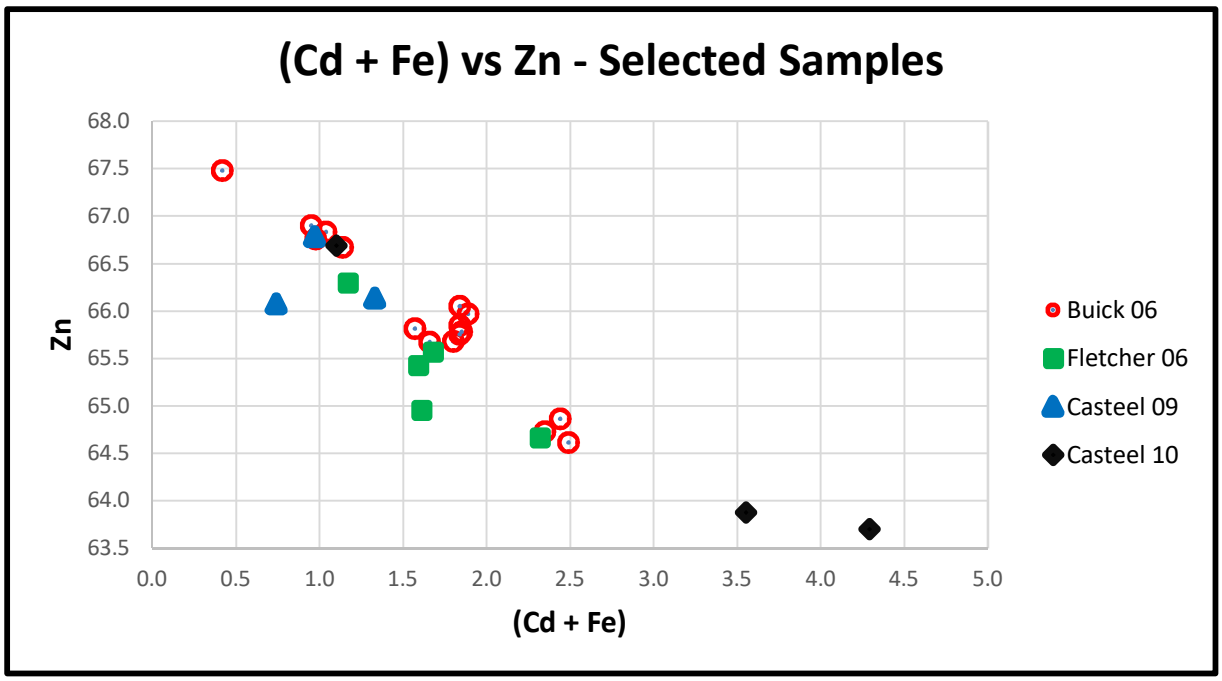

Figure 4.39: Cd + Fe vs. Zn in sphalerite from selected samples. All data in %.

4.3.2 Petrography Conclusions

The Stratiform Replacement Zone is characterized by replacement of early galena (G1), sphalerite (S1) by paragenetically late sphalerite (S2). S1 sphalerite is less abundant whereas late green and yellow sphalerite (S2) is dominant throughout the entire zone. S2 sphalerite grew concurrently with and in some instances replaced D3 dolomite and always replaced earlier D2 dolomite. Bedding parallel styolite zones, some of which were thick (6-10”), were ubiquitous throughout the SRZ.

Replacement of G2 galena with S2 sphalerite is indicated by both cusp and carrie as well as island/mainland textures in both hand samples and thin sections. These textures characterize the contacts between sulfides, where late-stage minerals either protrude into (mainland texture) or produce a convex shape (cusp and carrie texture) into earlier

minerals. Figure 4.40 (A-B) illustrates the replacement of cubic galena (G2) by sphalerite (S2) in hand sample and the corresponding polished thin section from the Casteel mine. Figure 4.40 (C) shows cubic stage galena (G2) surrounded by vug filling dolomite (D3) in a hand sample from the Sweetwater Mine and Figure 4.40 (D) shows the corresponding thin section of sphalerite (S2) and dolomite (D3) growing around cubic galena (G2).

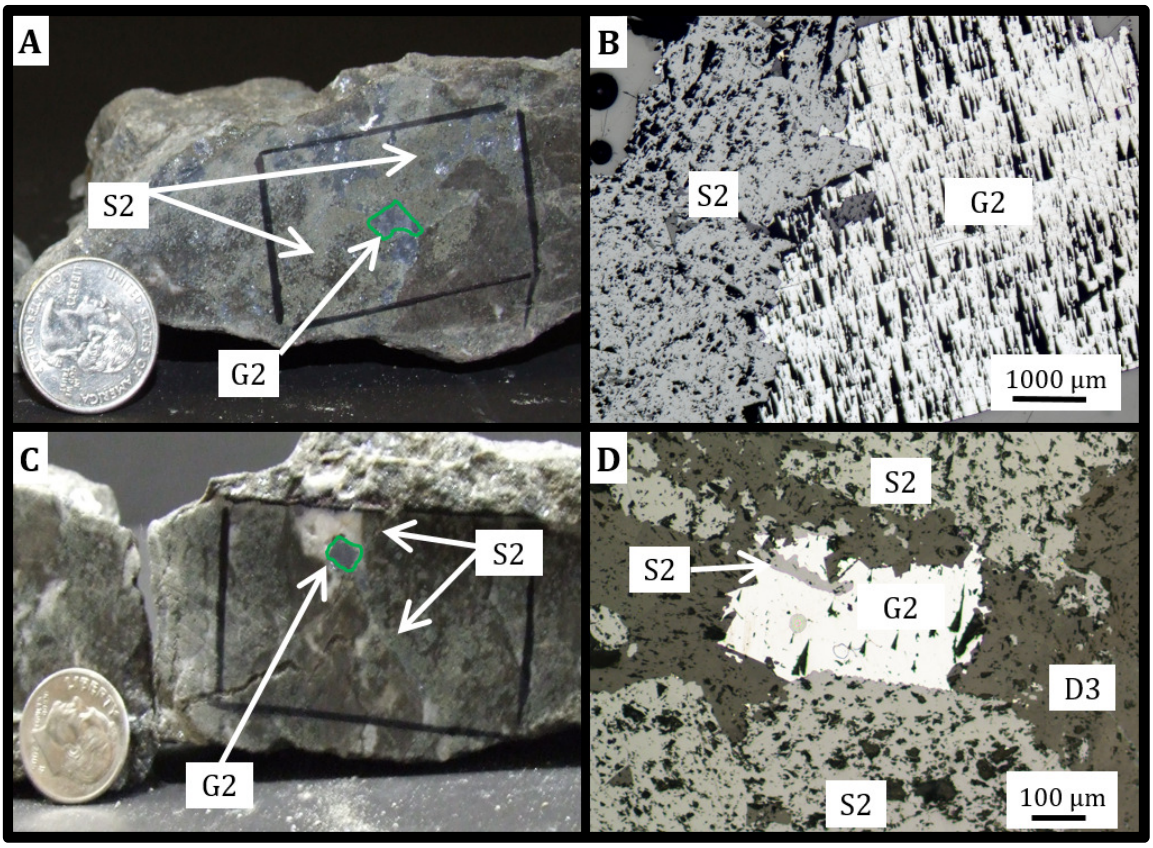

Figure 4.40: Late stage sphalerite (S2) replacing late galena (G2).
A) Hand sample from the Casteel Mine (sample Casteel 04) showing replacement of late cubic galena (G2) by late sphalerite (S2). B) Reflected Light Photomicrograph from the same sample as A showing cusp and carrie replacement of late cubic galena (G2) by late sphalerite (S2). C) Hand Sample from the Sweetwater Mine (sample Sweetwater 02) showing late cubic galena (G2) surrounded by vug and vein filling dolomite (D3) and late sphalerite (S2). D) Reflected light photograph of the same sample shown in C with late cubic galena (G2) surrounded by late sphalerite (S2) and dolomite (D3).

Figure 4.41 and Figure 4.42 show evidence of replacement of late dolomite (D3) by late sphalerite (S2) at the Casteel and Sweetwater Mines. The sphalerite grains in these samples contain blue mottling within sphalerite, which is indicative of organic rich inclusions (Cavender, 2015).

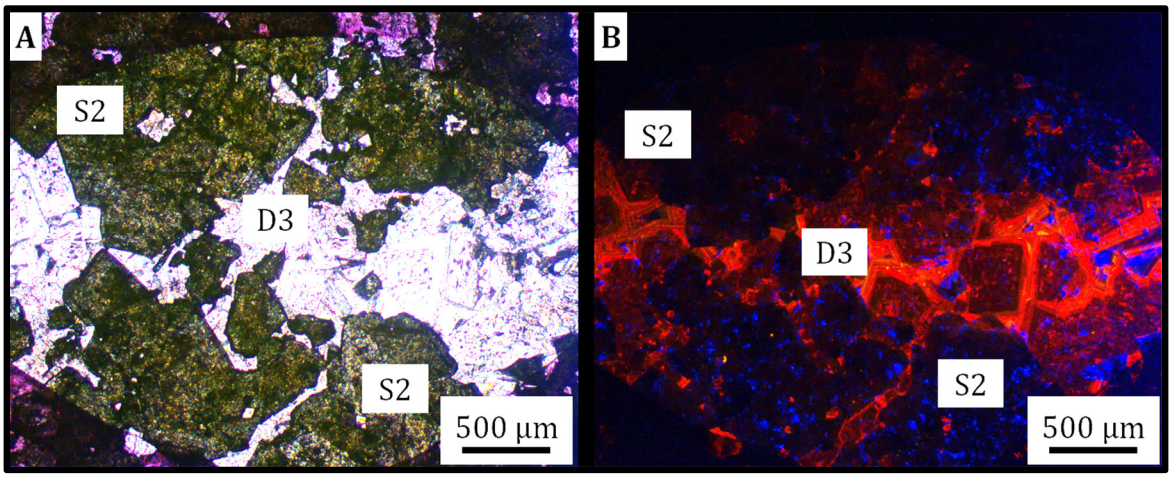

Figure 4.41: Late sphalerite (S2) with organic rich inclusions (blue), (sample Sweetwater 07, Sweetwater mine). A) PPL Image of sphalerite (S2) replacing D3 dolomite. B) CL image of same area.

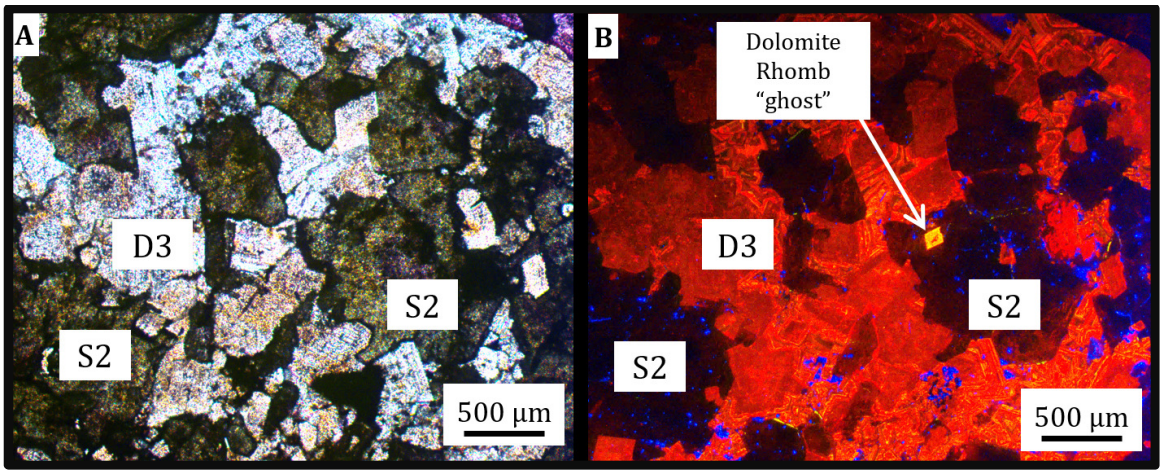

Figure 4.42: Late sphalerite (S2) with organic rich inclusions (blue)- Casteel Mine (sample 82V45) A) PPL Image of late sphalerite (S2) replacing late vein and vug filling dolomite (D3). B)CL Image of same area. Note the ghost of a grain of idiotopic dolomite rhomb (D3) which has been completely replaced by S2 sphalerite (center right of image).

Styolites in the stratiform replacement zone created zones of pre-existing weakness for later dolomitizing and mineralizing fluids to exploit. Figure 4.43 is an example of late dolomite (D3) which preferentially formed along a pre-existing zone of permeability created by a sub-horizontal styolite in a Sweetwater sample.

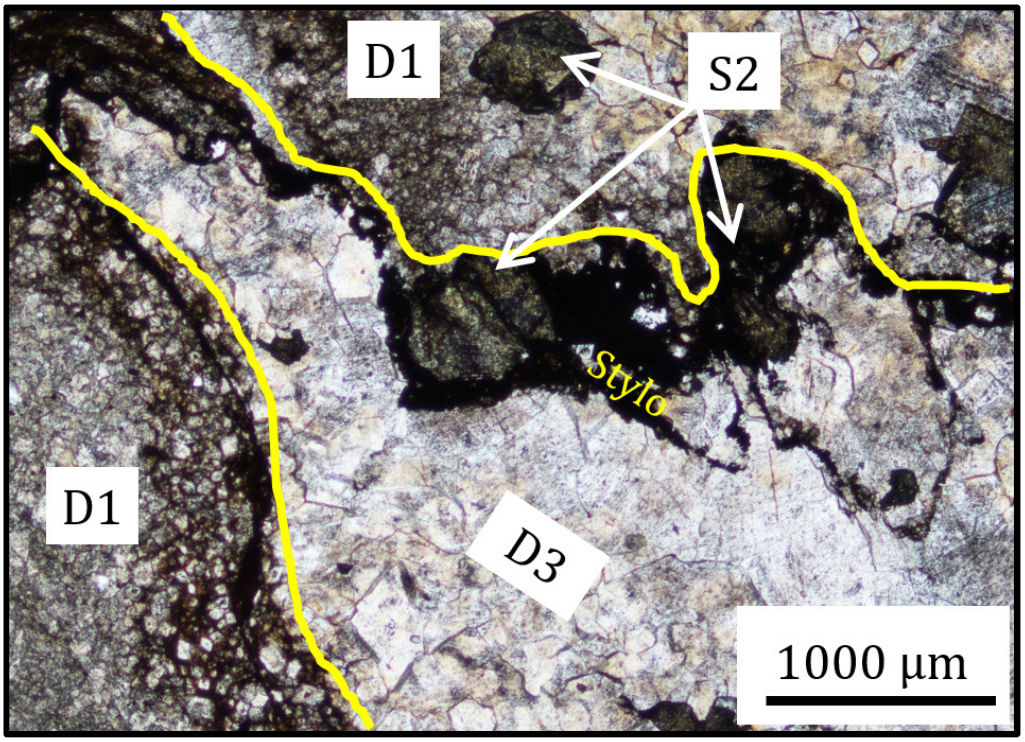

Figure 4.43: Pre-D3 Styolite with dolomite (D3) growing along the edges of the styolite plane (sample Sweetwater 02, Sweetwater mine).

4.4 Stable Isotopes

4.4.1 Bulk Carbon and Oxygen Isotopes

Bulk carbon and oxygen isotopic compositions were obtained from different dolomite textures in all 56 samples, while *in situ* SIMS data was collected on select representative barren and mineralized samples.

Samples were taken for the host dolomite (D1) as well as recrystallized dolomite (D2) and dolomite veinlets (D3). Some samples had no dolomite veinlets, so only the host dolomite (D1) or recrystallized dolomite (D2) in those samples were sampled. Most samples did not contain an identifiable recrystallized dolomite texture (D2) in hand sample, and the ones

which did were excluded from the dataset due to a poor analysis caused by high sulfide or iron concentrations (Section 3.6, p. 45). Some samples have more than one value (e.g. two values for host dolomite) because these samples were micro drilled two or three times within the same texture to assess intra-sample variability Table 4.2 shows the results of the intra-sample variability for D1 and D3 dolomites. Overall, the oxygen isotope variation within each sample is significant.

Table 4.2: Intra-Sample Variability of Oxygen Isotopes (VSMOW) D1 & D3 Dolomite Types.

Dolomite Generation	Avg. ‰ Difference	Min	Max	Count
D1	0.42	0.1	1.0	12
D3	0.45	0.1	0.9	14

Table 4.3 shows the carbon and oxygen isotopic data for unmineralized samples.

Table 4.3: Carbon and oxygen isotope data for host (D1) and dolomite veinlets (D3) from unmineralized drill core samples.

Sample	Dist. (ft) From Ugd. Workings (Ore Zones)	Dolomite Type	$\delta^{13}C$ - VPDB (‰)	$\delta^{18}O$-VSMOW (‰)	Mine
08DR3	2,203	Host Dol (D1)	1.01	22.59	Buick
89DR13	784	Host Dol (D1)	-0.33	22.00	Buick
93DR7	473	Host Dol (D1)	0.17	22.31	Buick
99DR7	201	Host Dol (D1)	-0.01	23.22	Buick
99DR7	201	Host Dol (D1)	0.08	22.28	Buick
58W32	611	Host Dol (D1)	-0.27	23.26	Casteel
82V69	642	Host Dol (D1)	-0.06	22.25	Casteel
LC-150	647	Host Dol (D1)	-0.32	22.23	Casteel
61W104	2,837	Host Dol (D1)	-0.29	22.45	Fletcher
61W29	2,336	Host Dol (D1)	-0.33	22.84	Fletcher
62W102	292	Host Dol (D1)	-0.31	21.72	Fletcher
64W67	764	Host Dol (D1)	-0.07	22.14	Fletcher
LC-486	2,893	Host Dol (D1)	0.71	25.34	Sweetwater
LC-499	2,200	Host Dol (D1)	0.46	21.96	Sweetwater
LC-584	1,695	Host Dol (D1)	-0.51	22.41	Sweetwater
LC-617	155	Host Dol (D1)	-1.31	23.38	Sweetwater
LC-681	1,419	Host Dol (D1)	0.49	26.06	Sweetwater
LC-710	2,101	Host Dol (D1)	-0.22	22.08	Sweetwater
93DR7	473	Veinlet (D3)	0.26	22.59	Buick
58W32	611	Veinlet (D3)	-0.12	22.98	Casteel
59W28	559	Veinlet (D3)	0.01	22.81	Casteel
82V69	642	Veinlet (D3)	-0.20	22.27	Casteel
LC-150	647	Veinlet (D3)	-3.67	23.27	Casteel
61W104	2,837	Veinlet (D3)	-1.67	21.83	Fletcher
61W29	2,336	Veinlet (D3)	-0.23	22.66	Fletcher
64W67	764	Veinlet (D3)	-0.22	22.91	Fletcher
73C26	288	Veinlet (D3)	-0.18	22.21	Fletcher
LC-486	2,893	Veinlet (D3)	1.43	25.91	Sweetwater
LC-498	3,960	Veinlet (D3)	-0.99	22.86	Sweetwater
LC-499	2,200	Veinlet (D3)	-4.61	23.59	Sweetwater
LC-584	1,695	Veinlet (D3)	2.18	21.96	Sweetwater
LC-617	155	Veinlet (D3)	-0.17	21.76	Sweetwater
LC-681	1,419	Veinlet (D3)	-0.20	24.32	Sweetwater
LC-710	2,101	Veinlet (D3)	-0.64	22.42	Sweetwater

Table 4.4 shows carbon and oxygen isotope data for mineralized samples.

Table 4.4: Carbon and oxygen isotope data for host dolomite (D1) and veinlet dolomite (D3) from mineralized underground samples.

Sample	Dolomite Type	$\delta^{13}C$ - VPDB (‰)	$\delta^{18}O$-VSMOW (‰)	Mine
Buick 03	Host Dol (D1)	-0.05	22.34	Buick
Buick 07	Host Dol (D1)	-0.42	22.25	Buick
Buick 07	Host Dol (D1)	-0.45	22.39	Buick
81V70	Host Dol (D1)	0.12	22.30	Casteel
Casteel 03	Host Dol (D1)	0.02	22.16	Casteel
Casteel 05	Host Dol (D1)	0.11	22.11	Casteel
Fletcher 01	Host Dol (D1)	0.03	22.32	Fletcher
Fletcher 02	Host Dol (D1)	-0.19	22.13	Fletcher
Fletcher 02	Host Dol (D1)	-0.30	22.08	Fletcher
Fletcher 03	Host Dol (D1)	0.05	21.74	Fletcher
Fletcher 03	Host Dol (D1)	0.04	21.81	Fletcher
Fletcher 04	Host Dol (D1)	-0.59	22.03	Fletcher
Fletcher 06	Host Dol (D1)	0.17	21.86	Fletcher
Fletcher 07	Host Dol (D1)	-0.33	22.35	Fletcher
Fletcher 07	Host Dol (D1)	-0.32	23.39	Fletcher
Sweetwater 01	Host Dol (D1)	-0.95	21.60	Sweetwater
Sweetwater 04	Host Dol (D1)	-0.60	22.11	Sweetwater
Sweetwater 05	Host Dol (D1)	-0.42	21.85	Sweetwater
Sweetwater 07	Host Dol (D1)	-0.18	22.19	Sweetwater
Sweetwater 08	Host Dol (D1)	-0.26	21.92	Sweetwater
Sweetwater 09	Host Dol (D1)	-0.11	22.20	Sweetwater
Sweetwater 10	Host Dol (D1)	0.09	21.76	Sweetwater
Buick 01	Veinlet (D3)	-0.07	22.39	Buick
Buick 01	Veinlet (D3)	-0.12	22.21	Buick
Buick 03	Veinlet (D3)	0.09	22.31	Buick
Buick 04	Veinlet (D3)	-0.31	22.40	Buick
Buick 04	Veinlet (D3)	-0.49	22.54	Buick
Buick 05	Veinlet (D3)	-0.21	22.40	Buick
Casteel 02	Veinlet (D3)	-0.21	22.97	Casteel
Casteel 04	Veinlet (D3)	0.04	22.22	Casteel
Casteel 05	Veinlet (D3)	0.18	22.41	Casteel
Casteel 08	Veinlet (D3)	0.04	21.97	Casteel
Fletcher 01	Veinlet (D3)	0.00	22.06	Fletcher
Fletcher 01	Veinlet (D3)	-0.06	22.18	Fletcher
Fletcher 03	Veinlet (D3)	-0.56	22.15	Fletcher
Fletcher 04	Veinlet (D3)	-0.90	22.63	Fletcher
Sweetwater 05	Veinlet (D3)	-0.52	22.16	Sweetwater
Sweetwater 06	Veinlet (D3)	-0.80	22.53	Sweetwater
Sweetwater 08	Veinlet (D3)	-0.16	22.47	Sweetwater
Sweetwater 09	Veinlet (D3)	-1.00	22.20	Sweetwater
Sweetwater 10	Veinlet (D3)	-0.78	21.50	Sweetwater

Overall, barren samples have a wide range in $\delta^{18}O$ values (21.8 to 26.1 ‰). $\delta^{18}O$ and $\delta^{13}C$ values do not correlate. The oxygen and carbon isotope values in the dolomite veinlets from barren samples have a wider variation than the host dolomite values (Figure 4.44).

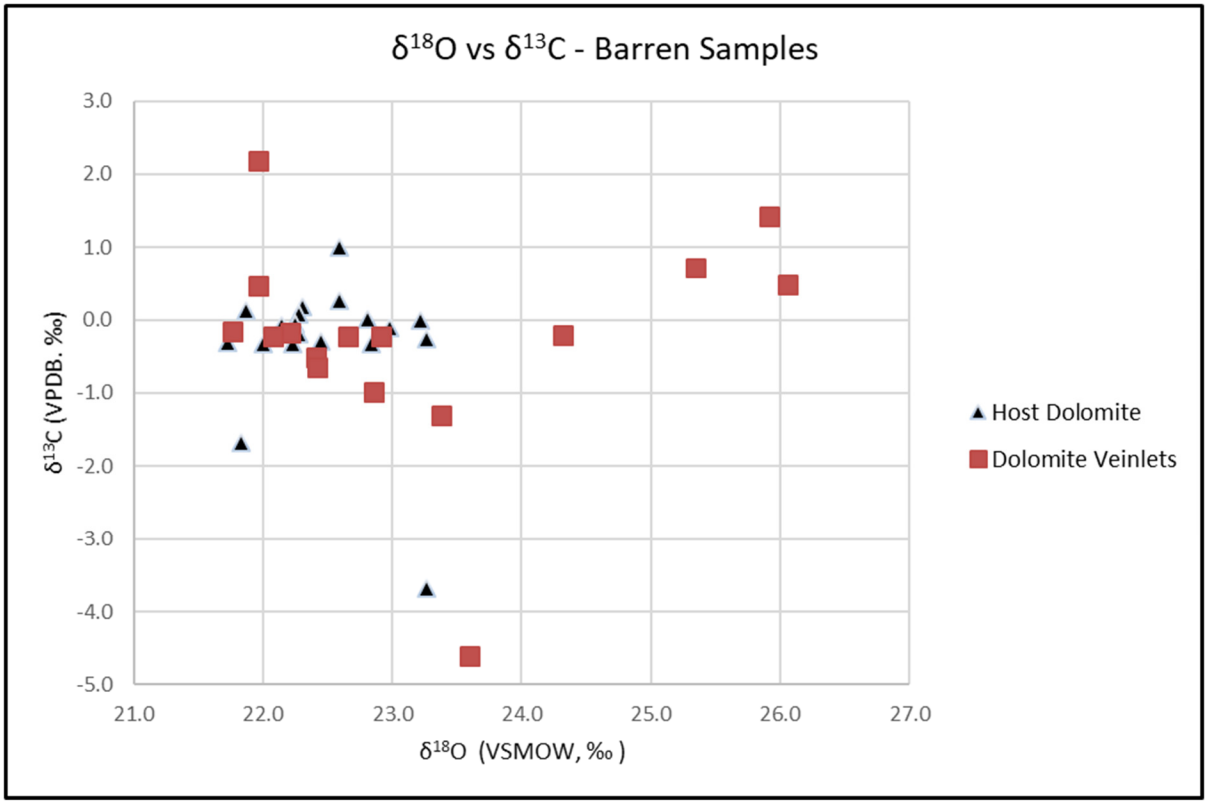

Figure 4.44: $\delta^{18}O$ vs. $\delta^{13}C$ values for dolomite from barren samples (data from Table 4.2)

The $\delta^{13}C$ and $\delta^{18}O$ values from mineralized samples also do not correlate (Figure 4.45). However, they do have a narrower range in $\delta^{18}O$ values (21.5 to 23.4 ‰) and $\delta^{13}C$ values (-1 to 0.2 ‰). While there is considerable overlap in the data for mineralized samples, dolomite veinlets (D3) display a shift towards higher $\delta^{18}O$ values compared with the host dolomite (D1) $\delta^{18}O$ values. In addition, the oxygen isotopes in the dolomite veinlets have

less variability than the host dolomites, which is opposite of what was observed for the barren values.

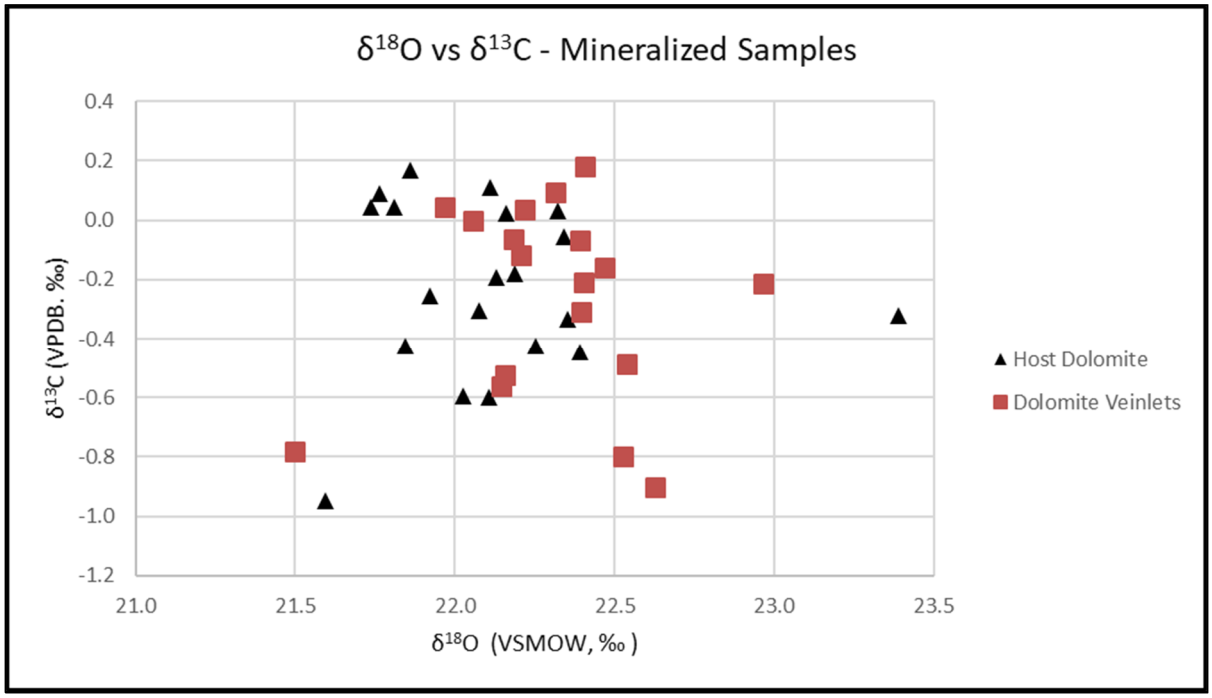

Figure 4.45 $\delta^{18}O$ vs. $\delta^{13}C$ values for dolomite from mineralized samples (data from Table 4.3)

4.4.1.1 Host Dolomite (D1)

Average oxygen isotopic compositions for host dolomites are summarized in Table 4.5. Overall, mineralized samples have lower $\delta^{18}O$ values compared with barren samples. In addition, the mineralized samples show a smaller standard deviation compared with the barren samples. For Buick and Fletcher, the differences in $\delta^{18}O$ values between barren and mineralized samples is subtle at 0.1-0.2 ‰. However, the difference in $\delta^{18}O$ values between barren mineralized samples from the Casteel and Sweetwater Mines is more significant.

Table 4.5: Average oxygen isotope values for host dolomite samples from mineralized and barren samples from the various mine areas.
Data is in per mil (‰) notation relative to Vienna Standard Mean Ocean Water (VSMOW).

Sample Type	Casteel	Buick	Fletcher	Sweetwater
Mineralized	22.19 ± 0.08 n=3	22.33 ± 0.06 n=3	22.19 ± 0.47 n=9	21.95 ± 0.21 n=7
Barren	22.58 ± 0.48 n=3	22.48 ± 0.41 n=4	22.29 ± 0.41 n=4	23.54 ± 1.61 n=6

D1 dolomite was sampled from drill core collected at various distances from the nearest mine workings (Figure 4.46). Overall, the oxygen isotope data for the host dolomites shows no correlation with distance from the mine workings.

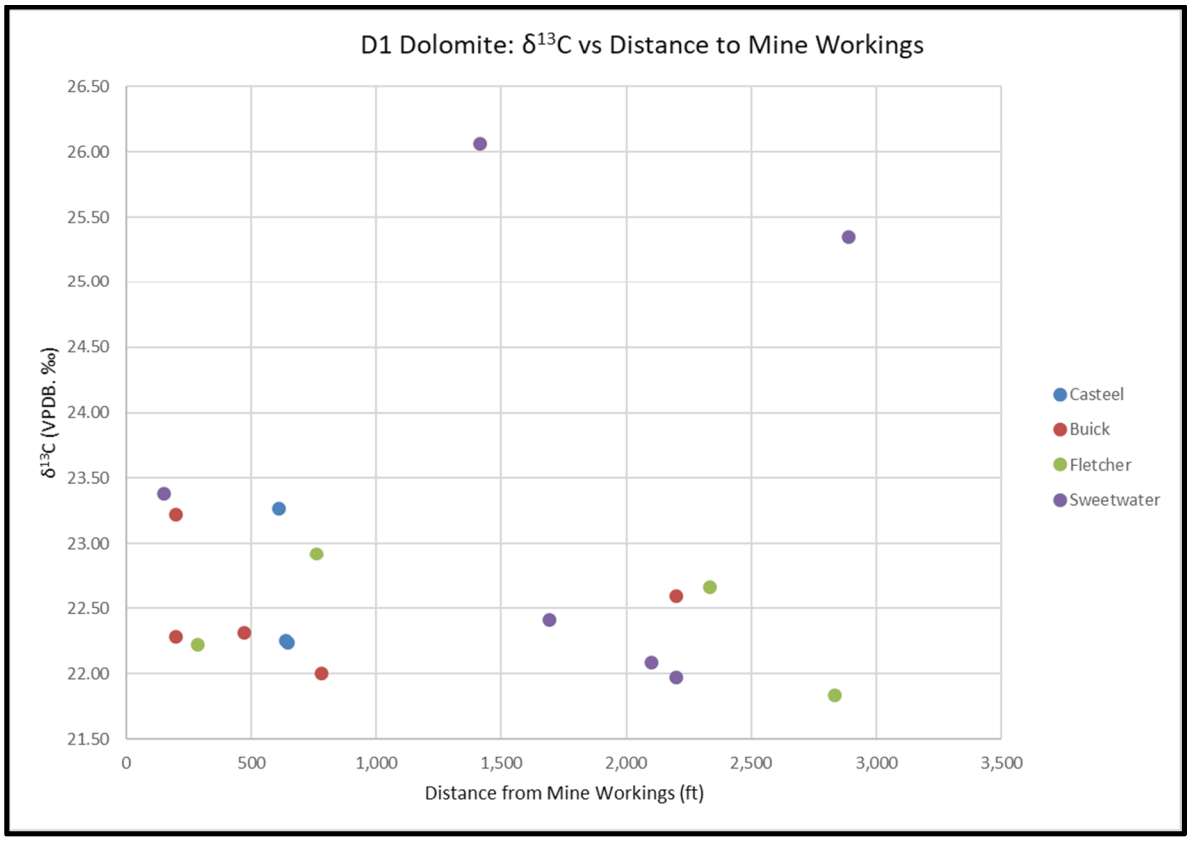

Figure 4.46: $\delta^{18}O$ values for barren host dolomite vs. distance from mineralization (Data from Table 4.3) .

Carbon isotope data for host dolomites are summarized in Table 4.6. The carbon isotope data also shows generally wider variation in data for barren samples.

Table 4.6: Average carbon isotope values for host dolomite samples from mineralized and barren samples.
Data is in per mil (‰) notation relative to Vienna Pee Dee Belemnite (VPDB).

Sample Type	Casteel	Buick	Fletcher	Sweetwater
Mineralized	0.09 ± 0.04 n=3	-0.31 ± 0.18 n=3	-0.16 ± 0.23 n=9	-0.35 ± 0.32 n=7
Barren	-0.22 ± 0.11 n=3	0.18 ± 0.44 n=4	-0.25 ± 0.11 n=4	-0.06 ± 0.70 n=6

The $\delta^{13}C$ values in host dolomite do not show any correlation with distance from mine workings (Figure 4.47).

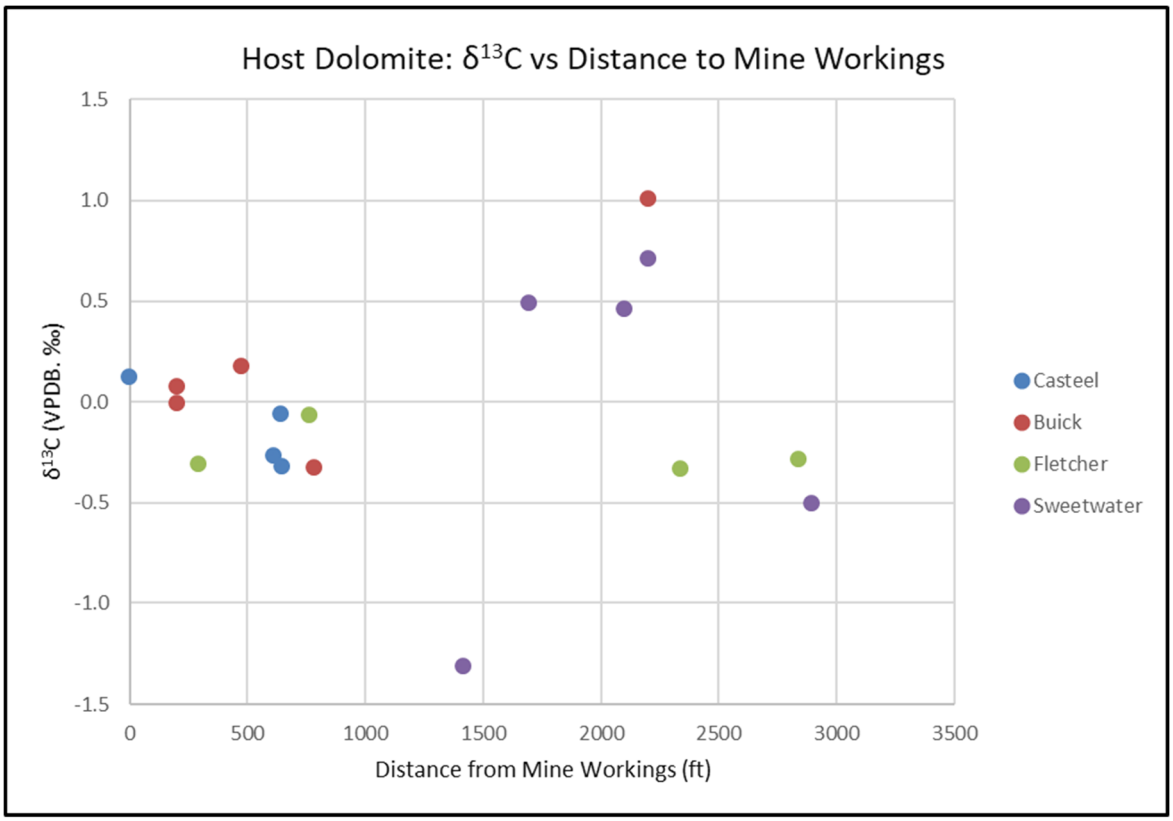

Figure 4.47: $\delta^{13}C$ values for barren host dolomite vs. distance from mineralization (data from Table 4.4)

4.4.1.2 Dolomite Veinlets (D3)

The average oxygen isotopic composition of dolomite veinlets (D3) is summarized in Table 4.7. Overall, the dolomite veinlets within the mineralized samples, much like the host dolomites, have lower $\delta^{18}O$ values relative to barren samples. The difference between mineralized and barren sample sets is small at Buick and Fletcher, but is more significant at

Casteel and Sweetwater, though is still within the range of error. The dolomite veinlets at Sweetwater, much like the host dolomites, display a large range of data.

Table 4.7: Average oxygen isotope values for dolomite veinlets.
Data is in per mil (‰) notation relative to Vienna Standard Mean Ocean Water (VSMOW).

Sample Type	Casteel	Buick	Fletcher	Sweetwater
Mineralized	22.39 ± 0.37 n=4	22.38 ± 0.10 n=6	22.25 ± 0.22 n=4	22.17 ± 0.37 n=5
Barren	22.83 ± 0.36 n=4	22.59 ± 0.05 n=1	22.40 ± 0.41 n=4	23.26 ± 1.37 n=7

Although there are minor differences in $\delta^{18}O$ values between barren and mineralized dolomite veinlets, there does seem to be a subtle trend of increasing $\delta^{18}O$ values with increasing distance from the mine workings for the Sweetwater and Fletcher mines and a slight decrease in $\delta^{18}O$ values with increasing distance for the Casteel mine (Figure 4.48). Isotopic data from Sweetwater is highly variable. The samples from the Buick mine only produced a single data point, so a trend for this mine could not be determined.

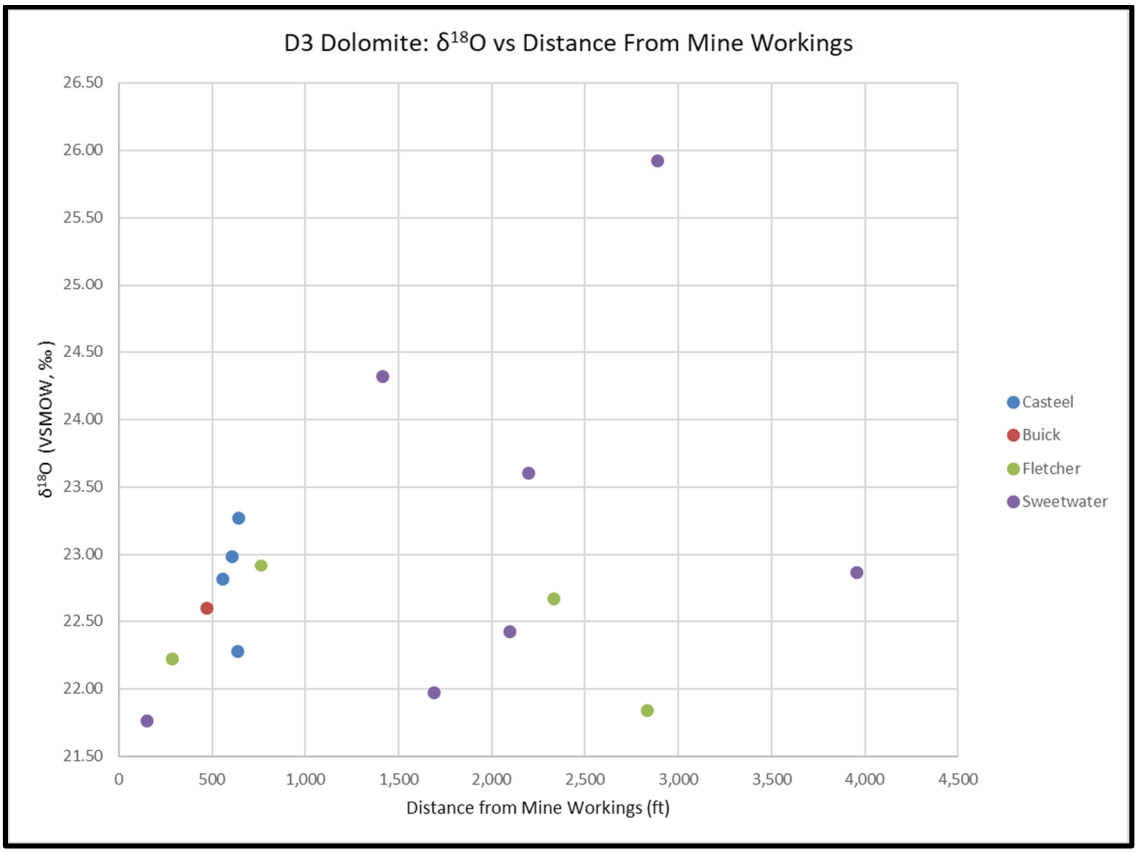

Figure 4.48: $\delta^{18}O$ values for barren dolomite veinlets vs. distance from mineralization (data from Table 4.5).

The average carbon isotopic composition of veinlets is summarized in Table 4.8. Similar to some of the previous bulk isotope results, the difference between $\delta^{13}C$ values for barren and mineralized samples is small. However, for mineralized samples, $\delta^{13}C$ values decrease from North to South (Casteel to Sweetwater).

Table 4.8: Average carbon isotope values for dolomite veinlets.
Data is per mil (‰) notation relative to Vienna Pee Dee Belemnite (VPDB).

Sample Type	Casteel	Buick	Fletcher	Sweetwater
Mineralized	0.01 ± 0.14 n=4	-0.18 ± 0.18 n=6	-0.38 ± 0.37 n=4	-0.65 ± 0.29 n=5
Barren	-1.00 ± 1.55 n=4	0.26 ± 0.10 n=1	-0.57 ± 0.64 n=4	-0.43 ± 2.01 n=7

For the Casteel mine, there is a slight overall decrease in $\delta^{13}C$ values with increasing distance from the mine, with a very weak correlation. None of the other mines display any meaningful trend. (Figure 4.49).

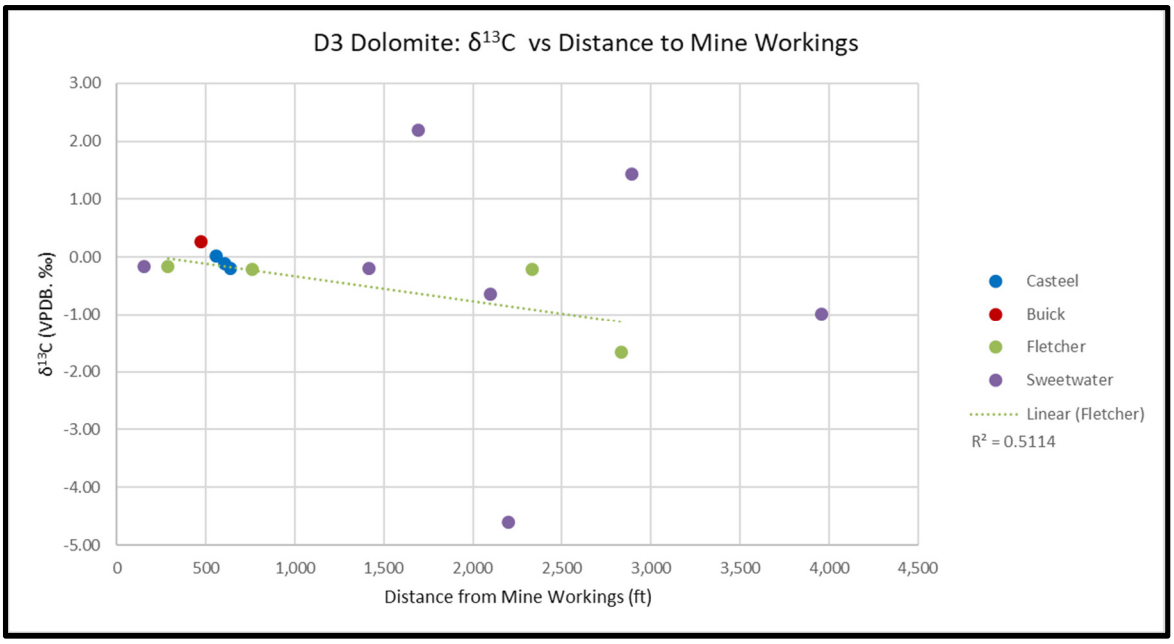

Figure 4.49: $\delta^{13}C$ of barren dolomite veinlets vs. distance to mine workings

4.4.1.3 Dolomite Veinlet Spatial Analysis

The oxygen isotope values were plotted and compared with results from the underground samples in the following section. Since micro drilled oxygen isotope and all carbon isotope values for the D1 assemblage show no relationship with mineralization, only oxygen isotope data for dolomite veinlets (D3) were plotted.

The map of isotope values for the Casteel area shows no relationship with the oxygen isotope values for D3 dolomite as the samples move further away from the mine workings (Figure 4.50).

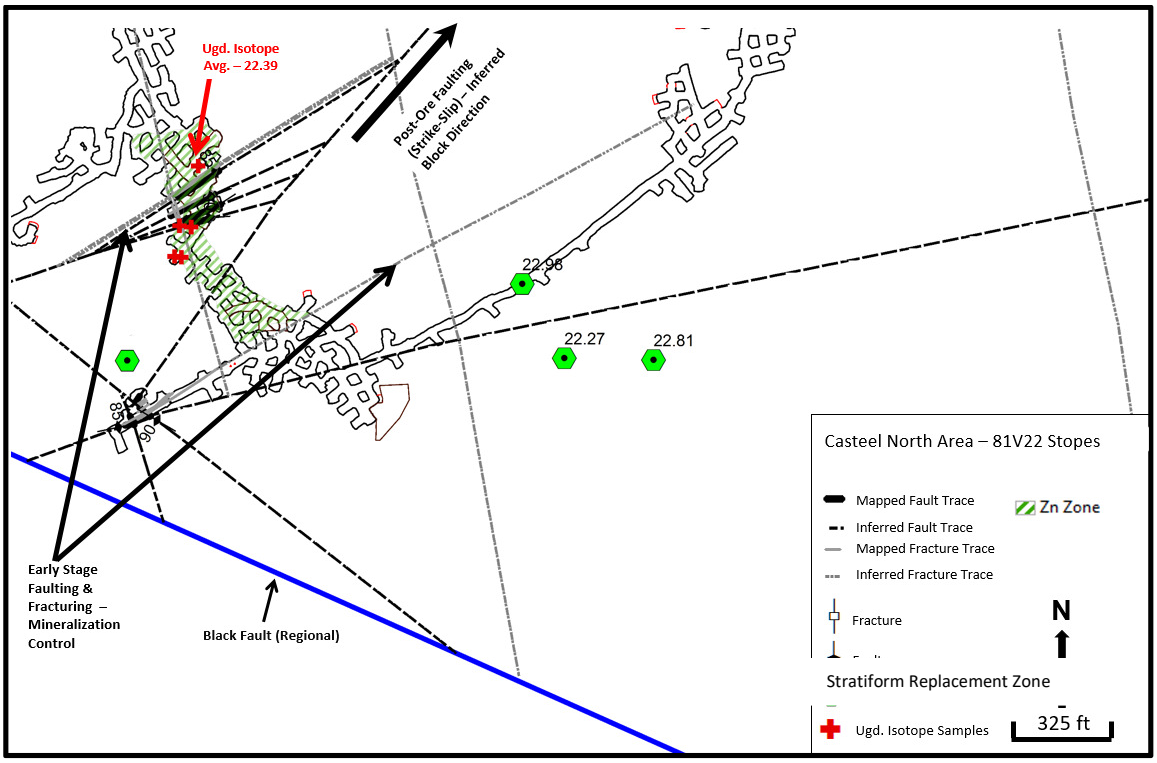

Figure 4.50: Casteel oxygen isotope (D3) map.

The map of oxygen isotope values for the Buick 93DRV3 stope has very little information available, but does show a small slight difference in the single sample with a value. The lack

of data points for the drill core samples (green hexagons) is due to the lack of D3 veinlets in the available drill core samples (Figure 4.51).

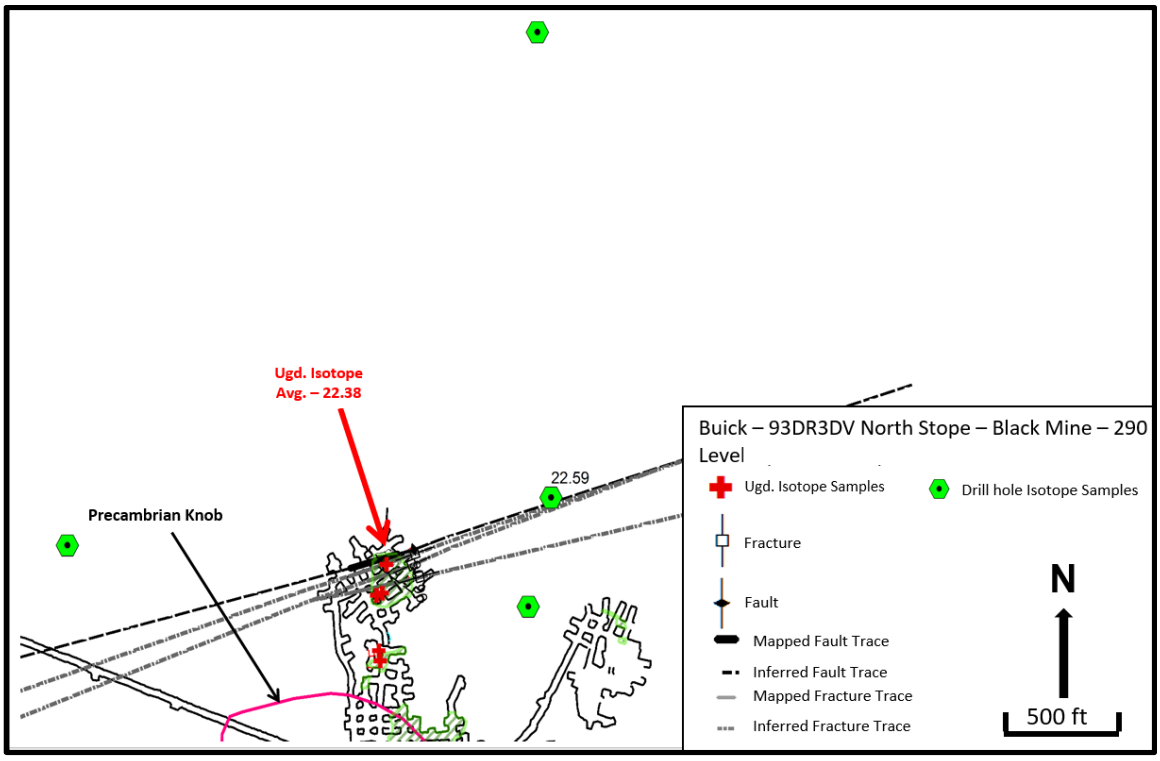

Figure 4.51: Buick 93DRV stope oxygen isotope (D3) map.

Isotope data for the J3UC stope at Fletcher is displayed in Figure 4.52. There is no relationship between the distance of the samples and the oxygen isotope values in the drill core samples.

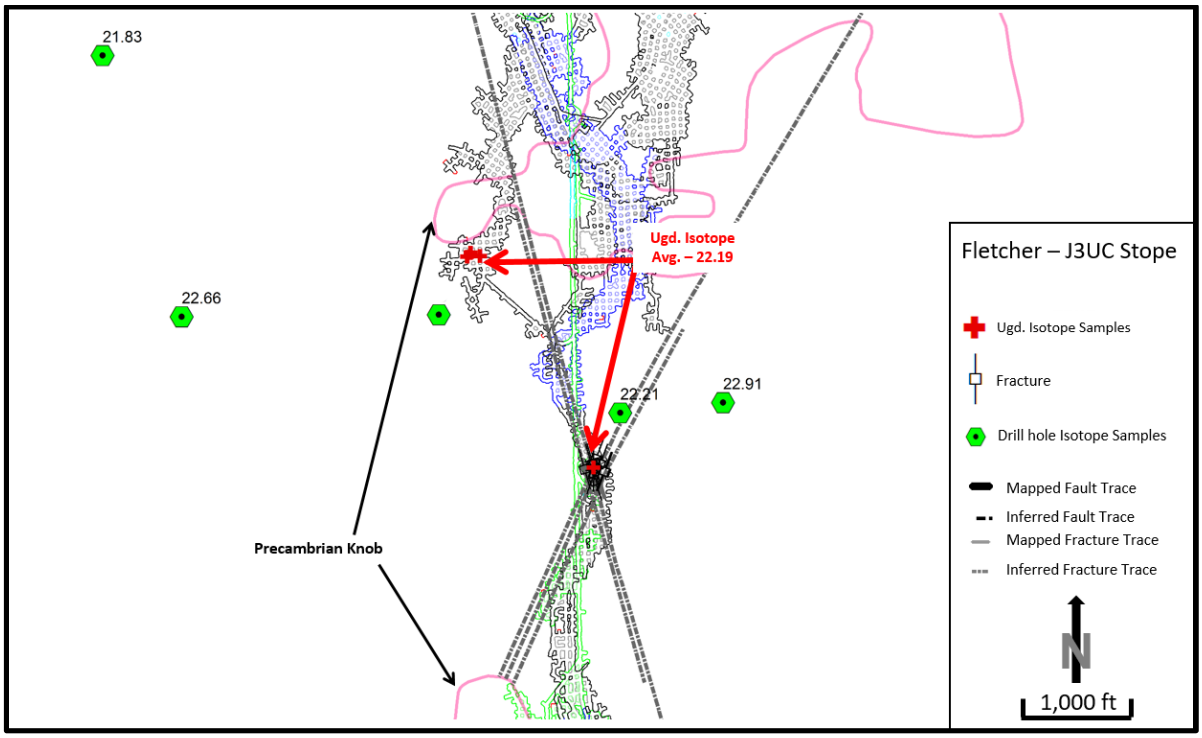

Figure 4.52: Fletcher J3UC oxygen isotope (D3) map.

Figure 4.53 shows the oxygen isotope values at Sweetwater from drill core samples compared with the underground sample locations. There is no relationship between the spatial location of the samples and the proximity to the SRZ.

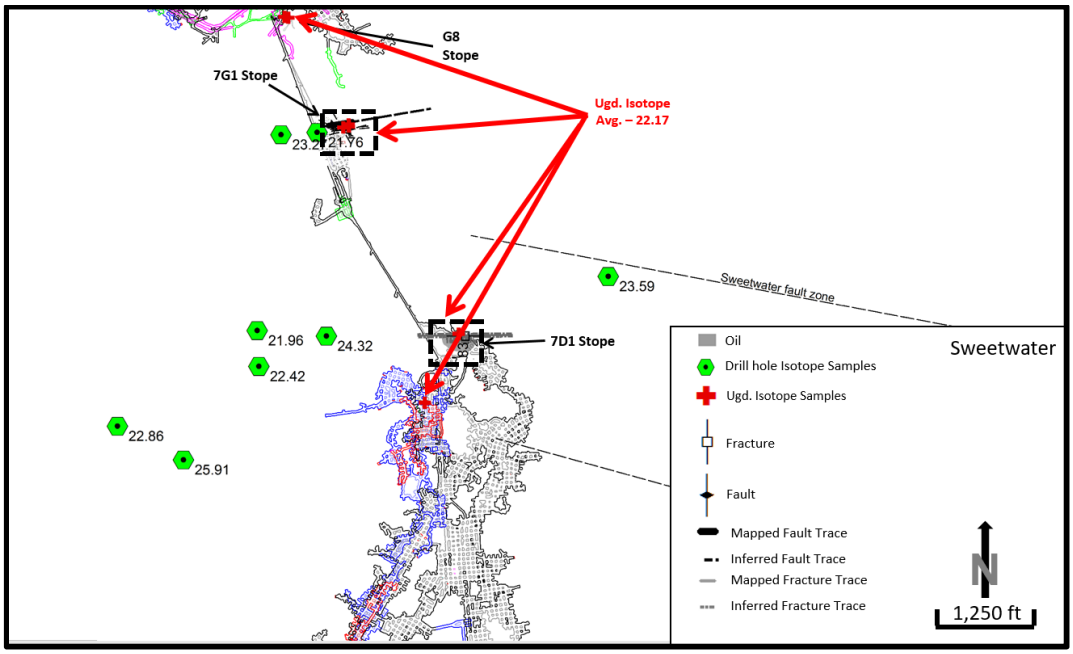

Figure 4.53: Sweetwater oxygen isotope (D3) map.

4.4.2 Secondary Ion Mass Spectrometry Isotope Data (SIMS)

Selected samples were analyzed for oxygen isotopes in dolomites using SIMS. The three main textures of dolomite analyzed using SIMS were: 1) hydrothermal dolomite veinlets and vugs (D3), 2) recrystallized dolomite (not in veinlets or vugs) (D2) and 3) host dolomite with no recrystallization textures (D1). Due to the small, thin section scale of the SIMS analysis, consistently identifying and analyzing recrystallized dolomite (D2) was possible, in contrast with the hand samples. It was not possible to consistently identify the D2 texture in hand samples due to its fine grain size.

Overall, the host dolomite shows the highest variability and has an average $\delta^{18}O$ value of 22.4 ‰ and a range from 19.8 to 24.7‰. Dolomite veinlets (D3) have an average value of 22.9 ‰ and a narrower range from 22.1 to 24.0‰. Recrystallized dolomite (D2) has the lowest average $\delta^{18}O$ value (21.8 ‰) with an overall range of 21.1 to 22.1 ‰ (Table 4.9).

Table 4.9: Oxygen isotopic composition averages of various dolomite textures obtained using SIMS. Samples in green are mineralized, while the others are barren.

Sample	Dolomite Type	$\delta^{18}O$-Avg. (‰)	Range	# of Analyses
Buick 03	Host Dolomite - D1	24.73	n/a	1
Buick 06	Host Dolomite - D1	23.26	n/a	1
Casteel - 60W117	Host Dolomite - D1	22.00	16.8 - 27.4	3
Casteel 82V69	Host Dolomite - D1	19.76	18.8 - 20.5	3
Casteel-82V45	Host Dolomite - D1	23.59	21.6 - 24.8	3
Fletcher 04	Host Dolomite - D1	24.10	22.4 - 25.8	2
Fletcher 06	Host Dolomite - D1	19.81	19.4 - 20.2	2
Sweetwater 03	Host Dolomite - D1	23.98	n/a	1
	Average	**22.65**		
	Total Range	**10.60**		
Buick 06	Dolomite Veinlet - D3	22.60	17.2 - 25.6	3

Casteel 82V69	Dolomite Veinlet - D3	24.03	22.5 - 25.0	4
Sweetwater 04	Dolomite Veinlet - D3	22.10	21.6 - 22.9	3
	Average	**22.91**		
	Range	**8.40**		
Casteel 04	Recrystallized Dolomite - D2	22.10	18.6 - 27.0	6
Casteel-82V45	Recrystallized Dolomite - D2	22.12	20.1 - 24.2	2
Fletcher 04	Recrystallized Dolomite - D2	21.10	20.4 - 21.8	2
Sweetwater 03	Recrystallized Dolomite - D2	21.79	19.4 - 25.1	6
	Average	**21.78**		
	Total Range	**7.60**		

Figure 4.54 (A) shows a thick section of a barren sample of host dolomite that is cut by a dolomite veinlet (D3) with the corresponding micro-drilled oxygen isotope values. Figure 4.54 (B) shows the corresponding thin section in plane polarized light with the SIMS $\delta^{18}O$ values from the same hydrothermal dolomite veinlet, and Figure 4.54 (C) shows the corresponding CL image. This figure shows that there is significant variation on the micron scale in both the D1 and D3 dolomite types. In addition, it shows that the D1 dolomite has more variation than the D3 dolomite isotope values.

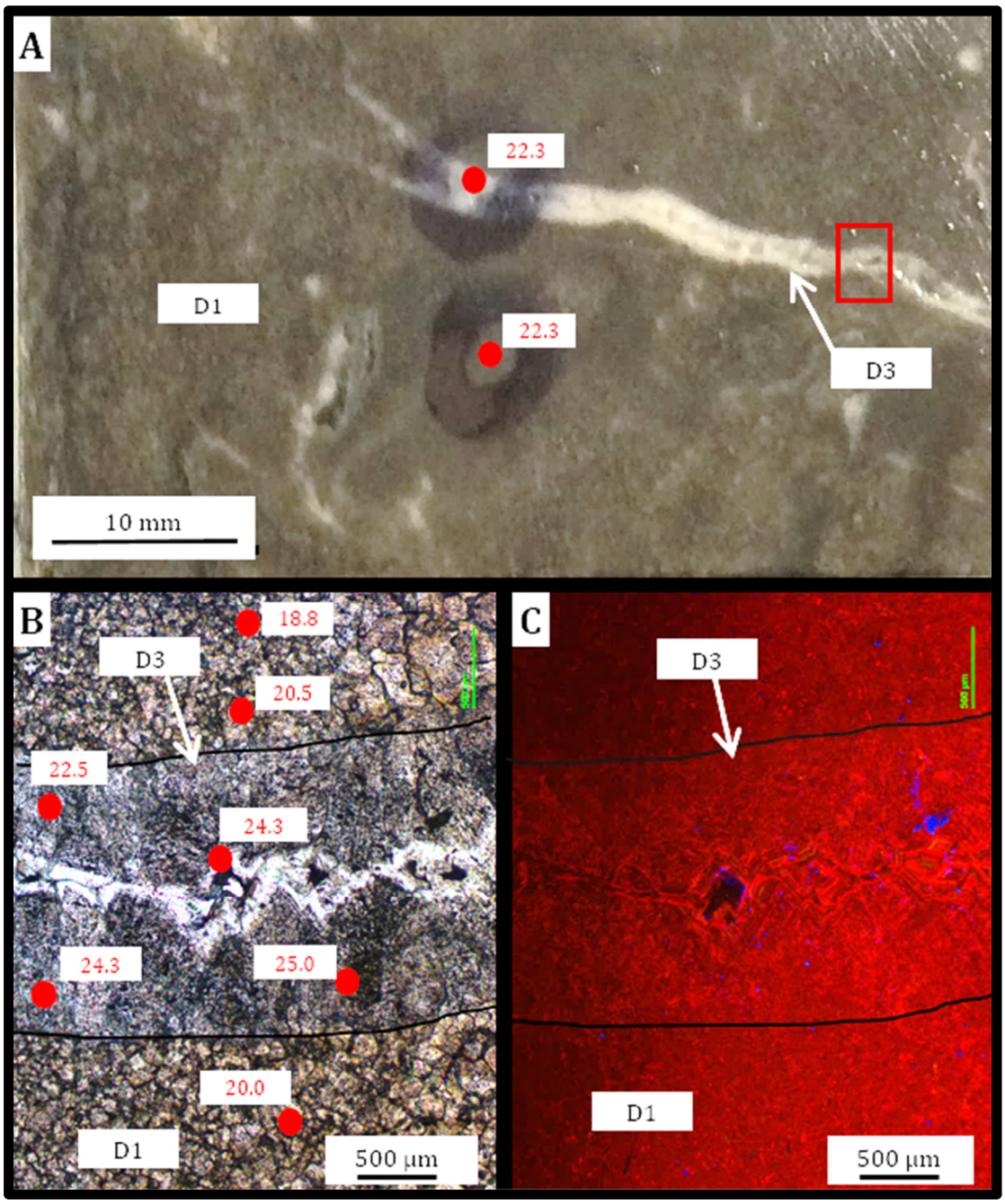

Figure 4.54: Micro drilled and SIMS analysis points for sample 89V64 (unmineralized) (Casteel mine).
A) Thick Section showing micro drilled analysis points and data, recrystallized dolomite veinlet (D3) cuts host dolomite (D1). Inset in center right is the location of the thin section images shown in B and C. B) Portion of a thin section showing SIMS analysis points and data. Recrystallized veinlet (D3) shows oxygen isotope variation within different generations of dolomite cement, but has less $\delta^{18}O$ variation than the host dolomite (D1). C) Cathodoluminescent image of the same area from B. While

most of the dolomite in this image is luminescent, the recrystallized veinlet (D3) shows banding within the cement which is similar to the cement types as defined by Voss et al. (1989).

4.4.2.1 Sulfur Isotopes in Sphalerite

The sulfur isotopic composition of sphalerite was measured using SIMS in key samples to compare the values with previous studies. Table 4.10 shows $\delta^{34}S$ values for sphalerite with different textures (replacement vs colloform), along with dolomite textures in proximity to the sphalerite.

Table 4.10: SIMS Summary Data for $\delta^{34}S$ of Sphalerites in the Stratiform Replacement Zone

Sample	Sphalerite Texture	Avg. $\delta^{34}S$ (‰)	Range (‰)	# of Analyses
60W117	Replacement	14.8	10.5 - 19.1	10
Buick 06	Colloform	15.2	11.9 - 18.6	8
Sweetwater 07	Replacement	12.2	10.7 - 13.8	6
Buick 03	Replacement	12.8	7.9 - 15.8	11
Fletcher 06	Colloform	11.4	6.4 - 17.8	6
Sweetwater 03	Replacement	13.4	10.4 - 15.1	2
	Average	**13.3**		
	Total Range	**12.7**		

Table 4.11 shows point SIMS data for sulfur in sphalerites. Significant variation is observed for all late stage sphalerites (S2) at the thin section scale.

Table 4.11: SIMS point data for $\delta^{34}S$ of sulfur within late stage sphalerite (S2)

Sample-Analysis Point	$\delta^{34}S$ (‰)	1σ	Mine
60W117 Spot 3 Pt 1	12.3	0.3	Casteel
60W117 Spot 3 Pt 2	13.1	0.3	Casteel
60W117 Spot 3 Pt 3	13.2	0.3	Casteel
60W117 Spot 3 Pt 4	10.5	0.3	Casteel
60W117 Spot 2 Pt 1	17.2	0.3	Casteel
60W117 Spot 2 Pt 2	16.8	0.3	Casteel
60W117 Spot 2 Pt 3	15.3	0.3	Casteel
60W117 Spot 1 Pt 1	19.3	0.3	Casteel
60W117 Spot 1 Pt 2	15.8	0.3	Casteel
60W117 Spot 1 Pt 3	14.8	0.3	Casteel
Buick 6 Spot 1 Pt 1	17.4	0.3	Buick
Buick 6 Spot 1 Pt 2	15.3	0.3	Buick
Buick 6 Spot 1 Pt 3	17.1	0.3	Buick
Buick 6 Spot 1 Pt 4	11.9	0.3	Buick
Buick 6 Spot 1 Pt 5	15.2	0.3	Buick
Buick 6 Spot 1 Pt 6	13.8	0.3	Buick
Buick 6 Spot 1 Pt 7	12.4	0.3	Buick
Buick 6 Spot 1 Pt 8	18.6	0.3	Buick
Buick 03 Spot 2 Pt 1	13.8	0.3	Buick
Buick 03 Spot 2 Pt 2	18.6	0.3	Buick
Buick 03 Spot 2 Pt 3	14.8	0.3	Buick
Buick 03 Spot 4 Pt 1	12.6	0.3	Buick
Buick 03 Spot 4 Pt 2	11.2	0.3	Buick
Buick 03 Spot 4 Pt 3	7.9	0.3	Buick
Buick 03 Spot 4 Pt 4	11.0	0.3	Buick
Buick 03 Spot 4 Pt 5	15.8	0.3	Buick
Buick 03 Spot 2 Pt 1	13.0	0.3	Buick
Buick 03 Spot 2 Pt 2	11.4	0.3	Buick
Buick 03 Spot 2 Pt 3	10.5	0.3	Buick
Sweetwater 03 Spot 1 Pt 1	14.6	0.3	Sweetwater
Sweetwater 03 Spot 1 Pt 2	10.4	0.3	Sweetwater
Sweetwater 03 Spot 1 Pt 3	15.1	0.3	Sweetwater
Sweetwater 03 Spot 3 Pt 1	14.3	0.3	Sweetwater

Sweetwater 03 Spot 3 Pt 2	9.8	0.3	Sweetwater
Sweetwater 07 Spot 2 Pt 1	11.9	0.3	Sweetwater
Sweetwater 07 Spot 2 Pt 2	11.3	0.3	Sweetwater
Sweetwater 07 Spot 2 Pt 3	12.9	0.3	Sweetwater
Sweetwater 07 Spot 2 Pt 4	13.8	0.3	Sweetwater
Sweetwater 07 Spot 2 Pt 5	12.4	0.3	Sweetwater
Sweetwater 07 Spot 2 Pt 6	10.7	0.3	Sweetwater
Fletcher 06 Spot 2 Pt 1	8.4	0.3	Fletcher
Fletcher 06 Spot 2 Pt 2	10.8	0.3	Fletcher
Fletcher 06 Spot 2 Pt 3	6.4	0.3	Fletcher
Fletcher 06 Spot 2 Pt 4	9.0	0.3	Fletcher
Fletcher 06 Spot 2 Pt 5	17.8	0.3	Fletcher
Fletcher 06 Spot 2 Pt 6	15.9	0.3	Fletcher

A colloform sample from the Buick Mine shows total variation in $\delta^{34}S$ values of 5.2 ‰ for late stage (S2) colloform sphalerite. The values oscillate back and forth from the center of the crystal to the outer rim (Figure 4.55).

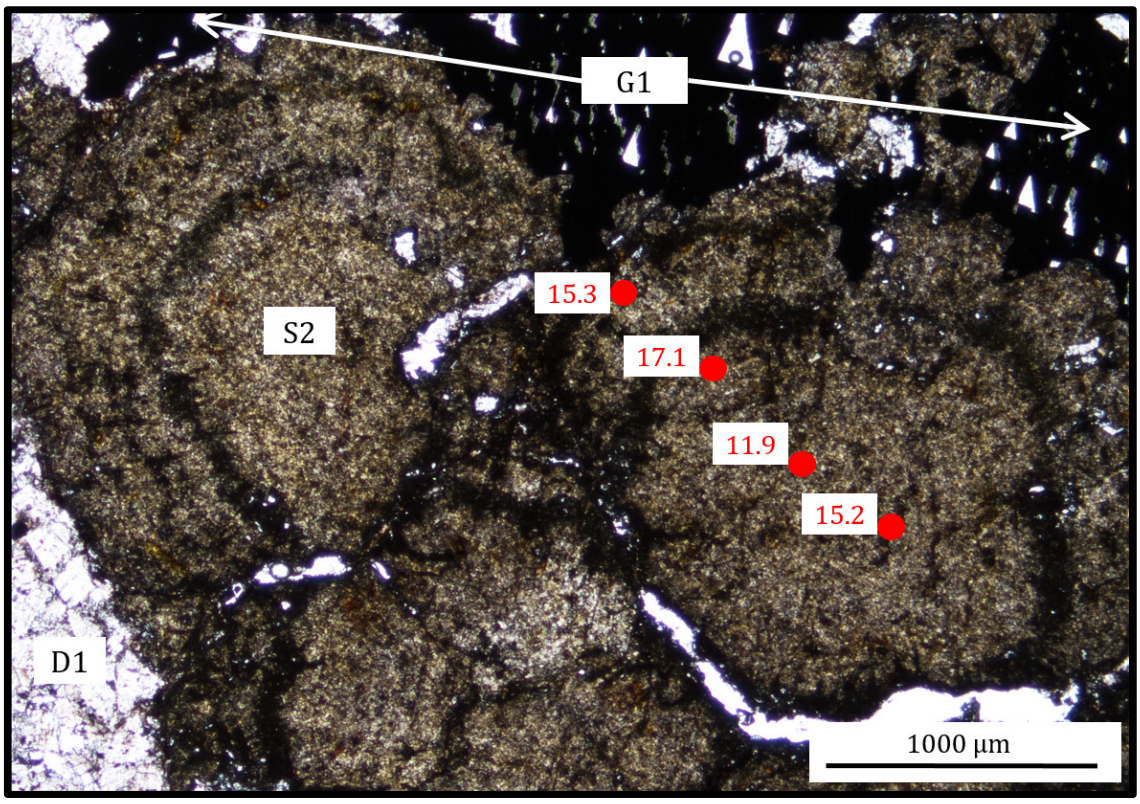

Figure 4.55: $\delta^{34}S$ values of late sphalerite (S2) from the Buick mine (sample Buick 06). data from Table 4.10.

$\delta^{34}S$ values for colloform sphalerite from the Fletcher Mine (Figure 4.56) show late sphalerite (S2) is complex and with a fluid history which evolved through time.

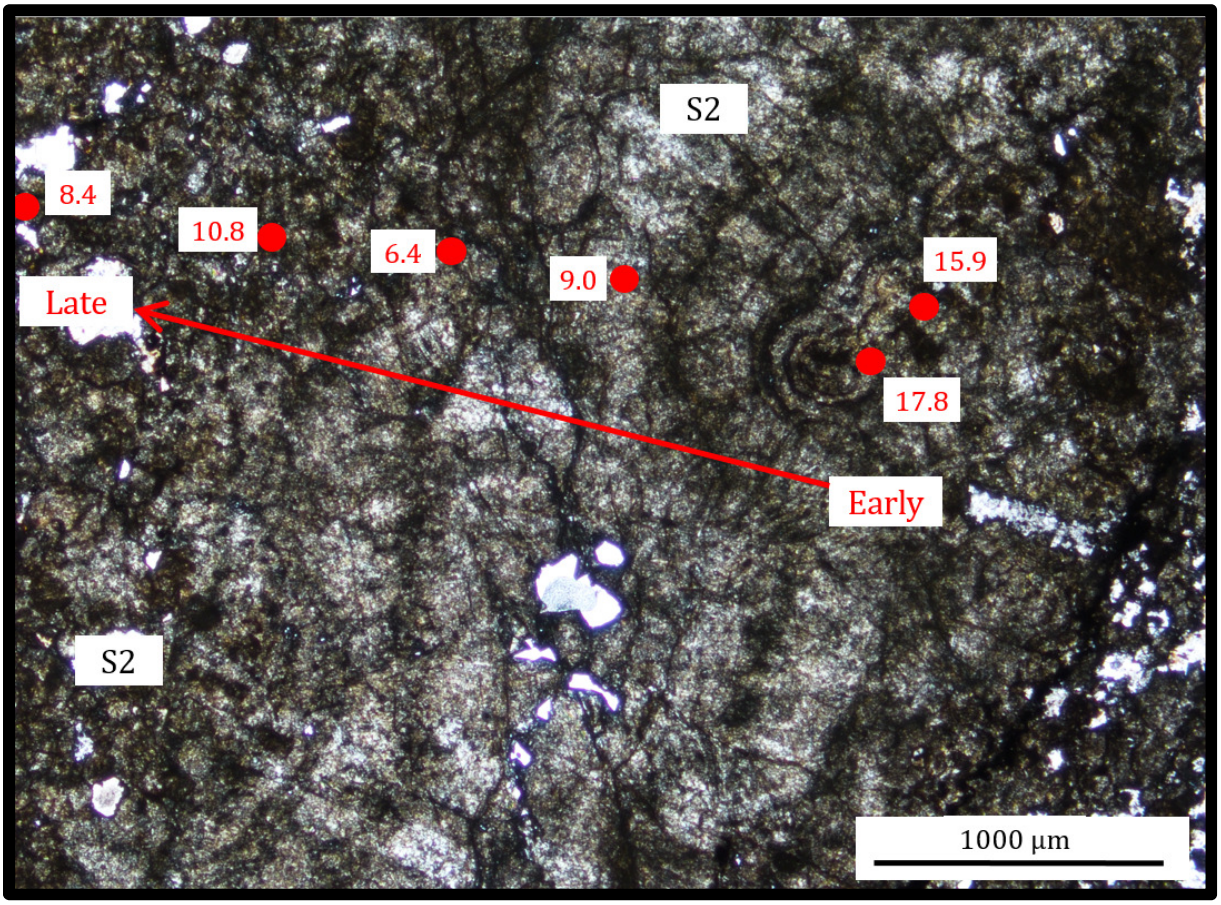

Figure 4.56: SIMS Data for $\delta^{34}S$ of late stage (S2) sphalerite at Fletcher mine. Data is from Table 4.11

Chapter 5: **Discussion**

5.1 Dolomite Textures & Geologic Relationships

Dolomite textures are variable and multiple dolomite textures can occur at the thin section scale within the same sample. These variations in dolomite crystal size and shape in the Stratiform Replacement Zone of the Viburnum Trend are controlled by 1) original depositional facies, 2) recrystallization due to diagenesis from different burial and exhumation events and 3) recrystallization related to hydrothermal fluids (Lyle, 1977; Gregg, 1985; Tobin, 1991; Gregg *et al.*, 1993).

Variation in host dolomite (D1) crystal size is substantial, with this texture representing multiple burial and exhumation events. These burial events preceded early galena and sphalerite (G1 & S1 in this study) (Tobin, 1991). Several samples contain late stage dolomite (D3), which appear along one side of a styolite (Figure 4.43, p. 101). This association was identified by Lyle (1977) and interpreted to be the result of early styolites themselves affecting the flow path of later dolomitizing fluids. They may have focused certain mineralizing fluids (in addition to the dolomitizing fluids), which could have resulted in one side of the styolites becoming more dolomitized than the other (Lyle, 1977).

Both Gregg (1985) and Tobin (1991) linked specific dolomite textures to lithology as well as stratigraphic position within the Bonneterre Formation. They suggested that the medium to large crystalline xenotopic dolomite texture was associated with the lower sections and the stromatlitic (reef) part of the Bonneterre Formation. The idiotopic-coarsely crystalline dolomite cement was linked with upper Bonneterre Formation and oolitic dolomite. The Stratiform Replacement Zone exclusively occurs in the upper

Bonneterre Formation within oolitic dolostone, but also occurs in micrite and other carbonate textures associated with other depositional zones. Therefore, the link between dolostone texture and stratigraphy is not valid for the Stratiform Replacement Zone.

The absence of consistent and correlatable dolomite cements of Voss et al. (1989) within the D2 or D3 generations of dolomite in this study could be evidence that the Stratiform Replacement Zone is unique and was subjected to different fluid dynamics than other areas on the Viburnum Trend. This is also indicated by the relationship of late stage euhedral quartz which is intergrown with sphalerite, which was observed underground and in hand samples at Sweetwater and Casteel. While sphalerite was never observed growing in vugs with a late generation of sphalerite in previous studies, late state quartz was observed replacing galena and marcasite at the Magmont West mine, as well as cementing certain mineralized breccias. This late stage quartz was deposited at approximately the same time as etching textures, which were interpreted to be part of a spatially broad leaching zone (Hagni & Trancynger, 1977). Geologic observations underground, combined with petrography indicate that the D3 dolomite generation is a long lived fluid event, with some aspects of the fluid intergrowing with S2 sphalerite.

5.2 Sphalerite Chemistry

Sphalerite in hand samples is homogenous in color, with only three varieties identified (brown, green and yellow). These colors correlate with different paragenetic stages of sphalerite identified in hand sample and thin section, with brown sphalerite being early (S1) and the green and yellow sphalerites being late (S2). Although there is some correlation in Fe and Cd concentrations with color at the thin section scale, there is no

correlation with colors of sphalerite in hand samples and color variation found in thin sections. All sites across the SRZ have similar variation of Cd and Zn level within sphalerite.

First, the early brown sphalerite (S1) was deposited at the same relative time as the main stage galena (S1) (both consistent with main stage mineralization). This was then leached and later replaced by a sphalerite generation (S2) which evolved through time in an open system. These fluids were constrained vertically within specific impermeable dolostone beds in the Bonneterre Formation, and shared a common fluid source as other late stage fluids, especially the Tri-State, Northern Arkansas and Central Missouri districts. The geochemistry of the sphalerite samples throughout this zone suggests that the S2 mineralizing fluids are generally homogenous and are likely the same generation throughout the entire 25 mile section of the SRZ. This data is consistent with the results from previous authors which demonstrated that chemical differences in sphalerite mineralization was related to the vertical position within the Bonneterre Formation, and that these differences were linked to differences in regional mineralizing fluid sources (Viets *et al.*, 1992; Cavender, 2015).

The Cd and Fe concentrations in late sphalerite (S2) from the SRZ are similar to concentrations in late stage mineralization from the, Tri-State, Central Missouri and Northern Arkansas mineral districts, with an average of 0.9% Cd and 0.7% Fe. This geochemical similarity suggests that the S2 sphalerite (the most volumetrically abundant sulfide in the SRZ) was related to other late stage galena and sphalerite rich fluids, which were sourced from a distinct sedimentary basin compared with the main stage fluids (Viets *et al.*, 1992; Fennel *et al.*, 1996).

5.3 Stable Isotopes

The lack of correlation of the carbon and oxygen isotopes as well as the overall high variability in oxygen isotopes outside of the mineralized zone in the SRZ is interpreted to be the result of several factors, including; 1) low water:rock ratios, 2) lack of dolomite recrystallization in association with the volumetrically dominant S2 sphalerite and 3) inadvertent inclusion of D2 dolomite within the D1 samples during micro drilling.

While there is some evidence from other MVT deposits which demonstrate comparatively low temperature mineralizing fluids can contribute to high variability (Fritz, 1969), it is unlikely that this alone is the cause of the scatter in isotope data from the unmineralized area within the SRZ. This is indicated by other stratiform MVT and SEDEX deposits which had similar or lower temperatures (70 - 130 °C), but showed a discrete halo of oxygen isotope values within recrystallized dolomite around mineralization (Pinckney & Rye, 1972; Savard *et al.*, 2000; Large *et al.*, 2001).

It is equally unlikely that the isotopic composition of the original mineralizing fluid contributed to the variability observed in this zone, because work has established that the original mineralizing fluids which dominated the SRZ were sourced from a separate basin, such as the Illinois or Forest City basins. These basins contain typical sedimentary brines with values which would have been similar to other deposits, such as the deposits in Northwestern Wisconsin, which showed strong oxygen isotope fractionation within recrystallized dolomites in association with mineralization (Pinckney & Rye, 1972; Taylor, 1974; Shelton *et al.*, 2009).

Most other MVT deposits contain open space filling as the dominant mode of mineralization, with vugs, faults and fractures being the primary source of mineralizing fluids (Heyl *et al.*, 1974). While it is clear that mineralization within the SRZ is also influenced significantly by certain early faults and fractures, petrographic work completed in this study has demonstrated that there is almost no dolomite recrystallization associated with the volumetrically abundant S2 sphalerite within the SRZ. This is markedly different from most other MVT deposits, where abundant calcite and dolomite recrystallization associated with mineralization is obvious on the hand sample scale. Distinct isotopic halos around mineralization in these deposits is usually limited to areas where visible recrystallization of the wall rock has occurred (Fritz, 1969; Pinckney & Rye, 1972). The dominant mechanism of sulfide deposition in the SRZ is replacement, which is a major reason why there is no clear, definable oxygen isotope depletion halo around mineralization.

A lack of correlation between carbon and oxygen isotopes in host dolomite along with carbon isotope values of (-2 to +1) (PDB) was used as evidence for local recycling of fluids in a closed system. The carbon source was organic rich, and was likely derived from oil field brines in the Upper Mississippi Valley Zinc District in Wisconsin (Hall & Friedman, 1969). While there are abundant organic rich styolites in the SRZ, the $\delta^{13}C$ values from the mineralized host dolomites (-0.8 to +0.2 ‰) (VPDB) do not support localized recycling of carbon from the styolites to the dolomite. Had isotopically light organic carbon been incorporated into the recrystallized dolomite veinlets, values in the -8 to -12 ‰ (VPDB) range would be expected (Hall & Friedman, 1969). Therefore, the organic carbon from the

styolites contributed little if any of the carbon isotope signature to late D3 dolomite veinlets in the SRZ.

A changing fluid composition within a closed system during late stage chalcopyrite and calcite mineralization at Magmont West, Viburnum Trend was used to explain the lack of correlation of carbon and oxygen isotope values in calcite and dolomite veinlets (Hannah & Stein, 1984). However, the multitude of dolomite and sphalerite textures and the lack of a trend in carbon isotopic composition for dolomites suggests a more complex fluid history for the SRZ and likely an open system dominated during and after the deposition of the volumetrically abundant late stage sphalerite (S2).

The carbon isotopic composition of dolomite veinlets does broadly correlate with distance from mineralization in Casteel (Figure 4.49, p. 112). However, the average values between mineralized and barren samples from each mine do not show a consistent trend or pattern (Table 4.8, p. 112). Given that carbon isotope values within the SRZ are consistent with early marine limestone, it is unlikely that these values were altered by any of the incoming mineralizing fluids (Hoefs, 2009).

The oxygen isotopic composition of the host dolomite from the unmineralized area within the SRZ does not correlate with proximity to mineralization. The difference in average oxygen isotopic composition of the host dolomite between mineralized and unmineralized samples varies between mine sites with a maximum difference of 1.59 ‰ at Sweetwater mine to only 0.10 ‰ at the Fletcher mine (Table 4.5, p. 107). The results are similar for dolomite veinlets, with the dolomite veinlets from the Sweetwater mine having the largest difference (1.1 ‰) between mineralized and barren samples, while samples from Fletcher

have the smallest difference (0.15 ‰), (Table 4.7, p. 110). This lack of correlation in the unmineralized areas of the SRZ for the oxygen isotope values within the host dolomites could be the result of a lower temperature of ore fluids within the host rocks, since lower temperatures have been shown to be associated with increasing variability within oxygen and carbon isotope values in other deposits (Hall & Friedman, 1969).

Early stage galena (G1) (octahedral in previous studies) has been shown to be sourced from red beds within the LaMotte Formation through isotope and geochemical work (Goldhaber & Mosier, 1990; Viets & Leach, 1990; Viets *et al.*, 1992; Goldhaber *et al.*, 1995). Multiple studies have documented the existence of an early galena (G1) within the same horizon that hosts the SRZ (Hagni & Trancynger, 1977; Crocetti & Holland, 1989; Mavrogenes *et al.*, 1992; Viets *et al.*, 1992; Shelton *et al.*, 1995). In addition, G1 galena was identified in mapping and petrography in multiple locations within the SRZ. Given this information, it is likely there was some contribution from fluids from the LaMotte Formation within the SRZ. These G1 galena and S1 sphalerite fluids, which are associated with D2 dolomites, could be influencing the values of the D1 dolomite because micro drilling may have inadvertently included some D2 dolomite, which is unavoidable because consistently identifying D2 recrystallization from D1 is impossible.

Figure 5.1 shows a scatter plot of oxygen and carbon isotopes for dolomite veinlets (D3) from mineralized samples in the SRZ compared to similar dolomite veinlets and mineralization-related recrystallized dolomite from other areas of the Viburnum Trend. Dolomite veinlets (D3) have higher $\delta^{13}C$ values and lower $\delta^{18}O$ values relative to similar dolomite the Viburnum Trend.

(Removed Due to Copyright)

Figure 5.1: Carbon & oxygen isotope plot of samples from the Stratiform Replacement Zone & Viburnum Trend.
Dolomite veinlets from mineralized samples from the SRZ (upper Bonneterre Formation) (Data from Table 4.4 and from other studies from the Viburnum trend, found in Appendix D). The data from Cavender (2015) is from the high grade Cu-Zn-Pb Deep Ore Zone (DOZ) at Brushy Creek (lower Bonneterre Formation), whereas the data from Gregg (1985) is from mineralized samples along the basal dolomite bed (lower Bonneterre Formation, sample locations not described in text). Data from Hannah & Stein (1985) are from the Magmont West mine (upper Bonneterre Formation). Samples from other studies were analyzed using the phosphoric acid method, and sampling was completed with either a micro drill, or crystals were hand-picked with a binocular microscope.

Both SRZ mineralization and the main deposits of the Viburnum Trend are hosted within the upper stratigraphic zone of the main mineralizing host (Gerdemann & Myers, 1972). Goldhaber *et al.* (1995), using the Pb isotopic composition of sulfides, showed that there are at least two different sources of metals for the Viburnum Trend. Late stage sulfide minerals from the upper part of the Bonneterre Formation have a distinctive Pb isotopic composition and were interpreted have a metal source from a different basin with common affinities to the Tri-State mineralizing fluids, and were distinct from fluids hosted within

lower sections of the Bonneterre Formation. Mapping, geological observations and petrographic analysis have shown that late stage sphalerite (S2) is the most abundant sulfide in the SRZ.

The petrographic data from this study, showing ubiquitous replacement of earlier generations of sulfides by sphalerite suggests a distinct fluid was responsible for sphalerite mineralization in the SRZ. In addition, the oxygen isotope data from hydrothermal dolomite veinlets (D3) from this study combined with the sulfur isotope data, support previous work by Goldhaber *et al.* (1995) and Viets *et al.* (1992) that at least two separate basins supplied fluids to early and late mineralizing fluids, which are more abundant in the lower and upper Bonneterre Formation, respectively.

Figure 5.2 is a plot of the carbon and oxygen isotopic composition of dolomite veinlets from the SRZ compared with dolomites associated with mineralization from the Polaris MVT Deposit in Northern Canada (Savard *et al.*, 2000). This comparison is relevant because the Polaris deposit is a low temperature, stratiform MVT deposit, although it is higher grade than any deposit on the Viburnum Trend (Savard *et al.*, 2000).

The carbon and oxygen isotopic composition of dolomite samples from the SRZ are more tightly clustered relative to comparable MVT deposits (Figure 5.2); and when compared to other areas from the Viburnum Trend (Fritz, 1969; Hall. & Friedman, 1969; Pinckney & Rye, 1972).

(Removed Due to Copyright)

Figure 5.2: Carbon & oxygen isotope plot-SRZ & Polaris deposit.
Dolomite veinlets from mineralized samples from Stratiform Replacement Zone (Data from Table 4.4) and from the Polaris MVT deposit (Data from Savard et. al. (2000), found in Appendix D).

Overall, there is substantial variation in carbon and oxygen isotopic compositions within the SRZ. However, compared with other MVT deposits worldwide, as well as other deposits on the Viburnum Trend, the data indicates that the late stage sphalerite (S2) within the mineralized zone of the SRZ was deposited at a comparatively high water:rock ratio and elevated temperatures relative to the unmineralized areas. In most other carbonate hosted ore deposits, elevated temperatures result in a decrease in isotope fractionation, which results in a depletion of oxygen isotope values (Hall & Friedman, 1969; Heyl *et al.*, 1974). In other MVT deposits, higher water:rock ratios have been interpreted to reduce isotopic fractionation with a resultant depletion in oxygen isotope values (Savard *et al.*, 2000).

5.3.1.1 Secondary Ion Mass Spectrometry (SIMS) Data

SIMS data has established that each dolomite texture is associated with distinct oxygen isotope values and variability. This variability is linked with recrystallization, with host dolomite (D1) showing the most variability (10.6 ‰), and hydrothermal dolomite veinlets (D3) showing less variability (8.4 ‰) (Table 4.9, p. 117).

This SIMS data confirmed the overall variability trends observed in bulk isotope data and suggests that recrystallization associated with the D2 and D3 dolomites resulted in lower oxygen isotope variability for these textures compared with the D1 dolomite. This is consistent with data from other MVT deposits, where the recrystallized dolomites and/or calcites were subjected to higher temperatures and water:rock ratios, which resulted in more homogenous oxygen isotope values (Fritz, 1969; Hall & Friedman, 1969; Pinckney & Rye, 1972; Heyl *et al.*, 1974; Taylor, 1974; Savard *et al.*, 2000). The SIMS data combined with the bulk isotope data suggests that the mineralizing fluids within the SRZ were associated with recrystallization which resulted in the D2 and D3 dolomite generations.

5.3.1.2 Sulfur Isotopes

The sulfur isotopic composition of sulfides averaged 13.8 ‰ with a total range of 12.7 ‰ (Table 4.10, p. 120) This is consistent with a sedimentary source for sulfur (Hoefs, 2009). This average and range is consistent with sulfur isotope data from late stage sphalerites identified in previous studies (Shelton *et al.*, 1995). The sulfur data from the SRZ in this study suggests that the mineralizing fluids associated with the S2 mineral stages were associated with late stage, vug filling mineralization. Figure 5.3 shows the paragenetic

stages of the Viburnum Trend with the associated sulfur isotope values related to these stages.

(Removed Due to Copyright)

Figure 5.3: $\delta^{34}S$ values of sulfides from the Viburnum Trend (Shelton *et al.*, 1995). The red box corresponds to the SRZ sulfur isotope values.

Sulfur isotopic compositions for sphalerite obtained by SIMS from the SRZ show similar variability as previous in-situ analytical sulfur isotope work (McKibben & Eldridge, 1995). The results of this study are consistent with sphalerite hosted in a vertically restricted zone, with a common link with regional, Tri-State, Central Missouri and Northern Arkansas mineralizing fluids. This separate regional fluid source is indicated because Cavender (2015) demonstrated a correlation between the sulfur isotopic composition of sphalerite, and the vertical position of the Bonneterre Formation. This, combined with earlier work completed by Viets & Leach, (1990), (Goldhaber *et al.* (1995) & Viets *et al.* (1992), showed

that galena and sphalerite mineralization hosted higher within the stratigraphic section of the Bonneterre Formation had a minor contribution of fluids from the LaMotte Formation, and a higher contribution of fluids which are related to fluids in the Tri-State, Central Missouri and Northern Arkansas mineral districts.

5.3.1.3 Stable Isotopes as an Exploration Tool

Using bulk carbon and oxygen isotopes as a vector towards mineralization for the SRZ is challenging, and overall yielded poor results. Previous work on host dolomite oxygen isotope values has established that un-dolomitized Bonneterre Formation (limestone) located dozens to hundreds of miles away from the Viburnum Trend has a range from 18.6 to 21.7 ‰ (SMOW) (Hannah & Stein, 1984). Carbon and oxygen isotope data for host dolomites (D1) does not correlate with distance from mineralization because of a lack of interaction with mineralizing fluids overall, which resulted in the isotope signature of the Bonneterre remaining largely unchanged.

In general, variation in oxygen isotopic composition of dolomite veinlets (D3) is low for the mineralized part of this zone. While some mines, such as Casteel appear to show a weak relationship on a scatter plot, when the values are plotted on a map, it is clear that there is no relationship or isotopic halo around mineralization. While there is a notable difference in oxygen isotope values from unmineralized drill cores relative to mineralized underground samples broadly, the map data clearly shows no relationship between distance to mineralization and the oxygen isotope values. Based on results from this study, it is clear that there is a difference in the oxygen isotope values of mineralized and barren D3 veinlets throughout the SRZ. The average oxygen isotope difference between

mineralized and barren D3 veinlets across all mines was 0.48 ‰, but this average is lower than the overall variability of the barren zone D3 veinlets (0.71 ‰). D3 dolomite veinlets that have interacted with heated mineralizing fluids (at sufficient water/rock ratios) have lower $\delta^{18}O$ values than samples that did not interact with mineralized fluids or interacted with the mineralized fluids at lower water:rock ratios.

At the Cave-in-Rock District in Illinois, an identifiable systematic trend in stable isotopic composition was identified that correlated with calcite recrystallization. The results from this district indicated a strong potential for the stable isotope method to be used as an aid in mineral exploration (Pinckney & Rye, 1972). Conversely, samples from the Upper Mississippi Valley district showed considerable scatter in their carbon and oxygen isotopic composition for both mineralized and barren samples. While a weak trend in distance to mineralization compared with oxygen and carbon isotopes was identified, the area of isotopic depletion was too narrow to be of use as an exploration tool in the Tri-State district (Hall & Friedman, 1969).

The SIMS data for carbon and oxygen isotopes underscores the challenge in using the oxygen isotopes as an exploration tool, since this study documented the maximum variability within one sample of 10.6 ‰. Such variability at a small scale likely precludes the successful use of oxygen isotopes as an exploration tool, regardless of the particular method chosen.

Chapter 6: **Conclusions**

6.1 Conclusions

1. The SRZ is a separate geologic zone within the Bonneterre Formation. This zone is dominated by late stage sphalerite (S2) that was deposited after the formation of fluids which resulted in the recrystallization of dolomite (D2 & D3). The S2 sphalerite mineralization is volumetrically abundant within the SRZ, and has genetic affinities with late stage mineralization associated with the Tri-State District (Viets & Leach, 1990; Goldhaber *et al.*, 1995). S2 sphalerite mineralization is particularly influenced by specific faults and fractures, and tends to increase in frequency in "mottled bedding zones" containing abundant D3 dolomite.
2. Certain zones of bedding parallel styolites may have channeled fluids both before and after deposition of late stage sphalerite (S2). Leaching occurred after deposition of main stage sulfides (G1 and S1), but prior to S2 mineralization.
3. Sphalerite was deposited in two stages, early brown sphalerite (S1), which was associated with early stage galena (G1) and late green & yellow sphalerite (S2), which resulted in whole rock replacement and vug fill.
4. SIMS oxygen isotopic analysis of different dolomite textures show that substantial variation occurs in all dolomite types at the micron scale. Host dolomite (D1) has the widest range in $\delta^{18}O$ values while the D2 and D3 dolomites have less variability overall. Lower water:rock ratios are likely the cause of the more heterogenous values for the host dolomite (D1) within the SRZ.

5. In an array of deposit types, if wall rock recrystallization (and associated mineralization) is associated with faults and fractures, then detailed mapping of oxygen isotopes can be a vector towards mineralization. This method has been applied as a vector towards mineralization and to map out thermal anomalies in porphyries, certain MVT's, carbonate replacement deposits, skarns and SEDEX deposits (Fritz, 1969; Matsuhisa *et al.*, 1985; Criss & Fleck, 1990; Dilles *et al.*, 1992; Naito *et al.*, 1995; Large *et al.*, 2001; Relvas *et al.*, 2006). Unfortunately, the lack of clear, well developed dolomite or calcite recrystallization in direct association with mineralization in the SRZ (and most of the Viburnum Trend) precludes the use of this method as a way of defining mappable halos around mineralization.
6. Oxygen isotope sampling on the Viburnum Trend, while useful for broadly differentiating general proximity to an ore zone, is ineffective as an exploration tool. The significant variability in oxygen isotope values on the thin section scale indicates that no method of bulk or micro drilled oxygen isotope samples would be effective, regardless of the geological constraints applied. While it is possible that there are some trends which would be detected with more samples and a more dense sampling grid, the sparse and sporadic location of most exploration drilling makes this unfeasible.

6.2 Alternative Exploration Techniques for the Stratiform Replacement Zone

The section below reviews previous research that was completed on the Viburnum Trend and elsewhere. The studies focused on a range of geologic and geochemical features, which were directly associated with mineralization. The work summarized below could be

incorporated into an exploration program, and increase the probabilities of an exploration drill hole intersecting mineralization.

Work completed at the Magmont West Mine in the 1980's focused on the relationship between bitumen and late stage mineralization. Bitumen blebs were analyzed using Rock-Eval pyrolysis to determine trace elements, elemental ratios of bitumen and total sulfur content of the bitumen blebs. The method is only semi-quantitative, but does give important information on the hydrogen and oxygen index of organic material so that the kerogen type can be identified as well as the overall maturation. While it is clear that most of the bitumen and organic matter was deposited after sulfide mineralization, one of the bitumen blebs was enriched in Zn (1,000 ppm), Pb (150 ppm) and Cu (30 ppm) but depleted in Ni and V. The chemistry of the bitumen bleb was interpreted as evidence that the organic material was in contact with Pb-Zn minerals prior to final deposition (Marikos *et al.*, 1986).

Work completed at the Sweetwater Mine in the late 1980's focused on classifying the organic matter present as well as defining the paragenetic relationship of the organic matter with different stages of sulfide mineralization. Paragenetic relationships indicated that metal bearing fluids were in contact with petroliferous compounds during late stage Pb-Zn mineralization. In one case, cubes of galena were found growing inside an open cavity of a tacky bitumen compound. The relationship of the various organic compounds to mineralization was interpreted as evidence that the organic compounds were in contact with ore bearing solutions prior to mineralization processes ceasing (Niewendorp, 1987).

Henry *et al.* (1992) identified a 12 mile wide organic matter alteration zone around the Viburnum Trend, based on detailed petrographic and chemical analysis of different organic compounds in and around the Buick Mine. They utilized the reflectance differences of a specific variety of organic matter (algine) to identify an alteration halo and determined that the entire mineralized area had been heated to temperatures in the oil window while samples outside the Viburnum Trend had not. In addition, total organic carbon (TOC) was analyzed and variations of TOC within samples was linked to proximity of samples to orebodies. Mineralized zones had higher TOC's than unmineralized ones.

The indirect relationship between organic matter and mineralization suggests that the presence of organic matter within samples could be used as a proxy for mineralization and consequently as an exploration tool on the Viburnum Trend. Since all three studies demonstrated a connection of organic compounds to late mineralization in three separate areas of the Viburnum Trend, analyzing the organic matter within targeted horizons of barren and mineralized samples in the Bonneterre Formation may be an effective tool to prospect within the SRZ. This method would be particularly useful because it would permit barren holes, which were likely close to an ore zone (higher TOC content) to be distinguished from barren holes which were likely not close to an ore zone (lower TOC content).

Total organic content is an analysis which is readily and cheaply available at most commercial labs, and gives an accurate analysis of carbon which has been derived from organic sources and not carbonate minerals. Judicious sampling of barren and mineralized drill hole intercepts for TOC data within the SRZ (and other zones) could allow the

compilation of this data and subsequent contouring of values to provide an additional tool to vector towards mineralization.

Work completed on shale samples at the base of the Davis Formation near the Buick Mine was evaluated to determine if there were any geochemical variations that may be detectable in clay minerals in and around the Viburnum Trend. Potassium concentrations were analyzed using whole-rock samples from the lowest 30 ft. of shale perpendicular to the main ore zone for a distance of up to 30 miles from the Viburnum Trend. Overall, samples above the ore zones were depleted in potassium compared with samples located further away. The mechanism that caused this is a result of hot fluids interacting with shale in a process called smectite-illitization (Panno & Moore, 1994).

Since only a small portion of this section needs to be sampled to utilize this method (the bottom 1-2 ft. of Davis Formation), the cost would be low compared to drilling costs and could be useful as an additional exploration tool.

Zinc isotopes are a new and emerging field of isotope research that hold great promise. Studies from MVT deposits in Ireland have shown that $\delta^{66}Zn$ values have a trend in high grade core samples from hydrothermal systems are higher, whereas more distal and lower grade parts of the orebody have lower $\delta^{66}Zn$ values. This is important because it allows the prospector the ability to sample trace sphalerite from any sample and can help identify the relative proximity to the ore zone of the deposit (Wilkinson *et al.*, 2005).

Another area of promise for prospecting on the Viburnum Trend is a geophysical survey method known as spontaneous polarization. This is one of the oldest geophysical survey methods known (discovered in the mid-1800's) and relies on the fact that a submerged

sulfide ore body generates its own electrical energy, much like a battery. The current flows from the lower part of the ore body (reducing conditions) to the upper part (oxidizing) as long as the ore zone is conductive. Interpretation of the data relies simply on assessing the peak negative response of the instrument and is based on the surface measurement of electrochemical reactions of a sulfide ore body with the water table. The method is sensitive to the amount of pyrite/marcasite in the rock, as well as any man-made conductive objects (buried pipe, drill casing etc.), and can produce false positive anomalies if such objects are not taken into consideration during interpretation (Jébrak & Marcoux, 2015).

A spontaneous polarization survey was conducted over three mines along the Viburnum Trend to determine if orebodies could be remotely detected with deep overburden thicknesses (50-150 ft.) and relatively deep ore zones (700-1,200 ft. below surface). Multiple surveys were conducted, including downhole, underground and on surface. The surveys were conducted at #28 Mine, #29 Mine and the Brushy Creek Mine. Orientation studies were generated first over areas where known mineralization was already blocked to ensure there was validity to the method. While some of the self-potential anomalies detected during the surface survey were weak due to the great depth from surface, clear negative anomalies were detected during the surface surveys, which outlined mineralization for most ore bodies. The authors were able to differentiate from surface the relative size of the ore bodies and whether the mineralization was massive or disseminated (Sivenas & Beales, 1982).

Work was conducted to evaluate the effectiveness of utilizing publicly available trace element data from streams and wells as a regional reconnaissance for mineral exploration in Southeast Missouri and in three other mineral districts in the Midwest. Data was extracted on streams and wells which included dissolved Zn, Pb and sulfate. Overall, the researchers determined that in Southeast Missouri, dissolved sulfate data was sharply elevated in areas around the Viburnum Trend, the Old Lead Belt and the Tri-State District. While the survey results indicated that the method was highly successful, it is limited as a regional tool to identify anomalous areas for follow-up prospecting and has no use in mine-scale exploration (<5 miles) (Lewis, 1980).

In conclusion, the geochemical and geophysical surveys briefly discussed above provide the geologist an arsenal of methods which can both identify an anomalous area of mineralization as well as provide mine scale vectoring towards prospective mineralization. These methods are relatively low-cost, have already been researched and applied on the Viburnum Trend (except for zinc isotopes) and could be effective in finding mineralization.

Table 6.1 summarizes multiple geochemical and geophysical survey methods not currently in use but which have promise to assist exploration efforts to identify new areas for potential mineralization on both on the Viburnum Trend and regionally in Southeast Missouri.

Table 6.1: Potential Geochemical and Geophysical Survey Methods for the Stratiform Replacement Zone

Method	Survey Type	Scale	Intended Use	Advantages	Disadvantages
Total Organic Matter Analysis	Geochemical	Mine/District Exploration	Vector towards Mineralization	Cheap analysis, easy to contour	Large amount of samples required
Potassium in Base of Davis Analysis	Geochemical	Mine/District Exploration	Vector towards Mineralization	Cheap analysis, easy to contour	Large amount of samples required
Dissolved Sulfate & Metals in Waterways	Geochemical	District Exploration	Narrow Region for Exploration	Free open source data, easy to contour data	Limited to regional scale use
Spontaneous Potential Survey	Geophysical	Mine Scale	Vector towards Mineralization	Cheapest and simplest geophysical survey method	Results affected by iron rich zones, false positives due to man-made metallic interferences (drill casings etc.)
Zinc Isotope Micro Drilling	Geochemical	Mine Scale	Vector towards Mineralization	Compliments oxygen isotope data, identify higher grade core of system	Relatively new, not tried on the Viburnum Trend, expensive analysis ($260/sample)

References

Appold, M.S. & Garven, G. (1999) The hydrology of ore formation in the Southeast Missouri District; numerical models of topography-driven fluid flow during the Ouachita Orogeny. *Economic Geology*, **94**, 913–935.

Barton, P. (1970) Sulfide Petrology. *Mineralogical Society of America*, **3**, 187–198.

Cavender, B.D. (2015) Atypical MVT, Zn-Cu-rich mineralization in the lower portion of the Bonneterre Dolomite, Viburnum Trend, Southeast Missouri, U.S.A. Unpublished Master's Thesis, Columbia, University of Missouri, 167 pp.

Claire, R.-B. & Carbonne, J.M. (2011) Determination of SIMS matrix effects on oxygen isotopic compositions in carbonates. *Journal of Analytical Atomic Spectrometry*, **26**, 1285.

Clendenin, C.W. (1991) Structure, stratigraphy, and mineralization; an interrelationship triangle and the Southeast Missouri Mississippi valley-type deposits. *Economic Geology*, **86**, 179–184.

Clendenin, C.W. (1993) Small-scale positive flower structures. *Mineralium Deposita*, **28**, 22–27.

Clendenin, C.W. & Duane, M.J. (1990) Focused Fluid Flow and Ozark Mississippi Valley-type deposits. *Geology*, **18**, 116–119.

Clendenin, C.W., Niewendorp, C.A. & Lowell, G.R. (1989) Reinterpretation of faulting in southeast Missouri. *Geology*, **17**, 217–220.

Clendenin, C.W., Niewendorp, C.A., Duane, M.J. & Lowell, G.R. (1994) The paleohydrology of Southeast Missouri Mississippi Valley-Type Deposits; Interplay of Faults, Fluids, and Adjoining Lithologies. *Economic Geology*, **89**, 322–332.

Craig, J.R. (2001) Ore-Mineral Textures and The Tales They Tell. *The Canadian Mineralogist*, **39**, 937–956.

Craig, J.R. & Carpenter, A.B. (1977) Fletcherite, Cu(Ni,Co) 2 S 4 , a new thiospinel from the Viburnum Trend (New Lead Belt), Missouri. *Economic Geology*, **72**, 480–486.

Craig, J.R. & Vaughan, D.J. (1994) *Ore microscopy and ore petrography*. 2nd ed. Wiley, New York, 434 pp.

Criss, R.E. & Fleck, R.J. (1990) Oxygen isotope map of the giant metamorphic-hydrothermal system around the northern part of the Idaho batholith, U.S.A. *Applied Geochemistry*, **5**, 641–655. Water-Rock Interactions Special Memorial Issue Ivan Barnes (1931–1989).

Crocetti, C.A. & Holland, H.D. (1989) Sulfur-lead isotope systematics and the composition of fluid-inclusions in galena from the Viburnum Trend, Missouri. *Economic Geology*, **84**, 2196–2216.

Dilles, J.H., Solomon, G.C., Taylor, H.P. & Einaudi, M.T. (1992) Oxygen and hydrogen isotope characteristics of hydrothermal alteration at the Ann-Mason porphyry copper deposit, Yerington, Nevada. *Economic Geology*, **87**, 44–63.

Dunn, R.G.J. & Grundmann, W.H. (1989) Geology of the Casteel Mine: Copper Rich Ore in a MVT Setting. *SEG Guidebook Series*, **5**, 31–55.

Fayek, M., Harrison, T.M., Ewing, R.C., Grove, M. & Coath, C.D. (2002) O and Pb isotopic analyses of uranium minerals by ion microprobe and U–Pb ages from the Cigar Lake deposit. *Chemical Geology*, **185**, 205–225.

Fennel, M.J., Hagni, R.D., Bradley, M.F. & Sangster, D.F. (1996) Mineralogy, paragenetic sequence, mineral zoning, and genesis at the Magmont-West Mine, Southeast Missouri lead district. *Society of Economic Geologists*, **Special Publication No. 4**, 597–610.

Fritz, P. (1969) The oxygen and carbon isotopic composition of carbonates from the Pine Point lead-zinc ore deposits. *Economic Geology*, **64**, 733–742.

Gerdemann, P.E. & Myers, H.E. (1972) Relationships of Carbonate Facies Patterns to Ore Distribution and to Ore Genesis in the Southeast Missouri Lead District. *Economic Geology*, **67**, 426–433.

Goldhaber, M.B. & Mosier, E.L. (1990) *Sulfur sources for southeast Missouri Mississippi Valley-type ores--implications for ore genesis*. USGS Circular 1043, US Government Printing Office.

Goldhaber, M.B., Church, S.E., Doe, B.R., Aleinikoff, J.N., Brannon, J.C., Podosek, F.A., Mosier, E.L., Taylor, C.D. & Gent, C.A. (1995) Lead and sulfur isotope investigation of Paleozoic sedimentary rocks from the southern Midcontinent of the United States; implications for paleohydrology and ore genesis of the Southeast Missouri lead belts. *Economic Geology*, **90**, 1875–1910.

Google Maps (2016): Map of Missouri, retrieved on Oct 4th, 2016, From http://maps.google.com/.

Gregg, J.M. (1985) Regional epigenetic dolomitization in the Bonneterre Dolomite (Cambrian), southeastern Missouri. *Geology*, **13**, 503–506.

Gregg, J.M., Laudon, P.R., Woody, R.E. & Shelton, K.L. (1993) Porosity evolution of the Cambrian Bonneterre Dolomite, south-eastern Missouri, USA. *Sedimentology*, **40**, 1153–1169.

Hagni, R.D. (1995) The Viburnum Trend, Missouri. Pp. 42–78 in: *Carbonate-Hosted Lead-Zinc-Fluorite-Barite Deposits of North America* (K.C. Misra, editor).

Hagni, R.D. (2006) Directions of Ore Fluid Flow in the Southeast Missouri Lead-Zinc District as Inferred from Asymmetrical Distributions of Orebodies around Precambrian Knobs and from Mineral/Metal Zoning Patterns. Pp. 6–40 in: *International Field Conference Guidebook*. St. Louis, Missouri.

Hagni, R.D. & Trancynger, T.C. (1977) Sequence of Deposition of The Ore Minerals at The Magmont Mine, Viburnum Trend, Southeast Missouri. *Economic Geology*, **72**, 451–464.

Hall & Friedman. (1969) *Oxygen And Carbon Isotopic Composition of Ore and Host Rock of Selected Mississippi Valley Deposits*. Geological Survey Research 1969, Chapter C, Report.

Hannah, J.L. & Stein, H.J. (1984) Evidence for Changing Ore Fluid Composition; Stable Isotope Analyses Of Secondary Carbonates, Bonneterre Formation, Missouri. *Economic Geology*, **79**, 1930–1935.

Henry, A.L., Anderson, G.M. & Heroux, Y. (1992) Alteration of Organic Matter In The Viburnum Trend Lead-Zinc District of Southeastern Missouri. *Economic Geology*, **87**, 288–309.

Heyl, A.V., Landis, G.P. & Zartman, R.E. (1974) Isotopic Evidence for the Origin of Mississippi Valley-Type Mineral Deposits: A Review. *Economic Geology*, **69**, 992–1006.

Hoefs, J. (2009) *Stable Isotope Geochemistry*. Sixth Edition. Springer, Berlin, 285 pp.

Jébrak, M. & Marcoux, É. (2015) *Geology of Mineral Resources*. Second Edition. Mineral Deposits Division of the Geological Association of Canada, Quebec, Canada, 668 pp.

Keller, T.J., Gregg, J.M. & Shelton, K.L. (2000) Fluid migration and associated diagenesis in the Greater Reelfoot rift region, Midcontinent, United States. *GSA Bulletin*, **112**, 1680–1693.

Kisvarsanyi, G. (1977) The role of the Precambrian igneous basement in the formation of the stratabound lead-zinc-copper deposits in Southeast Missouri. *Economic Geology*, **72**, 435–442.

Koob, K. (2014) Casteel Mine Tour Guide. *SEG Guidebook Series*, **45**, 25–33.

Large, R.R., Bull, S.W. & Winefield, P.R. (2001) Carbon and Oxygen Isotope Halo in Carbonates Related to the McArthur River (HYC) Zn-Pb-Ag Deposit, North Australia:Implications for Sedimentation, Ore Genesis, and Mineral Exploration. *Economic Geology*, **96**, 1567–1593.

Larsen, K.G. (1977) Sedimentology of the Bonneterre Formation, Southeast Missouri. *Economic Geology*, **72**, 408–419.

Lasmanis, R. (1997) Tri-State and Viburnum Trend Districts: An Overview. *Rocks & Minerals*, **72**, 400–419.

Leach, D.L., Fey, D.L., Diehl, S.F. & Saltus, R.W. (2010) A deposit model for Mississippi Valley-Type lead-zinc ores. P. 52 in: *Mineral Deposit Models for Resource Assessment*. 2010th-5070th-A edition. Scientific Investigations Report, U.S. Geological Survey.

Lewis, E.S. (1980) Trace Element Content of Surface and Groundwaters in Northwest Ohio in Relation to Mississippi Valley-Type Mineralization. Unpublished Master's Thesis, Bowling Green State University, 59 pp.

Lohmann, K.C. & Frank, M.H. (1982) Cathodoluminescence and isotopic analyses of diagenetically altered dolomite, Bonneterre Formation, southeast Missouri. *Geol. Soc. America Abstracts with Programs*, **14**, 491–491.

Lyle, J.R. (1977) Petrography and Carbonate Diagenesis of The Bonneterre Formation in The Viburnum Trend Area, Southeast Missouri. *Economic Geology*, **72**, 420–434.

Marikos, M.A., Laudon, R.C. & Leventhal, J.S. (1986) Solid insoluble bitumen in the Magmont West orebody, Southeast Missouri. *Economic Geology*, **81**, 1983–1988.

Matsuhisa, Y., Morishita, Y. & Sato, T. (1985) Oxygen and carbon isotope variations in gold-bearing hydrothermal veins in the Kushikino mining area, southern Kyushu, Japan. *Economic Geology*, **80**, 283–293.

Mavrogenes, J.A., Hagni, R.D. & Dingess, P.R. (1992) Mineralogy, Paragenesis, and Mineral Zoning of the West Fork Mine, Viburnum Trend, Southeast Missouri. *Economic Geology*, **87**, 113–124.

McKibben, M.A. & Eldridge, C.S. (1995) Microscopic Sulfur Isotope Variations in Ore Minerals from the Viburnum Trend, Southeast Missouri; a SHRIMP Study. *Economic Geology*, **90**, 228–245.

Mouat, M.M. & Clendenin, C.W. (1977) Geology of the Ozark Lead Company Mine, Viburnum Trend, Southeast Missouri. *Economic Geology*, **72**, 398–407.

Naito, K., Fukahori, Y., Peiming, H., Sakurai, W., Shimazaki, H. & Matsuhisa, Y. (1995) Oxygen and carbon isotope zonations of wall rocks around the Kamioka Pb□Zn skarn deposits, central Japan: application to prospecting. *Journal of Geochemical Exploration*, **54**, 199–211.

Niewendorp, C.A. (1987) Possible Role of Petroliferous Materials in Sulfide Precipitation at the Frank R. Millikan Mine, Southeast Missouri. Unpublished Master's Thesis, Western Michigan University, 108 pp.

Niewendorp, C.A. & Clendenin, C.W. (1993) Paragenetic link between organic matter and late-stage ore deposition in the Sweetwater Mine, Viburnum Trend, Southeast Missouri. *Economic Geology*, **88**, 957–960.

Ohle, E.L. (1985) Breccias in mississippi valley-type deposits. *Economic Geology*, **80**, 1736–1752.

Paarlberg, N.L. & Evans, L.L. (1977) Geology of the Fletcher Mine, Viburnum Trend, Southeast Missouri. *Economic Geology*, **72**, 391–397.

Panno, S.V. & Moore, D.M. (1994) Mineralogy of The Clay-Sized Fraction Of The Davis Shale, Southeast Missouri; Alteration Associated With a Mississippi Valley-Type Ore Deposit. *Economic Geology*, **89**, 333–340.

Pinckney, D.M. & Rye, R.O. (1972) Variation of O 18 /O 16 , C 13 /C 12 , Texture, and Mineralogy in Altered Limestone in the Hill Mine, Cave-in-District, Illinois. *Economic Geology*, **67**, 1–18.

Ramdohr, P. (1969) *The Ore Minerals and Their Intergrowths*. 1st edition. Pergamon Press Ltd, 1193 pp.

Relvas, J.M.R.S., Barriga, F.J.A.S. & Longstaffe, F.J. (2006) Hydrothermal Alteration and Mineralization in the Neves-Corvo Volcanic-Hosted Massive Sulfide Deposit, Portugal. II. Oxygen, Hydrogen, and Carbon Isotopes. *Economic Geology*, **101**, 791–804.

Riciputi, L.R., Paterson, B.A. & Ripperdan, R.L. (1998) Measurement of light stable isotope ratios by SIMS:: Matrix effects for oxygen, carbon, and sulfur isotopes in minerals 3 3 Dedicated to the memory of Al Nier. *International Journal of Mass Spectrometry*, **178**, 81–112.

Rogers, R.K. & Davis, J.H. (1977) Geology of the Buick Mine, Viburnum Trend, Southeast Missouri. *Economic Geology*, **72**, 372–380.

Savard, M.M., Chi, G., Sami, T., Williams-Jones, A.E. & Leigh, K. (2000) Fluid inclusion and carbon, oxygen, and strontium isotope study of the Polaris Mississippi Valley-type Zn–Pb deposit, Canadian Arctic Archipelago: implications for ore genesis. *Mineralium Deposita*, **35**, 495–510.

Shelton, K.L., Burstein, I.B., Hagni, R.D., Vierrether, C.B., Grant, S.K., Hennigh, Q.T., Bradley, M.F. & Brandom, R.T. (1995) Sulfur isotope evidence for penetration of MVT fluids into igneous basement rocks, southeast Missouri, USA. *Mineralium Deposita*, **30**, 339–350.

Shelton, K.L., Gregg, J.M. & Johnson, A.W. (2009) Replacement Dolomites and Ore Sulfides as Recorders of Multiple Fluids and Fluid Sources in the Southeast Missouri Mississippi

Valley-Type District: Halogen-87Sr/86Sr-δ18O-δ34S Systematics in the Bonneterre Dolomite. *Economic Geology*, **104**, 733–748.

Sivenas, P. & Beales, F.W. (1982) Natural Geobatteries Associated with Sulphide Ore Deposits, II. Field Studies at the Viburnum Trend, Southeast Missouri, U.S.A. *Journal of Geochemical Exploration*, **17**, 145–160.

Snyder, F.G. & Odell, J.W. (1958) Sedimentary Breccias in the Southeast Missouri Lead District. *Geological Society of America Bulletin*, **69**, 899.

Stein, H.J. & Kish, S.A. (1985) The Timing of Ore Formation in Southeast Missouri; Rb-Sr Glauconite Dating At The Magmont Mine, Viburnum Trend. *Economic Geology*, **80**, 739–753.

Taylor, H.P. (1974) The Application of Oxygen and Hydrogen Isotope Studies to Problems of Hydrothermal Alteration and Ore Deposition. *Economic Geology*, **69**, 843–883.

Thacker, J.L. & Anderson, K.H. (1977) The Geologic Setting of The Southeast Missouri Lead District; Regional Geologic History, Structure and Stratigraphy. *Economic Geology*, **72**, 339–348.

The Doe Run Company. (2015) . <http://www.doerun.com/what-we-do/mining-and-milling> (20 October 2015).

Tobin, R.C. (1991) Diagenesis, thermal maturation and burial history of the Upper Cambrian Bonneterre Dolomite, southeastern Missouri; an interpretation of thermal history from petrographic and fluid inclusion evidence. *Organic Geochemistry*, **17**, 143–151.

Viets, J.G. & Leach, D.L. (1990) Genetic Implications of Regional and Temporal Trends in Ore Fluid Geochemistry of Mississippi Valley-Type Deposits in the Ozark Region. *Economic Geology*, **85**, 842–861.

Viets, J.G., Hopkins, R.T. & Miller, B.M. (1992) Variations in minor and trace metals in sphalerite from mississippi valley-type deposits of the Ozark region; genetic implications. *Economic Geology*, **87**, 1897–1905.

Voss, R.L., Hagni, R.D. & Gregg, J.M. (1989) Sequential Deposition of Zoned Dolomite and its Relationship to Sulfide Mineral Paragenetic Sequence in the Viburnum Trend, Southeast Missouri. *Carbonates and Evaporites*, **4**, 195–209.

Walker, W.B. (1977) Geology of the Sweetwater Mine, Viburnum Trend, Southeast Missouri. *Economic Geology*, **72**, 111–129.

Wilkinson, J.J., Weiss, D.J., Mason, T.F.D. & Coles, B.J. (2005) Zinc Isotope Variation In Hydrothermal Systems: Preliminary Evidence From The Irish Midlands Ore Field. *Economic Geology*, **100**, 583–590.

Appendix A: Thin-Section Descriptions

Thin Section Descriptions

Sample	Mineral	% of Sample	Grain Size (um)	Grain Shape	Notes
08DR3	Group 1 Dolomite	85	50-350	Xenotopic	Moderate CRM on grain boundaries,
	Vug Filling Dolomite	12.5	100-350	Idiotopic	
			100-300		
	Sphalerite	1.25	100	Annhedral	Purplish mottling in PPL, cuts galena.
	Galena	3.75			
58W32	Group 1 Dolomite	85	300-600	Idiotopic	Well shaped rhombs with very little CRM between grain boundaries. Tight interlocking grain boundaries.
	Group 2 Dolomite	5	80-200	Idiotopic	Abundant CRM between grain boundaries, tight, interlocking grains.
	Vug Filling Dolomite	8	50-1300	Idiotopic	Clear, sometimes zoned rims. Abundant micro-crystalline matrix that is un-identifiable.
	Pyrite	2	200	Annhedral	Replaces all zones of dolomite.

Thin Section Descriptions

Sample	Mineral	% of Sample	Grain Size (um)	Grain Shape	Notes
59W28	Group 1 Dolomite	99.75	300	Xenotopic	Abundant relict oolites which are nearly perfectly circular. Low-amplitude styols cut Group 1 fabric with no apparent re-crystallization apparent. Undulatory extinction common. Some Idiotopic dol. grains. Moderate to heavy CRM on grain boundaries.
	Pyrite	0.25	200-500	Annhedral	Associated with styolite's.
60W117	Group 1 Dolomite	30	200-600	Xenotopic	Irregular grain boundaries. Some zonation on crystals with cloudy core and clear rim.
	Group 2 Dolomite	50	100-400	Idiotopic	Clay rich material on grain boundaries. Recrystallized, tiny euhedral rhomb's. Occur as oval rafts and as lateral zones which parallel styolites . Edges of rafts are marked by a styolite in some cases. Sharp contacts between this

Thin Section Descriptions

Sample	Mineral	% of Sample	Grain Size (um)	Grain Shape	Notes
					Group and Group 1 and dol.
	Vug Filling Dolomite	10	200-300	Idiotopic	Clear zonation of cloudy core and clear rim.
	Styolites		n/a	n/a	Three styolite's cut sphal. and are spatially related to Group 2 re-crystallized zones.
	Sphalerite	5	150-700	Annhedral	Early generation of sphal., cut by annhedral galena. New bronze color texture in PPL that has not been seen before. Cut by styolite with grain rotation and physical transport of grains.
	Galena	2.5	600-900	Annhedral	Cuts sphalerite, annhedral crystal shape occurs at the contact of Group 1 and 2 at a styolite.

Thin Section Descriptions

Sample	Mineral	% of Sample	Grain Size (um)	Grain Shape	Notes
	Pyrite	2.5	10-750	Annhedral	Occurs as tiny specks strongly associated with the styolite, though some small specks found in Group 1 dol. Appear to cut styolites, and sphal.
61W29	Group 1 Dolomite	80	100-400	Xenotopic	Coarse xenotopic dolomite is correlatable with other phases and has micro-porosity in between dolomite grains in the form of broken up and micro dolomites (CRM rich) as well as standard vugs. Mod.-Str. CRM on grain boundaries.
	Group 2 Dolomite	10	50-100	Idiotopic	Occurs as horizontal zones parallel to styolites. Micro euhedral rhomb's with no apparent zonation. Rotated appearance. Only associated with styolites.
	Vug Filling Dolomite	9	170-600	Idiotopic	Fills vugs, no zonation apparent.

Thin Section Descriptions

Sample	Mineral	% of Sample	Grain Size (um)	Grain Shape	Notes
	Pyrite	1	75	Annhedral	Little specks associated with Group 2 dolomite strongly. Some appears to have "diffused" into Group 1 host dolomite, but still a strong association with Group 2.
61W104	Group 2 Dolomite	50	50-300	Idiotopic	Heavy CRM on grain boundaries which are rotated and flipped about. Many are zoned with a distinct grungy core and a white rim.
	Vug Filling Dolomite	50	500 -300	Idiotopic	Curved twin planes in some saddle dolomites found next to styolite. Most crystals are zoned substantially.
62W102	Group 1 Dolomite	69.5	50-200	Xenotopic	Finer grained than most other textures. Relict oolites pronounced throughout.
	Group 2 Dolomite	30	40-100	Xenotopic	Similar to other zones except this is Xenotopic and finer grained, though it has the same amount of CRM material on grain boundaries.
	Vug Filling Dolomite		40-300	Idiotopic	

Thin Section Descriptions

Sample	Mineral	% of Sample	Grain Size (um)	Grain Shape	Notes
	Pyrite	0.5	15-300	Annhedral	Cuts all zones of dolomite, but has a stronger association with Group 2. Occurs as irregular bleb and as some random tiny specks.
64W67	Group 1 Dolomite	59	200-300	Xenotopic	Moderate CRM between grain boundaries, irregular and variable grain boundaries. Parts of the sample have abundant relict oolites, others have none. Where there is no oolites the texture is coarser.
	Group 2 Dolomite	15	75-200	Xenotopic	Irregular with moderate CRM on grain boundaries – not the nice Xenotopic grains with heavy CRM demonstrated in other samples.
	Group 3 Dolomite	15	10-30	Xenotopic	Micro-crystalline, composed of Xenotopic dolomites with irregular crystal faces.
	Vug Filling Dolomite	10	200-400	Idiotopic	Well-developed rhomb's.
	Pyrite	1	50-100		Preferentially replaces Group 2 dol. Some random specks.

Thin Section Descriptions

Sample	Mineral	% of Sample	Grain Size (um)	Grain Shape	Notes
73C26	Group 1 Dolomite	75	200-400	Xenotopic	Abundant porosity in the form of mini vugs, which are unfilled. Relict oolites preserved throughout. Tight interlocking grains are perforated by very small (200 um) mini vugs which typically form at the junction of several dol. crystals.
	Vug Filling Dolomite	25	300-600	Idiotopic	Zoned –brown core and white rim.
81V70	Group 1 Dolomite	50	250	Xenotopic	Rotated fossil fragments and prominent oolites.
	Group 2 Dolomite	20	100	Xenotopic	Abundant CRM, occurs as oval and circular rafts. Some of these rafts are replaced by very minor sulfides.
	Vug Filling Dolomite	20	400	Idiotopic	Calcite and dol. rhomb's in vugs.
	Galena	5	100	Annhedral	Associated with Group 2 dol.
	Pyrite	5	10-600	Annhedral	Associated with pyrite and Group 2 dol. Odd stringy texture on mineral edges.
82V45	Group 1 Dolomite	20	100-300	Xenotopic	Original recrystallized dolomite fabric. Where sphalerite grains cut Group 1 dol, some

Thin Section Descriptions

Sample	Mineral	% of Sample	Grain Size (um)	Grain Shape	Notes
					recrystallization has occurred on grain boundaries.
	Group 2 Dolomite	20	100-210	Xenotopic	Many idiotopic grains. Heavy CRM on grain boundaries
	Sphalerite	59.5	30-80		Consistent near zonation of purple on sphal. rims in a triangular pattern. Some grains have a yellow mottled coloration. Much of the sphal. is concentrated near styolites.
	Pyrite	0.5	10-600	Annhedral	Wispy appearance with clear replacement of dolomite and sphalerite.
82V69	Group 1 Dolomite	42.5	150-350	Xenotopic	Moderate CRM on grain boundaries, tightly packed irregular grain boundaries, overall cloudy and grungy. Relict oolites.
	Group 2 Dolomite	30	50-150	Xenotopic	Recrystallized with heavy CRM on grain boundaries. Some idiotopic grains.

Thin Section Descriptions

Sample	Mineral	% of Sample	Grain Size (um)	Grain Shape	Notes
	Group 3 Dolomite	15	30-110	Xenotopic	Tighter interlocking boundaries. Smaller grain sizes from an increased degree of recrystallization. Higher CRM content than Group 2
	Vug Filling Dolomite	10	120-350	Idiotopic	Oriented crystals show clear growth from outside-inside of vein structure. Many are zoned, some are tightly packed Xenotopic.
	Pyrite	2.5	20-50	Annhedral	Occurs in Group 2 and vug filling dol. but has a stronger association with vug filling dol. veins which cut the sample.
89DR13	Group 1 Dolomite	45	80-300	Xenotopic	Tight interlocking grains, minor CRM on grain boundaries.
	Group 2 Dolomite	30	50-120	Idiotopic	Euhedral rhomb's with some space (filled with CRM) between grains.
	Vug Filling Dolomite	15	100-400	Idiotopic	Vug filling, zoned crystals with black grungy core and a white rim.
	Sphalerite	5	10-50	Annhedral	Green, no zonation, occurs on the hanging wall size of a medium amplitude styolite.
	Galena	2.5	200-350		Vug filling

Thin Section Descriptions

Sample	Mineral	% of Sample	Grain Size (um)	Grain Shape	Notes
	Pyrite	2.5	10-600	Annhedral	Preferentially associated with Group 2, occurs as specks.
93DR7	Group 1 Dolomite	5	80-350	Xenotopic	Tightly interlocking grain boundaries, moderate CRM on grain boundaries.
	Group 2 Dolomite	40	50-125	Idiotopic	Abundant CRM on grain boundaries. Moderate pyrite specks associated with this zone.
	Group 3 Dolomite	30	10-50	Xenotopic	Moderate CRM on grain boundaries, many are micro-crystalline.
	Vug Filling Dolomite	10	210-550	Idiotopic	Zonation present, cloudy brown core and white rims.
	Sphalerite	10	100-500	Annhedral	Occasional purple zonation and moderate purplish mottling. Crystals are cut by styolites and one sample shows organic inclusions within the crystal structure. Sphal. are concentrated near styolites, which are high amplitude. Sphalerites are finer grained than most other samples.

Thin Section Descriptions

Sample	Mineral	% of Sample	Grain Size (um)	Grain Shape	Notes
	Galena	2.5	100-2500	Annhedral	Cuts all dolomite types and Sphal. Associated with vugs. Preferentially follows CRM pathways around Group 2/3 grains- indicating it was emplaced after these events.
	Pyrite	2.5			Occurs as specks throughout most dolomite zones, though is most concentrated in the recrystallized zones.
99DR7	Group 1 Dolomite	20	100-400	Xenotopic	Moderate CRM between grain boundaries, which are tight with no matrix present. No zonation apparent. Many euhedral rhomb's, but they are in the minority.
	Group 2 Dolomite	40	90-180	Idiotopic	Abundant CRM on grain boundaries. Very small recrystallized grains.
	Vug Filling Dolomite	48	120-350	Idiotopic	Moderate CRM on grain boundaries. Some zonation on dol. rhomb's with grungy core and white rim.

Thin Section Descriptions

Sample	Mineral	% of Sample	Grain Size (um)	Grain Shape	Notes
	Pyrite	2	5-15		Cuts all dol. generations
Buick 01	Group 2 Dolomite	10	100-200	Xenotopic	Tightly packed grains, CRM on grain boundaries.
	Group 1 Dolomite	30	100-150	Xenotopic	Associated with sulfides – CRM on grain boundaries. Some grains crystals are idiotopic with well developed rhombedrons.
	Group 3 Dolomite	5	120-300	Idiotopic	Occurs in vugs
	Sphalerite	40	50-200	Annhedral	Occurs in large masses with indistinguishable crystals (70%), and individual grains (30%). Massive sphalerite appears lineated from carbonaceous material cutting it. Sphalerites are green with occasional mottling of purple/green.
	Marcasite	0.5	10-100	Annhedral	Cuts sphalerites, appears corroded and broken in some places.
	Galena	1	500-1000	Annhedral	Cuts sphalerite

Thin Section Descriptions

Sample	Mineral	% of Sample	Grain Size (um)	Grain Shape	Notes
Buick 02	Group 1 Dolomite	15	50-100	Xenotopic	Carbonaceous Material surrounding this phase of dolomite grains. Small grains, tightly interlocking, no matrix present.
	Group 2 Dolomite	30	80-120	Xenotopic	Associated with sphalerites, larger than Group 1. Inter-granular textures are tight and interlocking with little matrix present.
	Group 3 Dolomite	5	300-620	Idiotopic	growing in void space around sphalerite – Group 2 crystals replaced by Group 3? Some void space in vugs, but still largely tight interlocking textures.
	Sphalerite	48	50-320	Annhedral	Occurs in aggregate masses in many cases, with grain sizes several mm in size. Carbonaceous material cutting sphalerite and gives sphalerite a lineated appearance.
	Galena	2	100-600	Annhedral	Replaces sphalerite and dolomites. Some galena has a complicated texture with “loop” textures around sphalerites.

Thin Section Descriptions

Sample	Mineral	% of Sample	Grain Size (um)	Grain Shape	Notes
Buick 03	Group 1 Dolomite	25	30-70	Idiotopic	Heavy carboneacous material on grain boundaries. Well shaped tiny rhomb. Dolomites. Late, cross cuts other features.
	Group 2 Dolomite	15	50-200	Xenotopic	Near sphalerites, grains are recrystallized into an almost unrecognizable crystal shape.
	Group 3 Dolomite	20	80-210	Idiotopic	Associated with vugs – disem. grains of sphalerite throughout this zone.
	Sphalerite	30	60-180	Subhedral	Green with some mottling of crystals.
	Galena	5	200-5000	Annhedral	Occurs as massive annhedral crystal and as smaller replacing crystals.
	Pyrite	0.1	5-400	Subhedral	Former pyrite cubes which have been cut and broken up by later carboneacous material.
	Marcasite	4.9	5-500	Subhedral	Forms as extremely fine grained hexagonal crystals about 5um in size scattered throughout sample in all mineral phases except sphalerite. Replaces galena

Thin Section Descriptions

Sample	Mineral	% of Sample	Grain Size (um)	Grain Shape	Notes
Buick 04	Group 1 Dolomite	50	25-150	Xenotopic	Associated with subhedral sulfides, carbonaceous material at grain boundaries.
	Group 2 Dolomite	20	25-75	Xenotopic	Associated with smaller sphalerite crystals.
	Sphalerite 2	5	10-100	Annhedral	Smaller, associated with Group 2 crystals. Cut by galena.
	Sphalerite 1	15	80-210	Annhedral	Associated with Group 1 crystals. Pre-galena.
	Galena	9	15-200	Annhedral	Inter-granular between dolomite grains.
	Pyrite	1	Microcrystalline	Annhedral	Occurs in an annhedral mass surrounding dolomite grains, cutting sphalerite. Replaced Group 1 and Group 2 dolomites.
Buick 05	Group 1 Dolomite	60	100-210	Xenotopic	Tightly interlocking crystals.
	Group 2 Dolomite	10	60-150	Idiotopic	Late feature which cuts Group 1 dolomites. Large open spaces filled with sphalerites, evidence of fluid flow with broken, rotated dolomite rhomb's. Abundant carbonaceous material flooded with this stage.

Thin Section Descriptions

Sample	Mineral	% of Sample	Grain Size (um)	Grain Shape	Notes
	Sphalerite 1	30	100-400	Annhedral	Replaces Group 1 crystals with "atoll" dolomite rhomb's within crystals.
	Sphalerite 2	5	80-500	Subhedral	Larger crystals associated with late event which caused re-crystallization of dolomites and abundant CRM.
	Galena	4	25-150	Annhedral	Minor, fills Group 2 grain boundaries after sphalerite.
	Pyrite	1	5-200	Subhedral	Fills Group 2, no association with other sulfides. Some speckled material looks remobilized by another fluid which may have caused break up of original euhedral crystal.
Buick 06	Group 2 Dolomite	30	80-120	Xenotopic	Associated with vein structure which cuts original host rock. Evidence of fluid movement and transport with rotated dolomite rhomb's from an external source. In-situ dolomites are finer grained than original dolomites and appear grungy and altered.

Thin Section Descriptions

Sample	Mineral	% of Sample	Grain Size (um)	Grain Shape	Notes
	Group 1 Dolomite	15	50-180	Xenotopic	Strong carbonaceous material throughout, cross cut by galena veins. Similar to other samples.
	Transported Dolomites	10	40-180	Idiotopic	Abundant open space between grains, rotated rhomb's which do not interlock or fit together. Interpreted as transported dolomite fragments from elsewhere.
	Group 3 Dolomite	5	100-210	Idiotopic	New dolomite generation – have not seen in other samples. Another generation of fluid?
	Sphalerite 1	30	60-700	Sub-Euhedral	Open space colloform textures, associated with Group 1 dolomites. Clear sphalerite growth rings in open space within vein. Indicative of multiple fluid pulses within this vein.
	Sphalerite 2	5	100-230	Subhedral	Occurs in Group 2 dolomite, evidence of leaching. Altered and grungy. Same generation as sphalerite 1, just altered.

Thin Section Descriptions

Sample	Mineral	% of Sample	Grain Size (um)	Grain Shape	Notes
	Galena	4	400-1300	Annhedral	Cuts both generations of dolomite, replaced by sphalerite.
	Pyrite	1	400-700	Annhedral	Cuts all minerals except for galena.
Buick 07	Group 1 Dolomite	50	80-160	Idiotopic	Many crystals subhedral, but most are rhombedran and are comparatively coarse grained.
	Group 2 Dolomite	15	30-90	Idiotopic	CRM throughout on grain boundaries, well formed rhombedran's which are very tiny.
	Vug-Filling Dolomite	10	25-200	Idiotopic	Fills vugs in Group 2 dolomites and vugs/fractures in sphalerites. Coarse, euhedral dolomites.
	Sphalerite	15	80-1300	Annhedral	Cuts both dolomite zones. Replacement of original host rock. Green, massive, grains broken up by late fracturing and replacement by other minerals.
	Sphalerite 2	2.5	400-600	Annhedral	Fills vugs in a seam of increased porosity across thin section. Late galena cuts sphalerite in these vugs.

Thin Section Descriptions

Sample	Mineral	% of Sample	Grain Size (um)	Grain Shape	Notes
	Galena	5	800-1300	Annhedral	Late feature, fills fractures, is post all fracturing. Fills open spaces, in association with vug filling dolomites.
	Pyrite	2.5	120-400	Annhedral	Grungy, forms on contact of massive sphalerite which cuts original dolomite. Cuts sphalerite and late dolomite recrystallization. Replaces other minerals.
Casteel 01	Group 1 Dolomite	83.5	100-300	Xenotopic	Small tightly packed xenotopic crystals. Overall, very little matrix identifiable in thin section. Gradational grain size throughout sample. Brown staining on grain boundaries.
	Group 2 Dolomite	10	150-300	Idiotopic	Large, idiotopic, but much later. Very little matrix identifiable in thin section. Associated with carbonaceous sulfides in veinlet and voids – clear recrystallization of sulfides. Iron staining on grain boundaries.

Thin Section Descriptions

Sample	Mineral	% of Sample	Grain Size (um)	Grain Shape	Notes
	Sphalerite	2.5	100-600	Sub-Euhedral-Euhedral	Sphalerite has a mottled, gray-green appearance and are subhedral-euhedral.. Some crystals have a distinct zonation of green-purple from one part of the crystal to the next. Crystals clearly cut Group 1 and Group 2 dolomites.
	Carbonaceous Material	2	Microcrystalline	Annhedral	
	Galena	1.5	50-100	Annhedral	Associated with carbonaceous material in sec. dol veinlet
Casteel 02	Group 1 Dolomite	50	80-200	Xenotopic	Small tightly packed xenotopic crystals. Overall, very little matrix identifiable in thin section. Rare disseminated iron staining
	Group 2 Dolomite	30	150-400	Xenotopic	In close proximity to sphalerite. Iron stained. Abundant iron staining on grain boundaries seems to form a “reaction front” where it cuts the z1 dolomites.

Thin Section Descriptions

Sample	Mineral	% of Sample	Grain Size (um)	Grain Shape	Notes
	Sphalerite 1	15	300-700	Subhedral	Black, some have greenish tint in ppl.
Casteel 03	Group 1 Dolomite	80	100-150	Xenotopic	Small, tightly packed annhedral-subhedral crystals with sulfides in between some grain boundaries. No matrix discernible.
	Group 2 Dolomite	15	150-500	Idiotopic	Relatively large subhedral to euhedral crystals which are in close proximity to a vein (white, now void space).
Casteel 04	Group 1 Dolomite	15	150-400	Xenotopic	Tightly packed xenotopic crystals. Overall, very little matrix identifiable in thin section. Dolomites display uniform extinction in crossed polars – which may be indicative of a similar recrystallization event. Larger grains of dolomite compared typical Group 1 dolomites, similar textures however

Thin Section Descriptions

Sample	Mineral	% of Sample	Grain Size (um)	Grain Shape	Notes
	Sphalerite	35	100-300	Subhedral	Sphalerites appear to cut Group 1 dolomites. Most sphalerites are green with some displaying clear zoning of a green euhedral hexagonal core rimmed by a reddish zone, probably due to organic matter. Some show oscillatory growth zoning.
	Galena	10	100-700	Annhedral-Subhedral	Fills vugs, is replaced by sphal.
	Marcasite	5	50-5000	Annhedral	Occurs in tiny grains and in large masses with complicated inter-granular relationships with sphalerite. Some have loop textures around sphalerite crystals in between sphal. grains.
Casteel 05	Group 1 Dolomite	10	150-300	Xenotopic	Forms clasts within a breccia.
	Group 2 Dolomite	15	300-950	Idiotopic	Cut by fractures
	Sphalerite	74	250-1000	Subhedral	Massive with lineaments and fractures throughout. Color is dominantly green, with many crystals forming a mottled reddish color.

Thin Section Descriptions

Sample	Mineral	% of Sample	Grain Size (um)	Grain Shape	Notes
	Galena	1	50-1000	Annhedral-Euhedral	Forms a cube as open space filling. This is late stage (correlated with Tri-state Pb) galena. Some tiny galena flecks within sphalerite.
	Marcasite	0.1	25	Annhedral	Occurs as tiny specs filling open spaces.
Casteel 06	Group 1 Dolomite	15	150-200	Xenotopic	Microbreccia, rotated clasts
	Group 2 Dolomite	15	250-600	Idiotopic	Occurs in open spaces and in fractures
	Sphalerite	65	400-1200	Subhedral	Occurs as individual grains
	Galena	5	500-1500	Annhedral-Euhedral	Fills open spaces in vugs - two types, cubic and annhedral
	Clay/Carbonaceous Material	5	n/a	Annhedral	Coats dolomite grains and occurs in open spaces and vugs.
	Marcasite	0.1	300	Annhedral	Occurs in vugs.
Casteel 07	Group 2 Dolomite	25	50-100	Xenotopic	Iron staining on grain boundaries, tightly packed.
	Group 1 Dolomite	45	100-200	Xenotopic	Sphalerites in this phase as discrete grains.
	Group 3 Dolomite	10	75-150	Idiotopic	Rhombedrans, associated with vugs. No sulfide association.

Thin Section Descriptions

Sample	Mineral	% of Sample	Grain Size (um)	Grain Shape	Notes
	Sphalerite	18	25-250	Subhedral	Green, no noticeable zonation. Associated with Group 2 dolomite, which it replaces at times leaving islands of dolomite within its matrix.
	Marcasite	2	25-50	Annhedral	Replaces sphalerite
Casteel 08	Group 2 Dolomite	25	50-150	Xenotopic	Tightly packed, iron staining on grain boundaries. These form clasts within this micro-breccia as well as parts of the wall rock.
	Group 1 Dolomite	50	80-200	Xenotopic	Less iron staining on grain boundaries, larger, forms sharp contacts with Group 1 dolomites.
	Group 3 Dolomite	5	100-200	Idiotopic	These formed in vugs within the sample. No iron staining present.
	Sphalerite	19.9	80-350	Annhedral	Many grains have inclusions within them that you can only see in xpl. Inclusions go extinct in ppl. Grains are mottled with purple/reddish coloration.

Thin Section Descriptions

Sample	Mineral	% of Sample	Grain Size (um)	Grain Shape	Notes
	Marcasite	0.1	30-60	Annhedral	Rare, forms in outlines around dolomite grains, cuts sphalerite grains.
Fletcher 01	Group 1 Dolomite	80	600-800	Xenotopic	Coarse, subhedral dolomite rhomb's. Some crystals are large (600) and euhedral with clear zonation of a cloudy core and clear rim.
	Group 2 Dolomite	15	300-500	Xenotopic	Becomes finer grained near galena with minor CRM rich on grain boundaries. Many dolomite grains are grungy and re-crystallized.
	Group 3 Dolomite	2.5	10-50	Xenotopic	Later re-crystallization, very microcrystalline, cuts Group 2 dolomite type. Barren with minor CRM on grain boundaries, not like other CRM rich late dolomite re-crystallization's.
	Galena	1	100-500	Annhedral	Clear replacement texture with islands of rotated dolomite rhomb's as islands within annhedral galena.
	Pyrite	0.5	10-50	Subhedral	Minor subhedral galena

Thin Section Descriptions

Sample	Mineral	% of Sample	Grain Size (um)	Grain Shape	Notes
Fletcher 02	Group 1 Dolomite	70	30-80	Idiotopic	Coarse, similar to other phases, but finer grained and more well shaped crystals. Minor CRM staining. Tightly packed crystals with minor overall brown grunge across all crystals. Minor vugs with large euhedral dolomite crystals.
	Group 2 Dolomite	25	100-300	Idiotopic	Similar to other re-crystallized dolomite zones, tiny idiotopic dol. Rhomb's with abundant CRM on grain boundaries.
	Group 3 Dolomite	5	50-70	Idiotopic	Occur as circular macro-blebs of re-crystallized dolomites. Tiny rhomb's with no CRM on grain boundaries.
Fletcher 03	Group 1 Dolomite	60	80-450	Xenotopic	Many are zoned with clear rims and cloudy/grungy cores. Many are nearly idiotopic. Minor CRM on grain boundaries. Occurs stratigraphically below coarse dolomite which hosts sulfides.

Thin Section Descriptions

Sample	Mineral	% of Sample	Grain Size (um)	Grain Shape	Notes
	Group 2 Dolomite	20	50-250	Idiotopic	CRM rich, microcrystalline that is associated with other late CRM rich recrystallization. Moderate CRM on grain boundaries, less than other samples.
	Vug Filling Dolomite	5	125-1250	Idiotopic	Secondary horizontal seam at top of sample. Filled with sulfides. Xenotopic, very large crystals. Crystals become massive closer to sulfides.
	Sphalerite	5	50-800	Annhedral	replaces chalc
	Galena	2.5	300	Annhedral	First generation, almost entirely replaced by sphalerite.
	Pyrite	2.5	75	Annhedral	Replaces chalcopyrite. Tiny grains replacing other sulfide phases. Tiny specks throughout all dolomite zones, but heaviest in Group 2.

Thin Section Descriptions

Sample	Mineral	% of Sample	Grain Size (um)	Grain Shape	Notes
Fletcher 04	Group 1 Dolomite	30	100-400	Xenotopic	Grains have minor CRM between grain boundaries, with grain edges that are truncated and rounded.
	Group 2 Dolomite	15	75-190	Xenotopic	Many grains are nearly idiotopic. Correlates with other late, CRM rich recrystallization dolomites in other samples. Contact with Group 1 is marked by a sharp contact consisting of thick CRM and tiny 1 um pyrite specks. Contact erodes other dolomites and sphalerites, even replacing them in some cases.
	Vug filling Dolomite	10	800-1200	Idiotopic	Clear zonation apparent – probable dolomite cement and CL zoning.
	Sphalerite	30	350-3000	Annhedral	Green, variable grain size. Replaces Group 2 and vug filling dolomites. Mostly massive with irregular crystal shapes
	Galena	7.5	100-3000	Annhedral	cut by sphal

Thin Section Descriptions

Sample	Mineral	% of Sample	Grain Size (um)	Grain Shape	Notes
	Pyrite	7.5	1-500	Annhedral	Tiny specks.
Fletcher 05	Group 1 Dolomite	50	105-500	Idiotopic	Correlatable, associated with sphalerite crystals.
	Group 2 Dolomite	20	40-160	Idiotopic	Classic, late CRM rich correlatable Group occurs as rafts and lenses with Group 1's throughout sample. Heavy CRM on grain boundaries, very small crystals.
	Vug Filling Dolomite	15	110-700	Idiotopic	Fills vugs. No zonation present.
	Sphalerite	5	400-2000	Annhedral	Replaces Group 1 crystals and forms in matrix where available.
	Galena	10	Massive	Annhedral	Replaces Group 1 crystals and sphalerite.
Fletcher 06	Group 1 Dolomite	15	250-500	Idiotopic	Zonation on the rim of the dolomite crystals, clear rim, cloudy cores. Crystals are replaced by sphalerite.
	Group 2 Dolomite	10	50-200	Idiotopic	Recrystallized, has 3 CRM veins cutting through the main part of this zone. Tight interlocking granular boundaries, abundant CRM in between grain

Thin Section Descriptions

Sample	Mineral	% of Sample	Grain Size (um)	Grain Shape	Notes
					boundaries. Cuts massive sphalerite.
	Sphalerite	70	Massive	Annhedral	Massive, replacement sphalerite. No individual grains present. Replaces Group 1 dolomite crystals. Zoned growth in one part of the massive section.
	Galena	3	300-5900	Annhedral	Early stage appears to be replaced by sphalerite
	Pyrite	2	600	Subhedral	Replaces sphalerite and Group 1 dolomite. Grain was clearly cubic and became altered and broken down by later fluids.
LC-150	Group 2 Dolomite	90	25-100	Idiotopic	Different visual appearance based on the quantity of CRM between grain boundaries. In general, larger more idiotopic grains tend to have more CRM than smaller grains which were recrystallized.

Thin Section Descriptions

Sample	Mineral	% of Sample	Grain Size (um)	Grain Shape	Notes
	Vug Filling Dolomite	9.75	100-1200	Idiotopic	Well shaped crystals with some calcite present as matrix in-fill.
	Pyrite	0.25	5-250	Annhedral	Associated with CRM rich zones specifically.
LC-486	Group 1 Dolomite	80	300	Xenotopic	Grains are coarser and have a different appearance than other typical Group 1 dolomites. Overall these are coarser and overall more cloudy than other dolomites. Grungy core and white cloudy rims common. Dolomite phase not seen in any other samples.
	Coarse “Breccia” Dolomite	20	300-2000	Idiotopic	Many crystals have a clear zonation of a grungy core and a white rim. These are surrounded by CRM rich material and have “flow” type textures which with the clearly rotated clasts is evidence that these were transported. Associated with glauconite. Some grains show a zonation of n the core with a sharp contact with a white rim. Occur as rotated, zoned

Thin Section Descriptions

Sample	Mineral	% of Sample	Grain Size (um)	Grain Shape	Notes
					clasts within a matrix of CRM rich material. Chlorite occurs as fluid type texture within the CRM Group as well.
	Pyrite	0.5	5-15		Pyrite associated with glauconite and CRM rich zones. Pyrite framboids identified in association with glauconite and CRM.
LC-498	Group 1 Dolomite	72.5	160-300	Xenotopic	Similar grain size as observed in mineralized samples with
	Group 2 Dolomite	5	100	Xenotopic	Occurs as oval rafts (~700 um) within Group 1 dolomite. CRM rich on grain boundaries.
	Broken/rotated Dol – Stylo Zone	15	550-700	Broken/Irregular	This dolomite texture appears to be rotated . Abundant CRM material as "matrix" surrounding dolomites. Loose inter-

Thin Section Descriptions

Sample	Mineral	% of Sample	Grain Size (um)	Grain Shape	Notes
					crystalline textures filled with CRM.
	Vug Filling Dolomite		150-1300	Idiotopic	Some internal crystal zonation observed.
	Pyrite	0.5		Annhedral	Associated with vug filling dolomite.
LC-499	Group 1 Dolomite	59.5	50-160	Xenotopic	Many grains have a clear zonation with a grungy core and a white rim. Typical Group 1 dolomite that is correlated with mineralized samples. Relict, though smaller than usual oolites present.
	Group 2 Dolomite	20	70-130	Idiotopic	Strong CRM on grain boundaries.
	Group 3 Dolomite	10	100-160	Xenotopic	Similar to Group 2 but recrystallized, Xenotopic with tighter interlocking grain boundaries.
	Vug Filling Dolomite	15	80-300	Idiotopic	Associated with abundant randomly oriented vugs and veinlets. Clear open space crystal growth from wall inwards. Veinlets these grow into only two Group(2/3) and

Thin Section Descriptions

Sample	Mineral	% of Sample	Grain Size (um)	Grain Shape	Notes
					appear random in length and geometry.
	Pyrite	0.5	5-10	Annhedral	Occurs largely as specks in all dolomite types.
LC-584	Group 1 Dolomite	65	50-200	Xenotopic	Very little CRM on grain boundaries. Much finer grained than coarse dolomite nearer in samples. Undulatory extinction in many grains.
	Styolite Zone	30	10-250	Xenotopic	Part of a large styolite zone. Heavy CRM on grain boundaries. Many rotated larger fragments of calcite and dolomite.
	Vug Filling Dolomite	5	50-850	Idiotopic	Some zoned crystals with a cloudy core and a white rim.
	Sphalerite	0.01	30-150	Annhedral	Grains are frequently corroded, with increasing corrosion in Group 2 examples.

Thin Section Descriptions

Sample	Mineral	% of Sample	Grain Size (um)	Grain Shape	Notes
	Pyrite	5	5-100	Annhedral	Occurs as specks and small annhedral fragments in both dolomite zones
LC-617	Group 1 Dolomite	80	100-490	Xenotopic	Minor CRM on grain boundaries. Relict oolites in some parts of the sample.
	Group 2 Dolomite	10	100-150	Idiotopic	Occurs as rafts and is strongly associated with styolites. Contains abundant CRM on grain boundaries and appears to cut earlier Xenotopic dolomite.
	Vug Filling Dolomite	9.5	250-600	Idiotopic	Cloudy crystals, no zonation apparent. Calcite cement? (fine grained, high bifrig.) surrounds vugs. Some vugs filling crystal display curved twin planes.

Thin Section Descriptions

Sample	Mineral	% of Sample	Grain Size (um)	Grain Shape	Notes
	Pyrite	0.5	10-200	Annhedral	Speckled/web texture from some fluid corroding/removing some of the pyrite later. Strongly associated with recrystallized fabrics (Group 2).
LC-681	Group 1 Dolomite	80	100-200	Xenotopic	Substantial amounts of CRM between grain boundaries, more than normal. Grains are smaller than observed elsewhere.
	Group 2 Dolomite	9.5	50-70	Xenotopic	Largely Xenotopic but some idiotopic grains with very high quantities of CRM.
	Group 3 Dolomite	10	30	Xenotopic	Xenotopic with even more CRM on grain boundaries.
	Vug Filling Dolomite		100-240	Idiotopic	Standard vug filling.
LC-710	Group 1 Dolomite	70	150	Xenotopic	Light CRM on grain boundaries.
	Group 2 Dolomite	24.5	100	Xenotopic	Tons of CRM on grain boundaries and in some cases throughout.
	Vug Filling Dolomite	5	700	Idiotopic	No apparent zonation.

Thin Section Descriptions

Sample	Mineral	% of Sample	Grain Size (um)	Grain Shape	Notes
	Pyrite	0.5		Annhedral	Associated with CRM rich zones across multiple dolomite zones.
Sweetwater 01	Group 1 Dolomite	50	100-400	Idiotopic	Cut by styolite (CRM vein) with some recrystallization of dolomite to Group 2 size and shape. Abundant glauconite(oval shapes) throughout sample.
	Group 2 Dolomite	20	25-90	Idiotopic	Occurs as oval and circular rafts approximately 2-3 mm in size.
	Vug Filling Dolomite	5	250	Idiotopic	Some are zoned with a cloudy core and clear rims.
	Sphalerite	20	60-2000	Annhedral	Green, some gray mottling. Occurs as individual grains and as an interconnected network of continuous mineralization. Cuts Group 1 dolomites. Does not occur in Group 2 dolomites.Sphalerites appear eroded with abundant open space

Thin Section Descriptions

Sample	Mineral	% of Sample	Grain Size (um)	Grain Shape	Notes
					which indicates they were remobilized during vug formation.
	Galena	3	1000-1500	Annhedral	Fills vugs
Sweetwater 02	Group 1 Dolomite	25	100-700	Xenotopic	Moderate CRM between grains, tight interlocking grain boundaries. Replacement of dol. by sphal. Some idiotopic grains present.
	Group 2 Dolomite	10	25-100	Idiotopic	Occurs within ~300 um of styolite's, consists of tiny idiotopic dolomites. Correlatable with other dol. generations in other sulfides.
	Group 3 Dolomite	5	5-15	Xenotopic	Micro-crystalline and not associated with any new sulfides. The crystals are too small to identify, but appear to be annhedral
	Vug Filling Dolomite	5	500-1200	Idiotopic	Fills vugs, some faint zonation apparent.

Thin Section Descriptions

Sample	Mineral	% of Sample	Grain Size (um)	Grain Shape	Notes
Sweetwater 03	Group 1 Dolomite	40	50-210	Xenotopic	Replaced by sphal. No evidence of recrystallization in association with sphal.
	Group 2 Dolomite	10	90-180	Xenotopic	CRM cut sphal. Light-moderate CRM on grain boundaries. Some idiotopic crystals.
	Vug-Filling Dolomite	15	300-500	Idiotopic	Small veinlets branch off from vug zones with zoned, euhedral dol cutting other textures.
	Sphalerite	20	40-2000	Annhedral	Odd zonation – broadly euhedral texture on one crystals in SW corner.
	Galena	10	90-2000	Annhedral	Fills vugs, good texture indicating replacement of vug filling dolomites and sphal.
	Pyrite	4.9	25-1000	Annhedral	Pyrite occurs in Group 2 recrystallized dolomites and as inclusions within chalcopyrite and galena – post sphal?

Thin Section Descriptions

Sample	Mineral	% of Sample	Grain Size (um)	Grain Shape	Notes
	Chalcopyrite	0.1	500	Annhedral	Complicated texture – almost looks resolved out of galena. Inclusion of pyrite (10 um) within chalco.
Sweetwater 04	Group 1 Dolomite	20	100-350	Xenotopic	Correlatable with other dolomite – cut by major sulfides.
	Group 2 Dolomite	25	70-190	Idiotopic	Abundant CRM.
	Vug Filling Dolomite	10	100-700	Xenotopic	Some idiotopic grains.
	Sphalerite	10	25-1800	Annhedral	Mostly locked by galena. Heavily fractured throughout.
	Galena	25	20-2500	Annhedral	Replaced by sphalerite. Evidence of replacement by dol phase? Open space textures present (cubic-galena).
	Pyrite	5	10-600	Annhedral	Exsolutions/inclusions within chalcopyrite and as single standalone crystals ~500 um in size. Emplaced before faulting and before Group 2 dol development. Strongly associated with vug filling dolomite.

Thin Section Descriptions

Sample	Mineral	% of Sample	Grain Size (um)	Grain Shape	Notes
	Chalcopyrite	5	30-100	Annhedral	Occurs as replacement of galena and as fine granular disseminations within the gangue phase.
Sweetwater 05	Group 1 Dolomite	65	220	Xenotopic	Not associated with galena or any sulfides.
	Group 2 Dolomite	25	20-150	Idiotopic	Occurs as oval rafts within a matrix of Group 1.
	Vug Filling Dolomite	5	350-900	Idiotopic	Strongly associated with galena growth.
	Sphalerite	2.5	20-75	Annhedral	Occur as inclusion which are replacing galena. Similar generation as SWT 04.
	Galena	1.5	1000-3000	Euhedral	Cuboctahedral and Cubic phases present. Associated with vug filling dolomites.
	Pyrite	0.5	250	Annhedral	Minor pyrite.
Sweetwater 06	Group 1 Dolomite	65			
	Group 2 Dolomite	20	100	Idiotopic	Occurs in oval rafts. Abundant CRM.

Thin Section Descriptions

Sample	Mineral	% of Sample	Grain Size (um)	Grain Shape	Notes
	Vug Filling Dolomite	5	600	Idiotopic	Vug filling, excellent zonation. CL stratigraphy ONLY applicable to galena – NOT sphalerite – despite presence of sphal near or in vugs. No CRM present.
	Sphalerite	5	250	Annhedral	Associated with vugs – deposited in them or were they already there and were dissolved by incoming fluids? No open space textures. Interpreted to be an earlier sphal. phase seen in most other samples.
Sweetwater 07	Group 1 Dolomite	20	100-280	Xenotopic	Light to moderate CRM on grain boundaries – gradational grain size with sphal. replacing large and small types.
	Group 2 Dolomite	5	Microcrystalline	Xenotopic	Occurs as small rafts which are oval in shape within sample. Grungy, appears heavily altered. Pyrite associated with this phase. Not associated with sphal.

Thin Section Descriptions

Sample	Mineral	% of Sample	Grain Size (um)	Grain Shape	Notes
	Vug Filling Dolomite	10	200-400	Idiotopic	Zoned crystals.
	Sphalerite	63	30-000's	Subhedral	growth textures on many sphalerites – indicating potential open space filling and multiple generations of fluid.
	Pyrite	2	10-200	Annhedral	Occur as fine specks within Group 2 dol and as grungy distorted grains within vug filling dolomites. Random specs in sphal.
Sweetwater 08	Group 1 Dolomite	60	300	Xenotopic	Moderate CRM on grain boundaries. Hard to differentiate from vug filling
	Vug Filling Dolomite	25	250	Idiotopic	Minor phase, does not seem associated with galena
	Galena	2.5	400-800	Euhedral	Both phases present, cuts Group 1 and Group 3 dolomite.
	Sphalerite	2.5	30-50	Annhedral	Cuts galena with cusp/carrie textures.
	Chalcopyrite	2.5	100-175	Annhedral	
	Pyrite	1	5-10	Annhedral	Replaces chalcopyrite
Sweetwater 09	Group 1 Dolomite	50	25		Replacement of both zone's by galena. This

Thin Section Descriptions

Sample	Mineral	% of Sample	Grain Size (um)	Grain Shape	Notes
					Group only occurs as minor rafts.
	Group 2 Dolomite	50	75		Recrystallized, cut by galena. Most of the rock is composed of this phase, except where galena cuts it.
Sweetwater 10	Group 2 Dolomite	20	2-210	Xenotopic	Abundant CRM material on grain boundaries, broken/rotated fossil fragments. Sharp contact between this
	Group 1 Dolomite	50	5-50	Xenotopic	CRM cuts through micro-crystalline zone, does not occur on grain boundaries. Flooding of Group with CRM common. Grains become substantially larger outside of CRM rich areas.
	Vug Filling Dolomite	10	100-600	Idiotopic	Cut by sphal? Clear zonation of dol.

Thin Section Descriptions

Sample	Mineral	% of Sample	Grain Size (um)	Grain Shape	Notes
	Sphalerite	15	25-45	Annhedral	here CRM appears to move into sample, color of sphal. changes to a dark purple. Re-crystallization event must have had some heat – perhaps it altered and incorporated CRM from the event into its crystal structure?
	Chalcopyrite		200-300	Circular, Ovoid, Rhombohedral	
	Pyrite	5	5-45	Subhedral	5-10 microns strong associated with Group 2 dolomite, some euhedral cubes.

Appendix B: Electron Microprobe Data

Table B1: Electron Microprobe Data

Sample - Analysis Point	Zn	Fe	Cd	S	Total
Casteel 10 Spot 3 Pt 1	66.69	0.43	0.67	32.99	100.96
Casteel 10 Spot 3 Pt 2	63.70	3.32	0.97	33.34	101.45
Casteel 10 Spot 3 Pt 3	63.88	2.52	1.03	32.87	100.52
Casteel 09 Spot 1 Pt 1	65.87	0.86	0.76	33.17	100.82
Casteel 09 Spot 1 Pt 2	65.92	0.79	0.77	33.12	100.84
Casteel 09 Spot 1 Pt 3	66.08	0.22	0.52	32.93	100.03
Casteel 09 Spot 1 Pt 4	66.14	0.43	0.90	33.35	101.03
Casteel 09 Spot 1 Pt 5	66.79	0.26	0.71	33.43	101.37
Casteel 09 Spot 2 Pt 1	66.11	0.82	0.69	33.11	100.85
Casteel 09 Spot 2 Pt 2	66.13	0.77	0.67	33.31	101.08
Casteel 09 Spot 2 Pt 3	65.50	0.85	1.00	32.80	100.33
Casteel 09 Spot 2 Pt 4	66.04	0.82	0.81	33.25	101.1
Casteel 09 Spot 2 Pt 5	66.01	0.19	0.61	33.00	99.97
Casteel 09 Spot 2 Pt 6	66.09	0.35	0.68	33.53	100.83
Buick 03 Spot 4 Pt 1	65.75	0.15	0.41	33.33	99.77
Buick 03 Spot 4 Pt 2	66.77	0.18	0.80	33.04	101.05
Buick 03 Spot 4 Pt 3	65.55	0.36	2.14	33.41	101.57
Buick 03 Spot 4 Pt 4	66.25	0.42	1.06	32.77	100.56
Buick 03 Spot 4 Pt 5	66.55	0.29	0.87	32.64	100.51
Buick 03 Spot 4 Pt 6	67.27	0.13	0.25	33.10	100.94
Buick 06 Spot 1 Pt 1	65.97	0.86	1.03	33.15	101.22
Buick 06 Spot 1 Pt 2	66.67	0.73	0.41	33.18	101.06
Buick 06 Spot 1 Pt 3	67.48	0.09	0.33	31.41	99.51
Buick 06 Spot 1 Pt 4	64.86	1.22	1.22	32.62	100.01
Buick 06 Spot 1 Pt 5	65.85	0.83	1.01	32.99	100.81
Buick 06 Spot 1 Pt 6	64.61	1.25	1.24	32.51	99.8
Buick 06 Spot 1 Pt 7	64.73	1.03	1.32	32.71	99.98
Buick 06 Spot 1 Pt 8	65.67	0.67	0.99	33.11	100.54
Buick 06 Spot 1 Pt 9	66.05	0.86	0.98	32.58	100.54
Buick 06 Spot 1 Pt 10	66.83	0.48	0.56	33.35	101.32
Buick 06 Spot 1 Pt 11	65.68	0.91	0.89	32.98	100.62
Buick 06 Spot 1 Pt 12	66.76	0.38	0.60	32.92	100.86
Buick 06 Spot 1 Pt 13	65.78	0.85	1.00	32.94	100.75
Buick 06 Spot 1 Pt 14	65.81	0.73	0.84	33.04	100.54
Buick 06 Spot 1 Pt 15	65.75	0.94	0.90	32.91	100.69
Buick 06 Spot 1 Pt 16	66.90	0.42	0.53	33.40	101.4
Buick 06 Spot 1 Pt 17	63.75	0.84	0.70	32.43	97.96
Buick 06 Spot 1 Pt 18	66.04	0.89	0.72	32.96	100.75
Buick 06 Spot 1 Pt 19	66.65	0.74	0.91	33.10	101.6
Buick 06 Spot 1 Pt 20	66.77	0.57	0.74	33.12	101.47
Buick 06 Spot 1 Pt 21	66.69	0.46	1.26	33.24	101.84
Buick 06 Spot 1 Pt 22	65.45	1.13	0.75	33.40	100.91

Sample - Analysis Point	Zn	Fe	Cd	S	Total
Buick 06 Spot 1 Pt 23	63.56	0.93	1.04	32.58	98.28
Buick 06 Spot 1 Pt 24	65.19	0.86	1.27	33.26	100.69
Buick 06 Spot 1 Pt 25	65.59	0.80	1.02	33.24	100.89
Buick 06 Spot 1 Pt 26	64.01	0.95	2.13	32.57	99.85
Buick 06 Spot 1 Pt 27	63.95	0.78	0.62	32.90	98.54
Fletcher 04 Spot 1 Pt 1	65.52	0.64	1.09	33.40	100.87
Fletcher 04 Spot 1 Pt 2	66.46	0.15	1.53	33.16	101.44
Fletcher 04 Spot 1 Pt 3	66.97	0.40	0.81	33.57	101.92
Fletcher 04 Spot 1 Pt 4	66.74	0.27	0.46	32.70	100.43
Fletcher 06 Spot 2 Pt 1	66.30	0.43	0.74	32.97	100.56
Fletcher 06 Spot 2 Pt 2	64.96	0.59	1.02	33.02	99.74
Fletcher 06 Spot 2 Pt 3	65.57	0.70	0.98	32.71	100.11
Fletcher 06 Spot 2 Pt 4	65.43	0.72	0.87	32.70	99.85
Fletcher 06 Spot 2 Pt 5	64.67	0.80	1.52	31.76	98.80
Sweetwater 04 Spot 2 Pt 1	66.00	0.44	1.52	32.93	101.14
Sweetwater 04 Spot 2 Pt 2	66.41	0.34	0.85	32.98	100.78
Sweetwater 04 Spot 2 Pt 3	64.60	0.75	1.15	32.35	99.16
Sweetwater 04 Spot 2 Pt 4	66.91	0.17	0.44	32.95	100.62
Sweetwater 04 Spot 2 Pt 5	64.80	0.67	1.55	32.71	99.88
Sweetwater 04 Spot 2 Pt 6	66.29	0.38	0.33	33.45	100.55
Sweetwater 04 Spot 2 Pt 7	66.26	0.30	0.79	33.24	100.8

Table B2: Electron Microprobe Standards

Element	Standard	Element	Standard	Element	Standard
Zinc	Sphalerite	Germanium	Ge	Bismuth	Bi2Se3
Lead	PbTe	Gallium	GaAs	Silver	Au80Ag20
Copper	Chalcopyrite	Cadmium	CdSe	Sulfur	Pyrite
Iron	Pyrite	Arsenic	Cobalt	Selenium	Bi2Se3
Cadmium	CdSe	Mercury	HgS	Manganese	Alabandite
Nickel	Pentlandite	Indium	InAs	Tin	Sn02
Cobalt	Elemental Cobalt	Magnesium	Olivine		

Appendix C: Secondary Ion Mass Spectrometry

Table C1: SIMS Dolomite Oxygen Isotope Data

Sample	Dolomite Type	$^{18}O/^{16}O$	1σ	$\delta^{18}O_{V\text{-}SMOW}$ (‰)$_{Uncorrected}$	$\delta^{18}O_{V\text{-}SMOW}$ (‰)$_{Corrected}$
Buick 06 Spot 2 Pt 1	Host (D1)	1.892416	1.2	31.93	18.36
Buick 06 Spot 2 Pt 2	Host (D1)	1.900170	1.2	36.16	22.59
Buick 06 Spot 3 Pt 1	Host (D1)	1.904682	1.2	38.62	25.05
Buick 06 Spot 3 Pt 2	Recrystallized (D2)	1.905660	1.2	39.15	25.58
Buick 06 Spot 3 Pt 3	Recrystallized (D2)	1.890246	1.2	30.75	17.17
Buick 06 Spot 3 Pt 4	Host (D1)	1.901401	1.2	36.83	23.26
Buick 03 Spot 1 Pt 1	Host (D1)	1.894877	1.2	33.27	24.73
Buick 03 Spot 2 Pt 1	Recrystallized (D2)	1.885672	1.2	28.25	19.71
Buick 03 Spot 2 Pt 2	Recrystallized (D2)	1.888518	1.2	29.80	21.26
Buick 03 Spot 2 Pt 3	Recrystallized (D2)	1.895477	1.2	33.60	25.05
Buick 03 Spot 3 Pt 1	Recrystallized (D2)	1.887601	1.2	29.30	20.76
Fletcher 06 Spot 1 Pt 1	Recrystallized (D2)	1.880173	1.2	19.85	22.26
Fletcher 06 Spot 1 Pt 2	Recrystallized (D2)	1.881345	1.2	20.49	22.90
Fletcher 06 Spot 1 Pt 3	Recrystallized (D2)	1.883227	1.2	21.51	23.92
Fletcher 06 Spot 1 Pt 4	Recrystallized (D2)	1.880955	1.2	20.28	22.69
Fletcher 06 Spot 3 Pt 1	Recrystallized (D2)	1.874868	1.2	16.97	19.39
Fletcher 06 Spot 3 Pt 2	Host (D1)	1.876442	1.2	17.83	20.24
Sweetwater 03 Spot 3 Pt 1	Veinlet (D3)	1.892370	1.2	26.47	25.14
Sweetwater 03 Spot 3 Pt 2	Veinlet (D3)	1.881822	1.2	20.75	19.42
Sweetwater 03 Spot 3 Pt 3	Veinlet (D3)	1.884734	1.2	22.33	21.00
Sweetwater 03 Spot 3 Pt 4	Veinlet (D3)	1.887257	1.2	23.69	22.37

Sample	Dolomite Type	$^{18}O/^{16}O$	1σ	$\delta^{18}O_{V\text{-}SMOW}$ (‰)$_{Uncorrected}$	$\delta^{18}O_{V\text{-}SMOW}$ (‰)$_{Corrected}$
Sweetwater 03 Spot 3 Pt 5	Host (D1)	1.890224	1.2	25.30	23.98
Sweetwater 03 Spot 1 Pt 1	Veinlet (D3)	1.886964	1.2	23.54	22.21
Sweetwater 03 Spot 1 Pt 2	Veinlet (D3)	1.883982	1.2	21.92	20.59
Fletcher 04 Spot 2 Pt 1	Recrystallized (D2)	1.881294	1.2	20.46	21.78
Fletcher 04 Spot 2 Pt 2	Recrystallized (D2)	1.878772	1.2	19.09	20.41
Fletcher 04 Spot 3 Pt 1	Host (D1)	1.888714	1.2	24.48	25.81
Fletcher 04 Spot 3 Pt 2	Host (D1)	1.882431	1.2	21.08	22.40
Sweetwater 04 Spot 2 Pt 1	Veinlet (D3)	1.878151	1.2	18.76	22.91
Sweetwater 04 Spot 2 Pt 2	Veinlet (D3)	1.876158	1.2	17.67	21.83
Sweetwater 04 Spot 2 Pt 3	Veinlet (D3)	1.875660	1.2	17.40	21.56
Casteel_82V69_Spot1_Pt 1	Veinlet (D3)	1.878493	1.2	20.09	22.53
Casteel_82V69_Spot1_Pt 2	Veinlet (D3)	1.881707	1.2	21.84	24.28
Casteel_82V69_Spot1_Pt 3	Veinlet (D3)	1.883078	1.2	22.58	25.02
Casteel_82V69_Spot1_Pt 4	Veinlet (D3)	1.881716	1.2	21.84	24.28
Casteel_82V69_Spot1_Pt 5	Host (D1)	1.871608	1.2	16.35	18.79
Casteel_82V69_Spot1_Pt 6	Host (D1)	1.873754	1.2	17.52	19.96

Sample	Dolomite Type	$^{18}O/^{16}O$	1σ	$\delta^{18}O_{V\text{-}SMOW}$ (‰)$_{Uncorrected}$	$\delta^{18}O_{V\text{-}SMOW}$ (‰)$_{Corrected}$
Casteel_82V69_Spot1_Pt 7	Host (D1)	1.874800	1.2	18.09	20.53
Casteel 09 Spot 1 Pt 1	Recrystallized (D2)	1.878456	1.2	20.07	20.08
Casteel 09 Spot 1 Pt 2	Recrystallized (D2)	1.885950	1.2	24.14	24.15
Casteel 09 Spot 1 Pt 3	Host (D1)	1.887113	1.2	24.77	24.78
Casteel 09 Spot 1 Pt 4	Host (D1)	1.886427	1.2	24.40	24.41
Casteel 09 Spot 1 Pt 5	Host (D1)	1.881189	1.2	21.56	21.57
Casteel 04 Spot 1 Pt 1	Recrystallized (D2)	1.887156	1.2	24.80	26.98
Casteel 04 Spot 1 Pt 2	Recrystallized (D2)	1.878737	1.2	20.22	22.41
Casteel 04 Spot 1 Pt 3	Veinlet (D3)	1.870166	1.2	15.57	17.76
Casteel 04 Spot 1 Pt 4	Veinlet (D3)	1.881363	1.2	21.65	23.84
Casteel 04 Spot 1 Pt 5	Veinlet (D3)	1.879867	1.2	20.84	23.02
Casteel 04 Spot 1 Pt 6	Veinlet (D3)	1.871712	1.2	16.41	18.59
60W117 Spot 3 Pt 1	Recrystallized (D2)	1.869893	1.2	15.42	16.80
60W117 Spot 3 Pt 2	Recrystallized (D2)	1.879031	1.2	20.38	21.76
60W117 Spot 3 Pt 3	Recrystallized (D2)	1.889507	1.2	26.07	27.45

Table C2: SIMS Sphalerite Sulfur Isotope Data

Sample	$^{34}S/S^{32}_{meas}$	1σ	$\delta^{34}S$
60W117 Spot 3 Pt 1	4.367847	0.3	12.29
60W117 Spot 3 Pt 2	4.371185	0.3	13.06
60W117 Spot 3 Pt 3	4.371634	0.3	13.16
60W117 Spot 3 Pt 4	4.359979	0.3	10.46
60W117 Spot 2 Pt 1	4.389236	0.3	17.24
60W117 Spot 2 Pt 2	4.387459	0.3	16.83
60W117 Spot 2 Pt 3	4.380950	0.3	15.32
60W117 Spot 1 Pt 1	4.398277	0.3	19.34
60W117 Spot 1 Pt 2	4.382843	0.3	15.76
60W117 Spot 1 Pt 3	4.378752	0.3	14.81
Buick 6 Spot 1 Pt 1	4.389837	0.3	17.38
Buick 6 Spot 1 Pt 2	4.381023	0.3	15.34
Buick 6 Spot 1 Pt 3	4.388565	0.3	17.09
Buick 6 Spot 1 Pt 4	4.366076	0.3	11.88
Buick 6 Spot 1 Pt 5	4.380410	0.3	15.20
Buick 6 Spot 1 Pt 6	4.374514	0.3	13.83
Buick 6 Spot 1 Pt 7	4.368154	0.3	12.36
Buick 6 Spot 1 Pt 8	4.395265	0.3	18.64
Buick 03 Spot 2 Pt 1	4.374440	0.3	13.81
Buick 03 Spot 2 Pt 2	4.395039	0.3	18.59
Buick 03 Spot 2 Pt 3	4.377285	0.3	14.85
Buick 03 Spot 4 Pt 1	4.367661	0.3	12.62
Buick 03 Spot 4 Pt 2	4.359670	0.3	11.20
Buick 03 Spot 4 Pt 3	4.345431	0.3	7.90
Buick 03 Spot 4 Pt 4	4.358896	0.3	11.02
Buick 03 Spot 4 Pt 5	4.377810	0.3	15.85
Buick 03 Spot 2 Pt 1	4.365554	0.3	13.00
Buick 03 Spot 2 Pt 2	4.358544	0.3	11.37
Buick 03 Spot 2 Pt 3	4.354617	0.3	10.46
Sweetwater 03 Spot 1 Pt 1	4.370597	0.3	14.61
Sweetwater 03 Spot 1 Pt 2	4.352465	0.3	10.40
Sweetwater 03 Spot 1 Pt 3	4.372899	0.3	15.14
Sweetwater 03 Spot 3 Pt 1	4.367496	0.3	14.33
Sweetwater 03 Spot 3 Pt 2	4.347850	0.3	9.76
Sweetwater 07 Spot 2 Pt 1	4.357006	0.3	11.89
Sweetwater 07 Spot 2 Pt 2	4.354387	0.3	11.28
Sweetwater 07 Spot 2 Pt 3	4.359327	0.3	12.87

Sample	$^{34}S/S^{32}_{meas}$	1σ	$\delta^{34}S$
Sweetwater 07 Spot 2 Pt 4	4.363385	0.3	13.81
Sweetwater 07 Spot 2 Pt 5	4.357389	0.3	12.42
Sweetwater 07 Spot 2 Pt 6	4.349797	0.3	10.65
Fletcher 06 Spot 2 Pt 1	4.338203	0.3	8.39
Fletcher 06 Spot 2 Pt 2	4.348626	0.3	10.82
Fletcher 06 Spot 2 Pt 3	4.329638	0.3	6.40
Fletcher 06 Spot 2 Pt 4	4.340638	0.3	8.96
Fletcher 06 Spot 2 Pt 5	4.376989	0.3	17.85
Fletcher 06 Spot 2 Pt 6	4.368433	0.3	15.86

Appendix D: Data used to Construct Figure 5.1 & Figure 5.2

Table D1: Data used to create Figure 5.1

Geologic Zone	Dolomite Type	$\delta^{13}C$ - VPDB	$\delta^{18}O$-VSMOW	Reference	Identifier on Chart
SRZ	Veinlet (D3)	-0.07	22.39	This Study	Red Box
SRZ	Veinlet (D3)	-0.12	22.21	This Study	Red Box
SRZ	Veinlet (D3)	0.09	22.31	This Study	Red Box
SRZ	Veinlet (D3)	-0.31	22.40	This Study	Red Box
SRZ	Veinlet (D3)	-0.49	22.54	This Study	Red Box
SRZ	Veinlet (D3)	-0.21	22.40	This Study	Red Box
SRZ	Veinlet (D3)	-0.21	22.97	This Study	Red Box
SRZ	Veinlet (D3)	0.04	22.22	This Study	Red Box
SRZ	Veinlet (D3)	0.18	22.41	This Study	Red Box
SRZ	Veinlet (D3)	0.04	21.97	This Study	Red Box
SRZ	Veinlet (D3)	0.00	22.06	This Study	Red Box
SRZ	Veinlet (D3)	-0.06	22.18	This Study	Red Box
SRZ	Veinlet (D3)	-0.56	22.15	This Study	Red Box
SRZ	Veinlet (D3)	-0.90	22.63	This Study	Red Box
SRZ	Veinlet (D3)	-0.52	22.16	This Study	Red Box
SRZ	Veinlet (D3)	-0.80	22.53	This Study	Red Box
SRZ	Veinlet (D3)	-0.16	22.47	This Study	Red Box
SRZ	Veinlet (D3)	-1.00	22.20	This Study	Red Box
SRZ	Veinlet (D3)	-0.78	21.50	This Study	Red Box
Cavender, 2015	Cement - LOZ Bright & Moderate	-1.02	26.40	Cavender, 2015	Blue Diamond

Geologic Zone	Dolomite Type	$\delta^{13}C$ - VPDB	$\delta^{18}O$-VSMOW	Reference	Identifier on Chart
Cavender, 2015	Cement - LOZ Bright & Moderate	-1.01	35.28	Cavender, 2015	Blue Diamond
Cavender, 2015	Cement - LOZ Bright & Moderate	-0.7	26.44	Cavender, 2015	Blue Diamond
Cavender, 2015	Cement - LOZ Bright & Moderate	-0.81	27.48	Cavender, 2015	Blue Diamond
Cavender, 2015	Cement - LOZ Bright & Moderate	-1.52	26.88	Cavender, 2015	Blue Diamond
Cavender, 2015	Cement - LOZ Bright & Moderate	-1.3	22.44	Cavender, 2015	Blue Diamond
Cavender, 2015	Cement - LOZ Bright & Moderate	-1.21	24.56	Cavender, 2015	Blue Diamond
Cavender, 2015	Cement - LOZ Bright & Moderate	-1.11	22.81	Cavender, 2015	Blue Diamond
Cavender, 2015	Cement - LOZ Bright & Moderate	-0.95	23.18	Cavender, 2015	Blue Diamond
Cavender, 2015	Cement - LOZ Bright & Moderate	-1.54	23.48	Cavender, 2015	Blue Diamond
Cavender, 2015	Cement - LOZ Bright & Moderate	-1.44	23.36	Cavender, 2015	Blue Diamond
Hannah & Stein 1984	Vein & Vug Filling	-1.1	21.50	Hannah & Stein 1984	Purple Circle
Hannah & Stein 1984	Vein & Vug Filling	-0.3	23.00	Hannah & Stein 1984	Purple Circle
Hannah & Stein 1984	Vein & Vug Filling	-1.2	22.70	Hannah & Stein 1984	Purple Circle
Hannah & Stein 1984	Vein & Vug Filling	-1.1	21.40	Hannah & Stein 1984	Purple Circle
Gregg, 1985	Cement - Basal Dol Bed	-1.4	23.18	Gregg, 1985	Green Triangle

Geologic Zone	Dolomite Type	$\delta^{13}C$ - VPDB	$\delta^{18}O$-VSMOW	Reference	Identifier on Chart
Gregg, 1985	Cement - Basal Dol Bed	-0.9	22.87	Gregg, 1985	Green Triangle
Gregg, 1985	Cement - Basal Dol Bed	-0.8	23.49	Gregg, 1985	Green Triangle
Gregg, 1985	Cement - Basal Dol Bed	-0.7	24.72	Gregg, 1985	Green Triangle
Gregg, 1985	Cement - Basal Dol Bed	-0.4	23.80	Gregg, 1985	Green Triangle
Gregg, 1985	Cement - Basal Dol Bed	-0.75	23.18	Gregg, 1985	Green Triangle

Table D2: Data used to create Figure 5.2

Geologic Zone	Dolomite Type	δ13C - VPDB	δ18O-VSMOW	Reference	Identifier on Chart
Mineralized Dolomite Cements	RD3	-1.4	21.9	Savard et al., 2000	Blue Diamond
Mineralized Dolomite Cements	RD3	-1.1	21.3	Savard et al., 2000	Blue Diamond
Mineralized Dolomite Cements	RD3	-1	21.6	Savard et al., 2000	Blue Diamond
Mineralized Dolomite Cements	RD3	-1	21.8	Savard et al., 2000	Blue Diamond
Mineralized Dolomite Cements	RD3	-0.9	21.8	Savard et al., 2000	Blue Diamond
Mineralized Dolomite Cements	RD3	-1.1	21.3	Savard et al., 2000	Blue Diamond
Mineralized Dolomite Cements	RD3	-0.2	22	Savard et al., 2000	Blue Diamond
Mineralized Dolomite Cements	RD3	-1.2	21.4	Savard et al., 2000	Blue Diamond
Mineralized Dolomite Cements	RD3	-0.9	21.2	Savard et al., 2000	Blue Diamond
Mineralized Dolomite Cements	RD3	-1.1	21.9	Savard et al., 2000	Blue Diamond
Mineralized Dolomite Cements	RD3	-0.9	21.9	Savard et al., 2000	Blue Diamond

Geologic Zone	Dolomite Type	δ13C - VPDB	δ18O-VSMOW	Reference	Identifier on Chart
Mineralized Dolomite Cements	RD3	-0.9	21	Savard et al., 2000	Blue Diamond
Mineralized Dolomite Cements	RD3	-1	20.5	Savard et al., 2000	Blue Diamond
Mineralized Dolomite Cements	RD3	-1.1	21	Savard et al., 2000	Blue Diamond
Mineralized Dolomite Cements	RD3	3.1	22.9	Savard et al., 2000	Blue Diamond
Mineralized Dolomite Cements	RD3	-0.8	21.6	Savard et al., 2000	Blue Diamond
Mineralized Dolomite Cements	RD3	2.9	24.7	Savard et al., 2000	Blue Diamond
Mineralized Dolomite Cements	RD3	2.7	23.6	Savard et al., 2000	Blue Diamond
Mineralized Dolomite Cements	RD3	-1.3	22	Savard et al., 2000	Blue Diamond
Mineralized Dolomite Cements	PD1	-1.1	21.7	Savard et al., 2000	Blue Diamond
Mineralized Dolomite Cements	PD1	-1.1	21.6	Savard et al., 2000	Blue Diamond
Mineralized Dolomite Cements	PD1	-1	21.2	Savard et al., 2000	Blue Diamond
Mineralized Dolomite Cements	PD1	-0.9	21.4	Savard et al., 2000	Blue Diamond
Mineralized Dolomite Cements	PD1	-1.5	21	Savard et al., 2000	Blue Diamond
Mineralized Dolomite Cements	PD1	-0.8	21.6	Savard et al., 2000	Blue Diamond
Mineralized Dolomite Cements	PD1	0.6	22.1	Savard et al., 2000	Blue Diamond

Geologic Zone	Dolomite Type	δ13C - VPDB	δ18O-VSMOW	Reference	Identifier on Chart
Mineralized Dolomite Cements	PD1	-0.7	21.4	Savard et al., 2000	Blue Diamond
Mineralized Dolomite Cements	PD1	-0.9	20.9	Savard et al., 2000	Blue Diamond
Mineralized Dolomite Cements	PD1	-1	20.8	Savard et al., 2000	Blue Diamond
Mineralized Dolomite Cements	PD1	-0.8	21.2	Savard et al., 2000	Blue Diamond
Mineralized Dolomite Cements	PD1	-5.1	18.7	Savard et al., 2000	Blue Diamond
Mineralized Dolomite Cements	PD1	-1	21	Savard et al., 2000	Blue Diamond
Mineralized Dolomite Cements	PD1	-0.9	20.9	Savard et al., 2000	Blue Diamond
Mineralized Dolomite Cements	PD1	0.5	21.8	Savard et al., 2000	Blue Diamond
SRZ Zone	Veinlet (D3)	-0.07	22.39	This Study	Red Box
SRZ Zone	Veinlet (D3)	-0.12	22.21	This Study	Red Box
SRZ Zone	Veinlet (D3)	0.09	22.31	This Study	Red Box
SRZ Zone	Veinlet (D3)	-0.31	22.40	This Study	Red Box
SRZ Zone	Veinlet (D3)	-0.49	22.54	This Study	Red Box
SRZ Zone	Veinlet (D3)	-0.21	22.40	This Study	Red Box
SRZ Zone	Veinlet (D3)	-0.21	22.97	This Study	Red Box
SRZ Zone	Veinlet (D3)	0.04	22.22	This Study	Red Box
SRZ Zone	Veinlet (D3)	0.18	22.41	This Study	Red Box
SRZ Zone	Veinlet (D3)	0.04	21.97	This Study	Red Box
SRZ Zone	Veinlet (D3)	0.00	22.06	This Study	Red Box
SRZ Zone	Veinlet (D3)	-0.06	22.18	This Study	Red Box
SRZ Zone	Veinlet (D3)	-0.56	22.15	This Study	Red Box
SRZ Zone	Veinlet (D3)	-0.90	22.63	This Study	Red Box

Geologic Zone	Dolomite Type	δ13C - VPDB	δ18O-VSMOW	Reference	Identifier on Chart
SRZ Zone	Veinlet (D3)	-0.52	22.16	This Study	Red Box
SRZ Zone	Veinlet (D3)	-0.80	22.53	This Study	Red Box
SRZ Zone	Veinlet (D3)	-0.16	22.47	This Study	Red Box
SRZ Zone	Veinlet (D3)	-1.00	22.20	This Study	Red Box
SRZ Zone	Veinlet (D3)	-0.78	21.50	This Study	Red Box